

Design of a Scanning Tunneling Microscope

Undergraduate Honors Thesis

Shannon Yee

V. V. Subramaniam, Advisor

Department of Mechanical Engineering
The Ohio State University
Spring, 2007

This work was supported in part by the College of Engineering and Lockheed Martin Corporation

Abstract

Applications in nanotechnology require the use of tools that can help visualize and manipulate structures at the nanoscale. A scanning tunneling microscope (STM) is a visualization tool that utilizes the quantum mechanical phenomenon of electron tunneling to image features and structures at these small scales. Tunneling results when a metallic probe tip is brought sufficiently close to an electrically conducting, biased sample without making physical contact. A small current is drawn as electrons jump (tunnel) across the gap between the tip and the sample. This current is so small that the medium between the tip and the sample does not break down and become electrically conducting. Once a tunneling current is drawn between the tip and the sample, which are separated by a gap, feedback controls in conjunction with piezoelectric actuators adjust the gap distance in such a way as to maintain a constant tunneling current as the tip scans across the sample surface. STMs utilize this monitoring of the gap adjustment in order to produce images of the sample surface with potentially near atomic resolution. The first STM was developed by Binnig and Rohrer in 1981 and these microscopes are now commercially available. Commercial microscopes, however, are expensive, and not easily integrated with other experiments and processes in the laboratory. The goal of this work is to design and build a relatively inexpensive STM in order to serve as a basic laboratory research apparatus that could be utilized in nanotechnology research. This approach consists of using off-the-shelf components and instrumentation commonly found in a university laboratory (such as oscilloscopes and multimeters) to construct a STM. Automatic feedback controls serve to acquire data and control the piezoelectric actuators to sub-nanometer displacements in order to obtain and maintain a tunneling current. This data is then recorded and analyzed by imaging software developed in MATLAB in order to produce topographical images of samples. A commercially available gold grid is successfully imaged and used as a calibration tool to quantify images of other samples such as a gold film on an alumina substrate. This home-made instrument is potentially capable of imaging surfaces with resolution comparable to those attainable with commercial STMs if placed under vacuum. This work turns into reality the goal of rendering a STM a laboratory instrument as quotidian as an oscilloscope for nanotechnology research.

Table of Contents

Abstract.....	1
List of Figures.....	3
List of Tables.....	4
Introduction.....	5
1.1) Historical Background.....	5
1.2) Quantum Mechanical Tunneling.....	6
1.3) Description of a STM.....	16
1.4) Review of the Relevant Literature.....	20
Motivation and Objectives.....	23
2.1) Motivation.....	23
2.2) Objectives.....	25
Design of the Microscope.....	26
3.1) Overview of the Design.....	26
3.2) Vibration Isolator.....	27
3.3) Scanner.....	31
3.4) Control Circuit.....	36
3.5) DAQ and Imaging Software.....	38
3.6) Cost.....	39
Procedure for Imaging.....	41
4.1) Procedure for Coarse Adjustment.....	41
4.2) Procedure for Fine Adjustment.....	44
4.3) Summary of Imaging Procedures.....	47
Results.....	49
5.1) Overview.....	49
5.2) Gold Calibration Grid.....	50
5.2) Sputtered Gold Film on an Alumina Substrate.....	55
5.3) STM Tungsten Probe Tip.....	59
5.4) SWCNT Bundle.....	60
Summary & Conclusions.....	61
Recommendations for Future Work.....	63
Appendix.....	64
A1) Schematic of the Scanner Assembly.....	65
A2) Schematic of the Control Circuit.....	74
A3) Explanation of the Software (ReadMe).....	78
A3.1 Data Acquisition.....	79
A3.2 Data Analysis.....	86
A4) MATLAB Scripts.....	94
A4.1 STM.m.....	94
A4.2 STMgui.m.....	95
A4.3 Settings.m.....	102
A4.4 removdup.m.....	107
References.....	108

List of Figures

Figure 1. Classic problem of a particle approaching a rectangular barrier.....	6
Figure 2. Classical physics predicts particle reflection.....	6
Figure 3. Quantum physics predicts particle tunneling as probable.....	7
Figure 4. Typical physical arrangement of tip and sample separated by a gap.....	8
Figure 5. Schematic showing the potential from tip to sample versus distance.....	9
Figure 6. Schematic of the WKB approximation.....	11
Figure 7. Schematic depicting tunneling.....	14
Figure 8. Constant height approach.....	16
Figure 9. Constant tunneling current approach.....	17
Figure 10. Commercial STM probe tip.....	18
Figure 11. IMB logo created from neon atoms imprinted on a nickel surface using a STM.....	24
Figure 12. Block diagram.....	26
Figure 13. Configuration of the coarse adjustment motorized translation stages.....	27
Figure 14. Photograph of the coarse adjustment motorized translation stages.....	28
Figure 15. Vibration isolation platform used to mount the motor controlled translation stages.....	30
Figure 16. Typical first order frequency response of piezoelectric actuators.....	32
Figure 17. Equivalent electrical element representation of piezoelectric crystal.....	32
Figure 18. More realistic electrical representation of the piezoelectric actuators.....	33
Figure 19. Schematic of the scanner assembly.....	35
Figure 20. Integral-derivative control scheme used in the prototype STM.....	36
Figure 21. Paschen's limit curve.....	42
Figure 22. Establishing the setpoint.....	44
Figure 23. Separation, sample bias, and current depiction during imaging.....	47
Figure 24. Photograph showing Nanosurf's sputtered gold grid used for calibration.....	50
Figure 25. Image of Nanosurf's sputtered gold grid taken with a commercial STM.....	50
Figure 26. 3D gold sputtered calibration sample.....	51
Figure 27. 2D gold sputtered calibration sample.....	52
Figure 28. Black and white image of gold sputter calibration sample.....	52
Figure 29. Center of gold sputtered calibration sample.....	53
Figure 30. 3D surface scratch.....	55
Figure 31. 2D surface scratch.....	56
Figure 32. Black and white image of the surface scratch.....	56
Figure 33. Rastering pattern encountering scratch.....	57
Figure 34. FFT of the data containing the scratch.....	57
Figure 35. Scan A, 3D surface scratch.....	58
Figure 36. Scan B, 3D surface scratch.....	58
Figure 37. Scan A, Black and white surface scratch.....	58
Figure 38. Scan B, Black and white surface scratch.....	58
Figure 39. Scan C, 3D STM tip.....	59
Figure 40. Scan D, 3D STM tip.....	59
Figure 41. Scan C, 2D STM tip.....	59
Figure 42. Scan D, 2D STM tip.....	59
Figure 43. Fiber 1, 3D SWCNT bundle.....	60
Figure 44. Fiber 2, 3D SWCNT bundle.....	60

Figure 45. Fiber 2, SWCNT bundle.....	60
Figure 46. Fiber 3, SWCNT bundle.....	60
Figure 47. Schematic of the scanner assembly.....	65
Figure 48. Close-up of scanner.....	66
Figure 49. Photograph of the scanner assembly.....	67
Figure 50. Mechanical drawing of the main support plate.....	68
Figure 51. Mechanical drawing of the large support plate.....	69
Figure 52. Mechanical drawing of the small plate.....	70
Figure 53. Mechanical drawing of the T-holder.....	71
Figure 54. Mechanical Drawing of the scanner assembly.....	72
Figure 55. Close-up of scanner assembly (side view).....	73
Figure 56. Close-up of scanner assembly (top view).....	73
Figure 57. Schematic of the power supply for the control circuit.....	74
Figure 58. Circuit diagram of the tunneling current transducer.....	75
Figure 59. Controls circuit.....	76
Figure 60. Control circuit for the lateral (XY) actuators.....	77
Figure 61. LabVIEW front panel for <i>STM DAQ&Analog Output.vi</i>	79
Figure 62. DAQ block diagram for <i>STM DAQ&Analog Output.vi</i>	80
Figure 63. DAQ assistant window.....	82
Figure 64. Signal generator window.....	83
Figure 65. Define signal window.....	84
Figure 66. Write to file window.....	85
Figure 67. STM graphic user interface (GUI).....	87
Figure 68. Settings window.....	89
Figure 69. MATLAB SPTool toolbox.....	90
Figure 70. Explanation pop-up window.....	90
Figure 71. Sample FFT.....	91
Figure 72. Example 3D image.....	92
Figure 73. Example 2D image.....	93
Figure 74. Example black and white image.....	93

List of Tables

Table I. Cost Estimate for the STM components ¹	40
--	----

Chapter 1

Introduction

1.1) Historical Background

The concept of tunneling was first investigated by nuclear physicist George Gamow who explained in 1928 how an alpha particle is able to escape the large potential energy barrier confining it to the nucleus, as a result of radioactive alpha decay. If a particle could tunnel out of a potential well, the next logical problem would be to investigate if a particle could tunnel through a barrier [1]. Max Born later realized the generality of tunneling as it applied as a quantum mechanical phenomenon where particles have the probability of tunneling both out of and into a potential well through a barrier. Later in the 1960's, solid-state physicist Ivar Giaever expanded on this concept as he "envisioned that if a potential difference is applied to two metals separated by a thin insulating film, a current will flow because of the ability of electrons to penetrate the potential barrier of insulating layers" [2].

Gerd Binnig, Heinrich Rohrer, and their colleagues [3] at the IBM Zurich Research Laboratory first applied the concept of tunneling to determine surface topology by obtaining the first image of a sample surface with atomic resolution in 1981. This accomplishment earned Binnig and Rohrer the Nobel Prize in Physics in 1986 for their design of a scanning tunneling microscope (STM) in 1985. Binnig and Rohrer's specific design utilized a novel technique involving piezoelectric actuators to control a sharpened metal probe tip and acquire a tunneling current in vacuum. While the tunneling phenomenon was well understood by the time Binnig and Rohrer designed their microscope, the field of scanning probe microscope (SPM) was still in its infancy. Several other scanning probe microscopes with high resolution have been developed since, with the most popular techniques being atomic force microscopy (AFM), scanning electrostatic force microscopy (SEFM), scanning magnetic microscopy (SMM), and scanning capacitance microscopy (SCM).

1.2) Quantum Mechanical Tunneling

An understanding of the quantum mechanical phenomenon of tunneling is essential to the design and operation of a STM. While the theory is mathematically intensive, the concept can be explained in a relatively simpler manner. First, consider the classic quantum physics problem of a particle of mass m impinging on a barrier, as illustrated in Fig. 1.

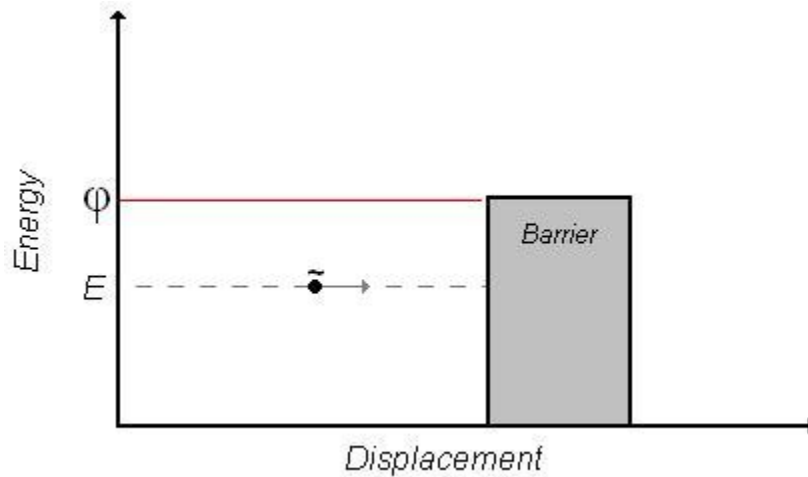


Figure 1. Classic problem of a particle approaching a rectangular barrier

The barrier has a potential energy height defined by the work function, ϕ , and a finite width. The particle has a total energy E . Suppose the energy of the particle is less than the work function necessary to liberate the particle classically. When the particle approaches the barrier with momentum mv , classical physics predicts that the particle will reflect as seen in Fig. 2.

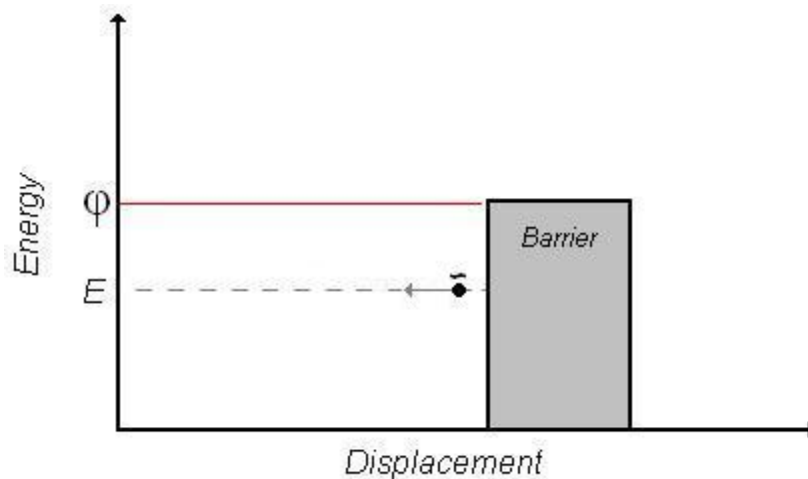


Figure 2. Classical physics predicts particle reflection

However, according to quantum mechanics, the particle exhibits wave-like characteristics with a wavelength defined by the DeBroglie wavelength, so that it may be able to penetrate the barrier if the characteristic length of the barrier is comparable to the wavelength as depicted in Fig. 3.

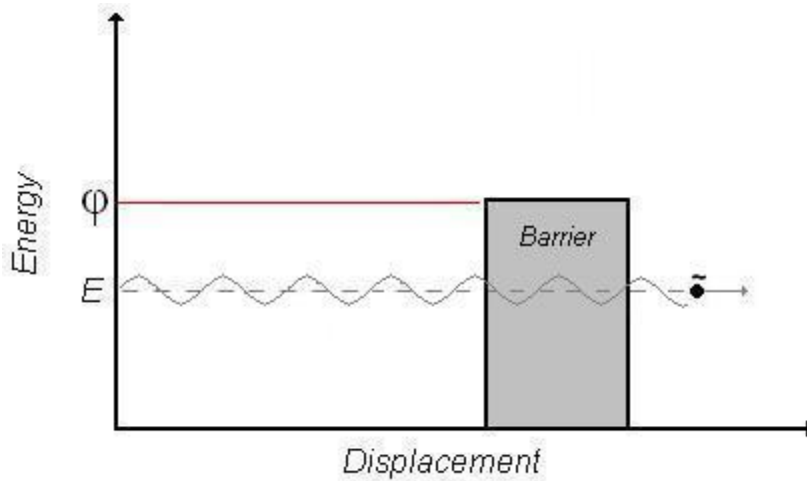


Figure 3. Quantum physics predicts particle tunneling as probable

The DeBroglie wavelength is defined as:

$$\lambda = \frac{h}{\gamma mv} \quad (1)$$

where

h = Planck's constant, 6.626×10^{-34} J-s

γ = Lorentz factor, $\gamma = \frac{c}{\sqrt{c^2 - v^2}}$

c = speed of light, 2.998×10^8 m/s

m = rest mass of the particle, kg

v = speed of the particle as observed in the time measured reference frame

For an object to exhibit wave-like characteristics, its DeBroglie wavelength must be comparable to or greater than a characteristic length, e.g. width of the barrier. Generally, this happens when the mass is small since Planck's constant, h , is a very small number. As a wave, there is a finite probability that the particle will "tunnel" through the barrier and appear on the other side. This is analogous to radio waves passing through buildings before a radio converts the signal into music.

The concept of tunneling can be applied to scanning tunneling microscopy where the particle of interest is an electron. The STM consists of a sharp, conducting probe tip, and an electrically conducting sample whose surface is to be imaged, which is separated from the probe tip by a small gap of length d . This gap may be open to air or be evacuated. Generally, the sharp probe tip is approximated as a sphere with a specific radius of curvature R . The sample must be electrically conducting because the conduction bands and Fermi levels of tip and sample play a key role in tunneling as will be discussed later. Figure 4 illustrates a typical physical arrangement.

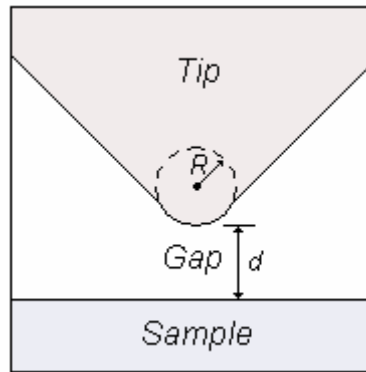


Figure 4. Typical physical arrangement of tip and sample separated by a gap

If a small potential difference, V , is applied between the tip and the sample, the resulting electric field can cause a tunneling current to flow. The polarity of the bias defines the direction in which electrons flow from occupied states in one conductor to vacant states in another conductor. For the remainder of this discussion, the tip will be presumed to be held at a lower potential than the sample. Thus, electrons will flow from the tip to the sample but a tunneling current can also be obtained with reverse polarity. The origin of the tunneling current may be more easily understood from the potential versus position diagram shown in Fig. 5.

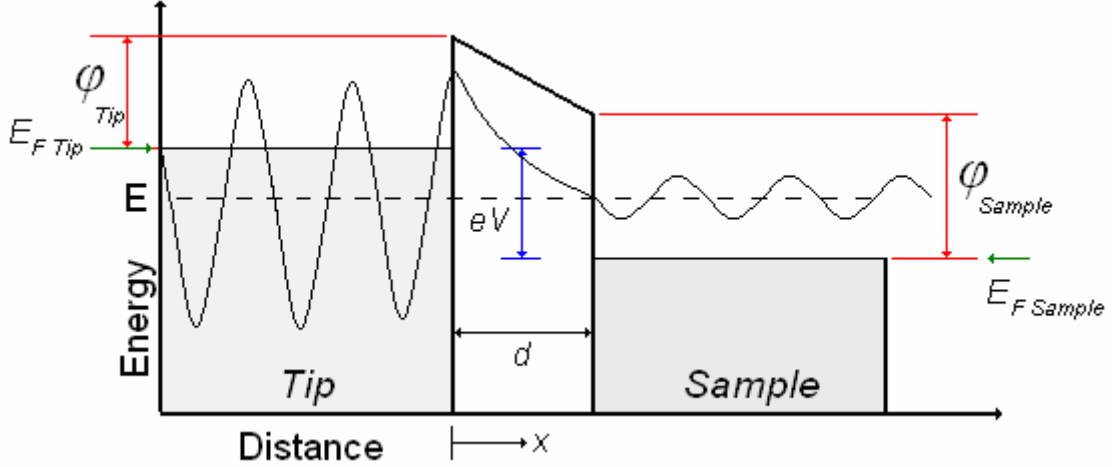


Figure 5. Schematic showing the potential from tip to sample versus distance

In Fig. 5, the effective work function necessary to liberate electrons from the tip is denoted by ϕ_{Tip} and the effective work function for liberating electrons from the sample is ϕ_{Sample} . The electron has an energy, E , which is less than the effective work function. The respective Fermi levels for the tip and the sample are $E_{F Tip}$ and $E_{F Sample}$. An electron at the Fermi level of the tip that drops to the Fermi level of the sample will experience a loss in energy equal to the difference eV where V is the applied voltage bias. The energy of an electron within the gap can be approximated as the average of the work functions. In other words, the potential energy of an electron between the tip and the sample may be taken to depend on the spatial coordinate, x , in the following manner:

$$V(x) = \begin{cases} (\phi_{Sample} - \phi_{Tip}) \frac{x}{d} + \phi_{Tip} & 0 \leq x \leq d \\ 0 & \text{Otherwise} \end{cases} \quad (2)$$

The wavelike nature of the electron is also depicted in Fig. 5.

Equation (2) may be used to estimate the tunneling current based on the probability that electrons flow from the tip to the sample. The probability of an electron tunneling through the barrier can be calculated from the one-dimensional, time-dependent Schrödinger equation, which can be expressed in the form given by Equation (3) for this situation.

$$E \frac{\partial}{\partial t} \Phi(x,t) = H\Phi(x,t) \quad (3)$$

where

E = energy of the electron

$\Phi(x,t)$ = the space and time dependent wave function

$H\Phi(x,t)$ = Hamiltonian of the system

The Hamiltonian for a tunnel junction for the electron is simply the sum of the kinetic and potential energy terms:

$$H\Phi(x,t) = -\frac{\hbar^2}{2m} \frac{\partial^2}{\partial x^2} \Phi(x,t) + V(x)\Phi(x,t) \quad (4)$$

where

\hbar = Dirac's constant, $\frac{h}{2\pi} = 1.055 \times 10^{-34}$ J-s

m = mass of the electron, 9.1096×10^{-31} kg

Taking the wave function to be separable with respect to space and time,

$$\Phi(x,t) = \Psi(x)Y(t) \quad (5)$$

$$\frac{\hbar^2}{2m} \frac{\partial^2}{\partial x^2} \Psi(x) = (V(x) - E)\Psi(x) \quad (6)$$

An approximate solution can be obtained using the WKB (Wentzel, Kramers, Brillouin) method. The WKB approximation makes the assumption that initially the Fermi levels for the tip and the sample are the same. As a voltage is applied across the gap, the Fermi levels displace so that the effective work functions of the tip and sample are ϕ_{Tip} and ϕ_{Sample} , respectively. In other words, the barrier across the gap from tip to sample is approximated as a rectangular barrier. The approximation is shown schematically in Fig. 6.

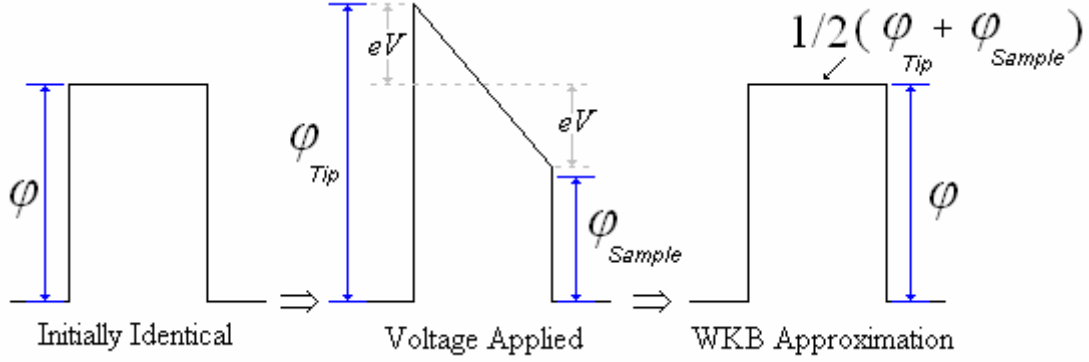


Figure 6. Schematic of the WKB approximation

Under the WKB approximation, the time-independent Schrödinger equation can be written as:

$$\frac{\partial^2}{\partial x^2} \Psi(x) \approx \frac{p(x)^2}{\hbar^2} \Psi(x) \quad (7)$$

where

$$p(x) \equiv \sqrt{2m(V(x) - E)} \quad (8)$$

Equation (7) has three solutions corresponding to the spatial regions: tip, gap, and sample. These solutions can be expressed in the following manner:

$$\Psi(x) \approx \begin{cases} Ae^{i|p(x)|\frac{x}{\hbar}} + Be^{-i|p(x)|\frac{x}{\hbar}} & x < 0 \\ \frac{C}{\sqrt{|p(x)|}} e^{-\frac{1}{\hbar} \int_0^x |p(x')| dx'} + \frac{D}{\sqrt{|p(x)|}} e^{\frac{1}{\hbar} \int_0^x |p(x')| dx'} & 0 \leq x \leq d \\ Fe^{i|p(x)|\frac{x}{\hbar}} + Ge^{-i|p(x)|\frac{x}{\hbar}} & x > d \end{cases} \quad (9)$$

The solution of the partial differential equation has six unknown constants, A , B , C , D , F , and G . The amplitude of the incident electron wave, A , is arbitrary. The coefficients B , D and G correspond to the amplitude of leftward moving electrons (i.e. from sample to tip). Specifically, B refers to reflected electrons at the edge of the tip, D refers to leftward moving electrons in the gap due to interactions occurring in the gap, and G refers to electrons that from the sample to the tip. Only rightward moving electrons are considered since electrons flow in the opposite direction of the applied electric field and the probability of leftward tunneling is assumed to be much smaller than the probability of rightward tunneling. In addition, it is assumed that operating temperatures are low enough that it is unlikely that electrons will thermally migrate from the sample to the tip. Under these conditions, the coefficients B , D , and G are zero. The coefficient C represents a constant defined in the WKB approximation as:

$$C^2 = A^2 \frac{d\theta}{dx} \quad (10)$$

where

A = amplitude of the wave associated with the rightward moving electron

$\frac{d\theta}{dx}$ = derivative of the phase of the wave associated with the rightward moving electron

The incident electron wave function then has the form:

$$\Psi_{rightward}(x) = Ae^{i\theta(x)} = Ae^{i|p(x)|\frac{x}{\hbar}} \quad x < 0 \quad (11)$$

or more simply:

$$\theta(x) = |p(x)|\frac{x}{\hbar} \quad x < 0 \quad (12)$$

$$\frac{d\theta}{dx} = \frac{|p(x)|}{\hbar} = \frac{\sqrt{2mE}}{\hbar} \quad x < 0 \quad (13)$$

The coefficient F represents the amplitude of the transmitted wave associated with the electrons. The ratio of the amplitudes for the transmitted and incident electron waves is essentially the total decrease produced by the rightward exponential decay in the tunneling region ($0 \leq x' \leq d$) since the wave function must be continuous.

$$\frac{|F|}{|A|} = \frac{|\Psi(d)|}{|\Psi(0)|} \approx \frac{\frac{C}{\sqrt{|p(x=d)|}} e^{-\frac{1}{\hbar} \int_0^d |p(x')| dx'}}{\frac{C}{\sqrt{|p(x=0)|}} e^{-\frac{1}{\hbar} \int_0^d |p(x')| dx'}} = \frac{\sqrt{|p(x=0)|}}{\sqrt{|p(x=d)|}} e^{-\frac{1}{\hbar} \int_0^d |p(x')| dx'} \quad (14)$$

The tunneling probability as a function of electron energy is then the ratio of the squares of the transmitted amplitude to the incident amplitude.

$$T(E) = \frac{|F|^2}{|A|^2} = \frac{|\Psi(d)|^2}{|\Psi(0)|^2} \approx \sqrt{\frac{(\varphi_{Tip} - E)}{(\varphi_{Sample} - E)}} e^{-\frac{2}{\hbar} \int_0^d |p(x')| dx'} \quad (15)$$

Note that if the effective work functions are equal then the tunneling probability reduces to [1]:

$$T(E) = \frac{|F|^2}{|A|^2} \approx e^{-\frac{2}{\hbar} \int_0^d |p(x')| dx'} = e^{-2\gamma(d)} \quad (16)$$

where

$$\gamma(d) = \frac{1}{\hbar} \int_0^d |p(x')| dx' \quad (17)$$

The tunneling current for electrons at an energy E is proportional to the tunneling probability for those electrons. The electrons that are free to tunnel are those electrons whose energies are between the Fermi level of the sample and the Fermi level of the tip. Since the energies of the electrons are quantized, the total tunneling current is proportional to the sum of the tunneling probability over all finite energy quanta within the range that are free to tunnel.

$$I \propto \sum_{E_{F,Tip} - eV}^{E_{F,Tip}} |\Psi(0)|^2 T(E) \quad (18)$$

By defining the local density of states (LDOS) as:

$$\rho_s(x, E) \equiv \frac{1}{eV} \sum_{E-eV}^E |\Psi(x)|^2 \quad (19)$$

the tunneling current can be expressed as:

$$I \propto V \rho_s(0, E_{F Tip}) e^{-2\gamma(d)} \quad (20)$$

The foregoing simplified analysis of tunneling reveals several key results. First, the tunneling current is directly proportional to the voltage bias applied between the tip and the sample. This voltage bias introduces other physical constraints which will be discussed later. Second, the tunneling current exponentially decreases as the gap distance is increased. Lastly, the tunneling current is actually a measure of the density of states for the tip and the sample. In the operation of a STM, the tunneling current does not represent an image of the nuclei of atoms but rather the probable regions where electrons are likely to flow. These regions tend to be around the positively charged nuclei but what is actually being detected is the availability or density of states at given locations. Figure 7 shows a schematic summarizing this discussion.

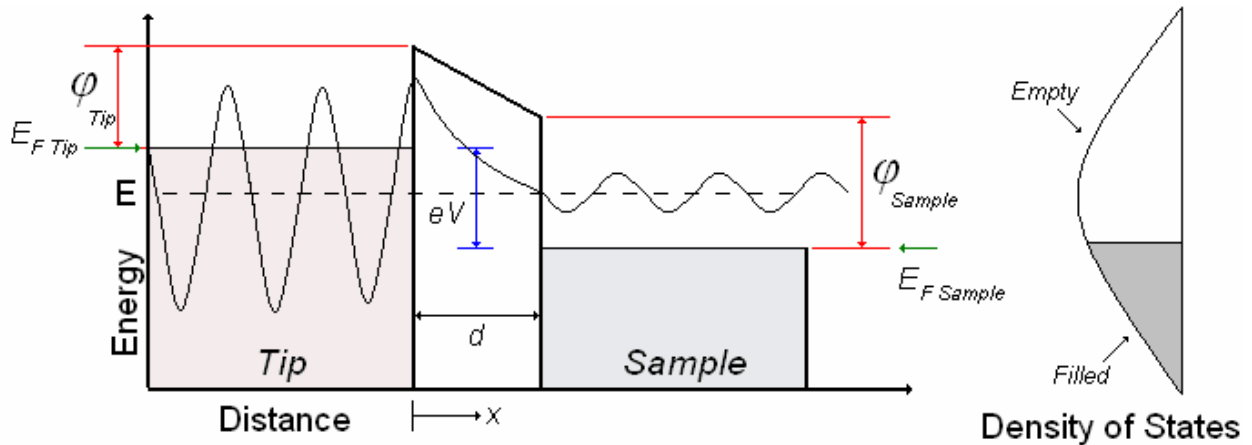


Figure 7. Schematic depicting tunneling.

Analysis of the tunneling phenomenon also enables the lateral resolution of the microscope to be determined. The general approach is to model the tip as a sphere with a radius of curvature R as depicted in Fig. 8. The s-wave model for the lateral resolution is extensive and was developed by Tersoff and Hamann in 1985[4], essentially verifying Binnig and Rohrer's experimental results. The results of the model are reproduced below and are valid when the radius of curvature of the tip is much greater than the gap separation distance.

$$Resolution = \sqrt{(2\text{\AA})(R + d)} \quad (21)$$

where

R = radius of curvature, \AA

d = gap distance, \AA

In summary, the theory behind the quantum mechanical phenomenon of tunneling provides a means of understanding the nature of images with near atomic resolution produced by a STM. While these images are not those of the nuclei of atoms, they represent the LDOS of the surface at locations that are associated with atoms. It is important to emphasize the exponential decay of the tunneling current with gap distance and the direct proportionality with the sample bias as key characteristics of STMs. It is also important to remember that the foregoing analysis is only valid for electrical conductors. This theory is not applicable for semiconductors and insulating bodies. The foregoing theory of tunneling current provides the framework for application and design of STMs.

1.3) Description of a STM

A STM uses the concept of tunneling in order to control the tip-to-sample distance and produce an image of the surface topology of a sample. There are two main types of STMs. One type relies on maintaining a constant tip-to-sample distance whereas the other relies on preserving a constant tunneling current. Both of these approaches utilize tunneling as the primary mechanism for producing an image of the sample, but the actuation and image voltage signals differ between the two approaches. In both approaches, a sharpened probe tip is brought close to a sample surface until a tunneling current is detected. Typical tunneling currents are on the order of nanoAmperes (nA). Once a tunneling current is drawn, the probe tip can be scanned laterally across the surface and the recorded tip-to-sample distance (or tunneling current) is used to image the sample surface.

For the constant tip-to-sample approach, the tip is brought close to a surface until a tunneling current is drawn. Once this current is detected, the tip and sample are held at a fixed distance with respect to each other along the vertical axis. In other words, the tip and the sample are not permitted to move vertically relative to one another. Next, the probe tip is scanned across the sample surface and the tunneling current varies with the surface topology. Figure 8 illustrates this strategy. Since the tunneling current is known to vary exponentially with the gap distance (Equation (20)), the surface topology can be inferred from the magnitude of the change in tunneling current relative to the tunneling current at the datum height. The change in tunneling current is recorded at various locations and represents relative distances from the tip to the sample.

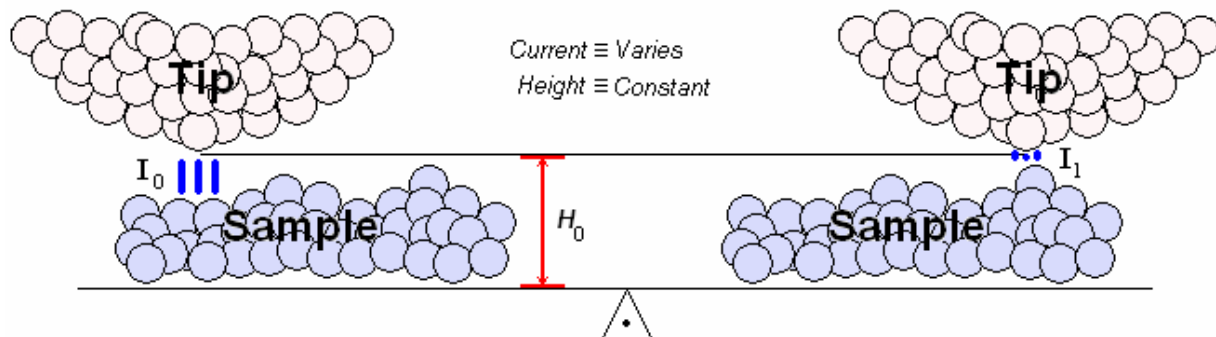


Figure 8. Constant height approach

In the constant current approach, the tip is also brought close to the sample surface until a tunneling current is detected. However, unlike the constant height approach, once this current is drawn, it is maintained by moving the tip up and down as the tip is scanned across the sample surface. This requires feedback control to be present in order to compensate for any current fluctuations by corresponding displacement variations. In other words, the tip and sample are permitted to move vertically relative to one another. The probe tip is then scanned across the surface and the height is varied relative to a datum with the surface topology. Figure 9 illustrates this approach.

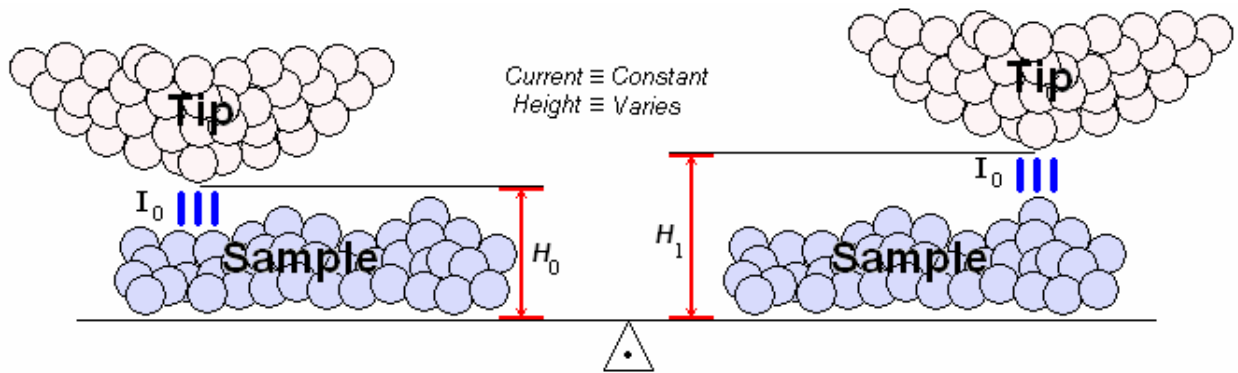


Figure 9. Constant tunneling current approach

There are advantages and disadvantages to both approaches. The major disadvantage of the constant height approach is its inability to determine surface topologies when the surface is rougher than a few nanometers. When the surface is rougher than a few nanometers the probe tip is likely to contact the sample as it scans since the tip-to-sample distance does not vary. A major advantage of this approach, however, is that it can be operated without complicated feedback control. Similarly a major disadvantage of the constant tunneling current approach is that a complicated control circuit is required. The actuators that move the tip relative to the sample must be able to respond rapidly to changes in the surface topology. However its major advantage is the ability to determine the surface topology of rougher surfaces. In addition, the constant current approach can produce higher resolution images,

Another aspect of a STM is its operating environment. STMs can either operate in vacuum or in an electrically insulating medium. Again, there are advantages and disadvantages to each. First, in order to operate in vacuum, vacuum chambers, pumps, and complicated automated coarse adjustment techniques must be employed. Operating in open air, however,

introduces other problems. Namely, oxide layers can form on the tip and sample depending on what materials constitute these two components. These oxide layers electrically insulate the tip and the sample, and introduce additional barriers to the tunneling current. However, once a tunneling current is drawn this oxide layer may act as a mechanical damper and helps to eliminate vibration. This is analogous to a thin film cushion on a surface. The presence of adsorbed molecules such as H_2O and CO_2 can also introduce additional barriers for the tunneling current.

Now that the basic operating principles of STMs have been described, the general design of a STM will be discussed. The components of a constant tunneling current design, open to air will be described first. A constant height approach or a vacuum STM has slightly different components, and will not be discussed in detail. A constant tunneling current type of STM open to air consists of three main components, a sharpened probe tip and scanner, a vibration isolator and sample stage, and a feedback controls and data acquisition system. The function of these individual components is briefly discussed.

STM probe tips are commercially available (Veeco Probes, Model TT). These tips are typically made from tungsten due to strength and chemical considerations. These probe tips are chemically etched so they are much sharper than any machined tip. Since the lateral resolution of a STM strongly depends on the tip's radius of curvature, a smaller radius yields a finer resolution. Typical tungsten probe tips have a radius of curvature of about 20 nm (see Figure 10).



Figure 10. Commercial STM probe tip

The probe tip is then mounted on a scanner. These scanners must be able to translate in three dimensions, and therefore consist of three actuators. The lateral actuators (X and Y direction) are used to move the probe tip over a desired area and the vertical actuator (Z direction) is used to move the probe tip up and down in order to maintain a constant tunneling current. These actuators are typically made from piezoelectric materials due to the very small displacements that can be achieved with these actuators.

The next component is the vibration isolator and sample stage. The sample stage is simply used to hold the sample and make electrical contact so a voltage bias can be applied between the sample and the probe tip. These motorized sample stages (Velmex, Model 6012K1) typically have a way of moving the tip or the sample with a resolution on the order of microns. This permits coarse placement and adjustment so specific regions can be scanned. Both the sample stage and the scanner are mounted on a vibration isolator. This vibration isolator must be capable of eliminating unwanted mechanical vibrations. Vibrations with amplitudes on the order of nanometers will adversely affect the tunneling current since it has a strong exponential dependence with the air gap.

Finally, a STM usually consists of a feedback controls circuit and a data acquisition system. The purpose of the feedback controls circuit is to convert the tunneling current into a voltage signal, which is then used to control the vertical actuators by means of controls logic. The voltage signal used to control the actuators is also sent to a data acquisition system where it is then interpreted by imaging software to produce an image of the surface.

While the basic concept behind a STM is simple, the actual design of each component is challenging. For example, eliminating unwanted mechanical vibrations to displacement levels below the nanometer scale is difficult. An individual walking past the microscope can produce mechanical vibrations on orders much greater than this tolerance. The feedback controls circuit also poses a challenge due to the need to detect extremely small tunneling currents. The piezoelectric actuators in the scanner also have inherent problems such as charge creep and hysteresis that must be considered when designing a controls system. The combination of these problems makes the design of a STM very difficult.

1.4) Review of the Relevant Literature

Several concepts and designs for STMs have been published in the archival literature. Binnig and Rohrer described the basic technique of STM in their Nobel Prize acceptance lecture entitled “Scanning Tunneling Microscopy- from Birth to Adolescence” [5]. Since their seminal work, scanning tunneling microscopy has matured to the point where the instrument has been commercialized. Güntherodt and Wiesendanger have published a series of books describing the theory, general principles, and basic designs governing STMs [6, 7]. Their two volume series discusses general techniques and approaches for preparing and imaging the surfaces of various samples. While their work and those of others provide guidelines for the design and operation of STMs, they lack the detail necessary to implement such designs into an actual functioning instrument.

An innate challenge in developing a STM is the integration of numerous components into a functioning system. In addition, individual components can be expensive so that the overall cost of the instrument can be prohibitive and limit its availability as a general purpose laboratory instrument. Several attempts have been undertaken to design and construct inexpensive STMs[8-12]. They vary in their goals, approaches, and cost. These works are reviewed briefly next, in order to place the present work in an appropriate context.

One of the earliest works in the field of designing STMs was that of Park et. al.[8]. While their design is not inexpensive, it is certainly thorough and serves as an excellent resource when it comes to circuit design. Following Park’s work, S. Kleindiek et al. developed a miniature scanner which demonstrated the ability to reduce the size of typical STMs[9]. Their design focused primarily on the scanner and could easily be combined with concepts from other STM designs. Kleindiek’s work was popularized by the idea of table top devices but their design is not inexpensive. Jayadevaiah et al. report development of a very compact STM with atomic resolution, which also falls into the category of a table top device[10]. This design is well outlined and utilizes common circuit components. The coarse adjustment utilizes the concept of an inertia slider as described by Pohl[13]. While Jayadevaiah’s design reduces the fabrication cost and improves the stability of the device (namely that associated with the coarse adjustment), the complexity of the overall device inhibits its use as a quotidian STM.

The work of Alexander focused on designing a STM for under \$100, excluding the cost of an oscilloscope, computer, and data acquisition systems[11]. Alexander's STM features common electronic components and a novel scanner design which mirrors a concept originally proposed by Koops[14]. Piezoelectric elements cannibalized from low-cost and readily available speakers are divided into quadrants and used to induce a rocking-type motion of a metal tip mounted on the piezoelectric elements. A close examination of this scanner design shows that it is difficult to reliably reproduce but is extremely inexpensive. Moreover, the piezoelectric components cannibalized from these low-cost speakers are of varying characteristics and response so that the resulting characteristics of the STMs also vary in an unpredictable manner. The control strategy for maintaining constant tunneling current, however, is quite useful and Alexander's control circuit design is adopted in this work.

Müller's STM project is an excellent resource for those interested in designing their own STMs[12]. Extensive resources are provided to aid in the design of homemade STMs. The running cost for this design, however, makes acquisition of a low-end commercial STM more desirable, especially when the effort in terms of number of hours devoted to the construction of the device is factored into the cost. Müller's design has several features that parallel the commercial easyScan STM developed by Nanosurf available for about \$13,000 (not including the cost of a computer).

In addition to the aforementioned works on the overall design of STMs, design of individual components used in a STM, such as the scanner, probe tip, control strategy, and piezoelectric actuators, are also discussed in the literature.. Some of these merit discussion. The works of Rogers et al.[15] and Gupta et al.[16] have both influenced the design of STMs. Rogers developed an inexpensive method for manufacturing STM probe tips. His method uses commercially available Pt-Ir wires cut and chemically etched to produce very inexpensive and durable probe tips. Since the cost of commercially available tungsten STM probe tips is relatively low (on the order of \$25), this latter option is used in the present work. Gupta, like Pohl, focuses on methods for coarse approach of the probe tip. It is necessary that the coarse and fine approach regimes have sufficient overlap. Gupta accomplished this task by using a piezoelectric walking device inside a tube, whereas Pohl relies on inertia sliders also inside a tube.

Control of the tunneling current or tip-to-sample distance and actuation of the scanning process are important to the design of a STM. References[17-20] discuss these aspects of STM design. Kuk et al.[17] generate an outline for the operation of STMs and include a discussion of physical and electronic designs associated with STM instrumentation. Maps[18] focuses on developing a raster generator which can be used in conjunction with piezoelectric actuators in order to trace a scanning area. Strom et al.[19] focus on designing inexpensive, high-voltage, low-current amplifiers for driving piezoelectric actuators. Lastly, Chen[20] focuses on selection of preamplifiers for piezoelectric actuators. These designs are simple and have been adapted by others in their attempts to reduce the cost associated with STMs.

The design described in the present work incorporates concepts from several of the aforementioned ideas described in the literature. Selection of the various subcomponents in the design of the STM is governed by the overarching requirements of lowering cost, using off-the-shelf components, and enhancing versatility. The design described here is unique because of its focus on the use of equipment commonly found in a laboratory such as a computer, oscilloscope, and multimeter. While the production of high resolution images is not strictly a goal of this work, every effort is made to attain as high a resolution as possible without sacrificing low cost and low complexity. The present design also differs from other existing work because it is more complete. Everything from the vibration isolator and controls circuit to the data acquisition system and graphic user interface have been developed for ease of use as well to allow the STM to be integrated with other experiments. The focus of this research is (1) to develop an inexpensive instrument from components readily available in a university research laboratory, (2) to make it as inexpensive as possible, and (3) to make it versatile enough so that the instrument can be used in conjunction with or in support of other nanotechnology experiments. The contribution of this work therefore lies in the integration of all the components into a well functioning STM.

Chapter 2

Motivation and Objectives

2.1) Motivation

STMs are commercially available instruments. Several companies specialize in building STMs and the associated accessories. This technology has been available for a few decades and the concept is rather simple while its promise is great. STMs and in general, scanning microscopy, are very useful in investigating micro and nanoscale phenomena. Even though these microscopes are commercially available, there are some drawbacks.

The first major consideration is the cost. While this type of microscopy has a limited and targeted market, namely research institutions, the cost of these microscopes prohibits their widespread use. A STM with near atomic resolution can cost around \$100,000, and more compact instruments with less resolution cost about \$13,000 (not including a computer). While the latter price is not unreasonable, it is still outside the range of affordability of many university research groups. Moreover, commercially available units are by their very nature, inflexible in terms of being used in-situ and in conjunction with other experiments. Home-made STMs allow the user this flexibility of potentially integrating the microscope with other experiments or processes involving nanomaterials and nanoscale processes.

Another issue with commercial STMs deals with the portability of such apparatus. Commercially available STMs are usually difficult to integrate with other laboratory apparatus that are part of other experiments. Therefore, STMs are usually used as stand-alone instruments to which samples must be brought. In some situations, it is difficult to prepare a sample that can be transported to the STM. For these applications, it would be convenient to bring the microscope to the sample rather than the sample to the microscope. This requires a STM that is versatile and easy to use.

Finally, many samples are not electrically conducting or cannot withstand local electric fields and therefore cannot be imaged by a STM. Other forms of scanning probe microscopy, however, can be used to accomplish this task. Since the sample to be imaged must be electrically conducting and durable, the market and therefore the applications for STM are inherently limited.

The promise of this technology, however, still makes STMs very attractive. With an increased interest in nanotechnology and manipulating structures on the nanoscale, STMs provide a unique solution. Early work at IBM has demonstrated that STMs can indeed be used to manipulate atomic structures. As shown in Fig. 11, the IBM logo was created out of neon atoms imprinted on a nickel surface. Not only did a STM place these neon atoms in the locations shown, but it also imaged the surface afterward.

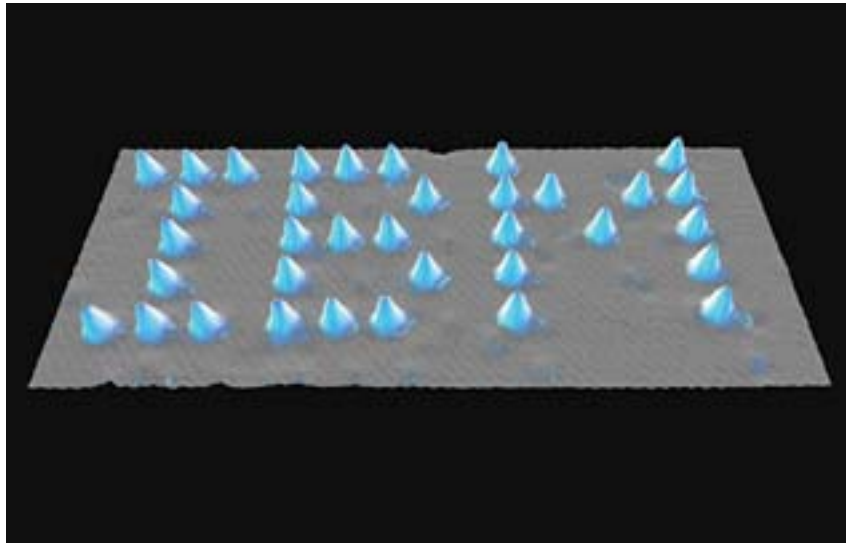


Figure 11. IBM logo created from neon atoms imprinted on a nickel surface using a STM

In this manner STMs can not only be used for atomic assembly, but also for their verification. As nanotechnology research becomes increasingly popular in research institutions, there is a growing need to image and manipulate nanostructures. Instruments such as STMs therefore need to be as commonplace as other laboratory tools such as oscilloscopes and multimeters. The focus of this thesis is on making this a reality for the STM.

2.2) Objectives

The goal of this research is to design a STM that can be used as a general purpose, quotidian laboratory instrument. The primary goal of this work is the design of an inexpensive and versatile STM, capable of integration with other experiments and apparatus. While the term inexpensive is relative, the focus here is to design a prototype for under \$500 (not including a computer) that has near atomic resolution. The microscope is targeted towards research institutions such as university laboratories.

A secondary goal of this work is to design the STM for portability. The majority of commercially available STMs are stand-alone instruments to which a sample must be brought. In contrast, an objective of this research is to develop a prototype STM that can be used parting conjunction with other experimental apparatus. This may require the STM to operate open to atmospheric air. The option of operating the STM in ambient air or under vacuum would make the instrument even more versatile. In addition to being inexpensive and portable, the STM must produce repeatable results under different levels of resolution. Ideally, the STM should have near atomic resolution; however, it should also be capable of imaging larger features, on the order of tens to hundreds of nanometers.

In addition to designing a functional microscope, imaging software must also be developed in order to make data manipulation user-friendly and to produce several easily interpreted images for the user. Specifically, post-processing and filtering need to be performed on the data. In addition, the software must also be capable of displaying a variety of images, ranging from 3D representations of a surface to 2D representations and contour plots.

The theory behind the STM is well understood and near atomic resolution has been attained with more expensive microscopes. In order to accomplish these objectives several individual component goals are met in this work. First, a versatile vibration isolator is designed. Second, a tunneling current is obtained while the microscope operates open to atmospheric air. Third, a control circuit capable of measuring and manipulating small currents is designed. Lastly, a scanner capable of actuating the probe tip to sub-nanometer tolerances is constructed. These objectives culminate in a working instrument.

Chapter 3

Design of the Microscope

3.1) Overview of the Design

The overall design of the microscope can be divided into categories involving three components: the vibration isolators, the scanner, and the control circuit. These components work together to collect data, which is then recorded by a data acquisition (DAQ) board and interpreted by imaging software. The purpose of the vibration isolator is to provide a stable base on which the scanner and sample are mounted. The scanner draws a tunneling current and sweeps across the surface. The circuit is used to control the scanner using feedback signals. These signals are sent to the DAQ board, which records and interprets the data. The simple block diagram shown in Fig. 12, illustrates this concept. The design of these individual components is described in the following sections.

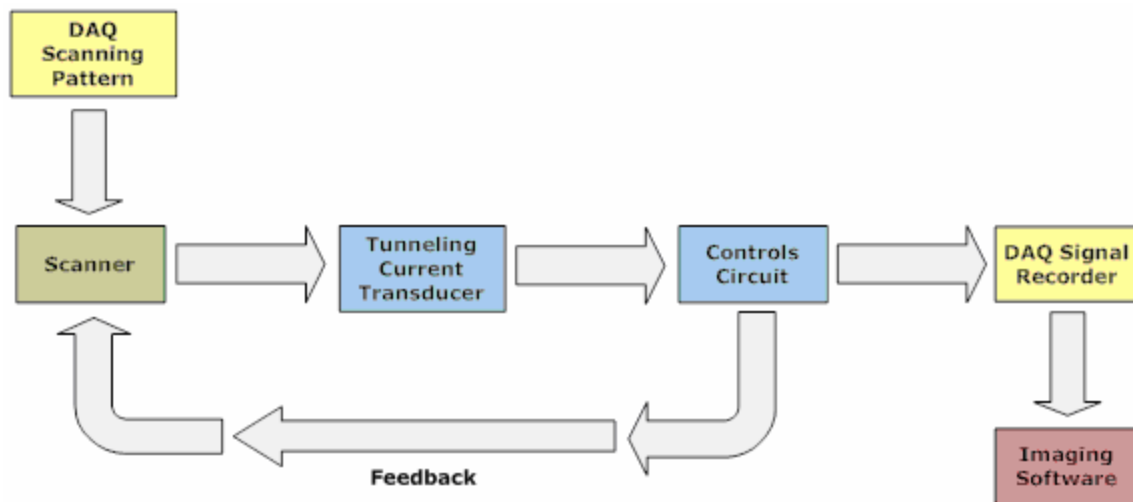


Figure 12. Block diagram

3.2) *Vibration Isolator*

The purpose of the vibration isolator is to eliminate mechanical vibrations that may adversely impact the microscope. The vibration isolator must be capable of attenuating both low and high frequency vibrations to displacement amplitudes less than one nanometer. Typically STMs are supported on pneumatic or hydraulic legs, similar to an air table. Air tables are so expensive that an inexpensive alternative is sought in this work. In addition, air tables tend to be very large and would limit portability of the microscope.

A strategy for the tip to approach the sample surface, without impacting it, is critical to successful operation of the STM. This approach consists of a coarse adjustment and fine adjustment. Coarse adjustment is necessary before tip-to-sample distances on the order of 1 nm can be achieved. The coarse adjustment system allows the sample and tip, to be roughly positioned near to one another such that the fine adjustment control can take over. In order to accomplish this task, two motor control stages (Velmex 6012K1) already available in the laboratory, are used. The K1 distinction in the model number of these stages describes the pitch of the screw used and corresponds to 10 revolutions per centimeter. These two motor stages are used to control the horizontal and vertical position of the STM tip relative to the sample. The motor stages are mounted on separate vibration isolated platforms and configured as shown schematically in Fig. 13.

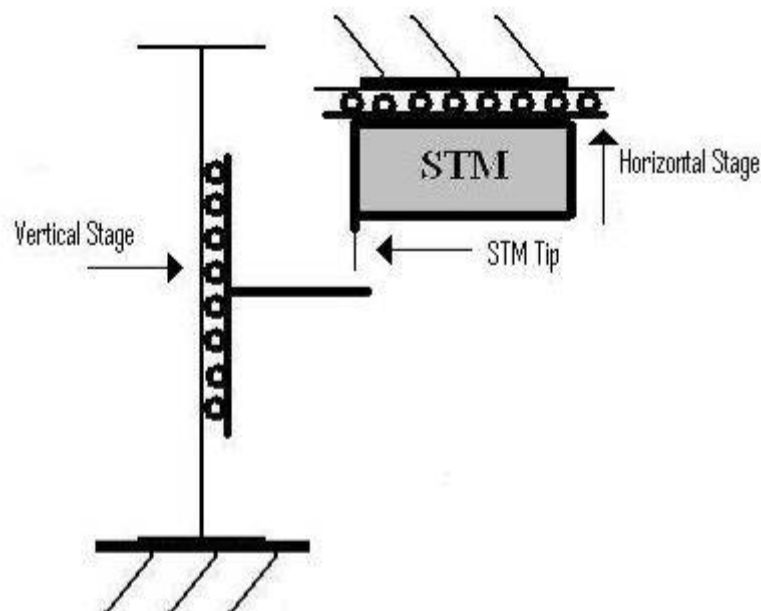


Figure 13. Configuration of the coarse adjustment motorized translation stages.

The accompanying motor controller for the Velmex stages has increments of 400 steps per revolution. This corresponds to 4000 steps per centimeter or $2.5 \mu\text{m}$ per step. This distance of $2.5 \mu\text{m}$ is too large of a gap between tip and sample to detect a tunneling current. Depending on the voltage bias, ambient pressure, geometry of the tip, and gap distance, breakdown of the air gap is possible as will be discussed later. This breakdown across the gap can be used to distinguish between currents due to arcing and tunneling. The motor controlled stages produce displacements that are much larger than what is optimum; nevertheless, they are used since they are readily available. Figure 14 shows a photograph of the motorized translation stages.



Figure 14. Photograph of the coarse adjustment motorized translation stages.

Due to the size of the stages, a vibration isolation platform larger than desired or necessary, was designed. It must be pointed out that this is unnecessarily large in dimension since much smaller stages can be used to accomplish the task at hand. As mentioned earlier, these stages were readily available and were therefore incorporated into the design of this prototype. The vibration isolation mount consists of a frame supported on foam blocks. The motor controlled translation stages are suspended by bungee cords (purchased from a local hardware store) from the Unistrut frame as shown in Fig. 15. Bungee cords are used because their elastic nature is very effective at reducing the amplitude of high frequency vibrations. Adjustable pneumatic air cylinders could also be used as dashpots in order to increase damping if necessary. These dashpots are very effective in reducing the amplitude of low frequency vibrations. However, it was ultimately determined that these dampers are unnecessary since low frequency vibrations were not an issue.

The vibration isolation platform simply consists of the motor controlled translation stages suspended by a number of bungee cords in parallel. The bungee cords are attached to the Unistrut frame by adjustable hooks (also available at a local hardware store) so that the stages can be leveled by adjusting the hooks. The frame itself is mounted on foam blocks. These foam blocks offer additional vibration isolation and prevent the frame from rocking. Figure 15 shows the vibration isolation platform used in the prototype STM.

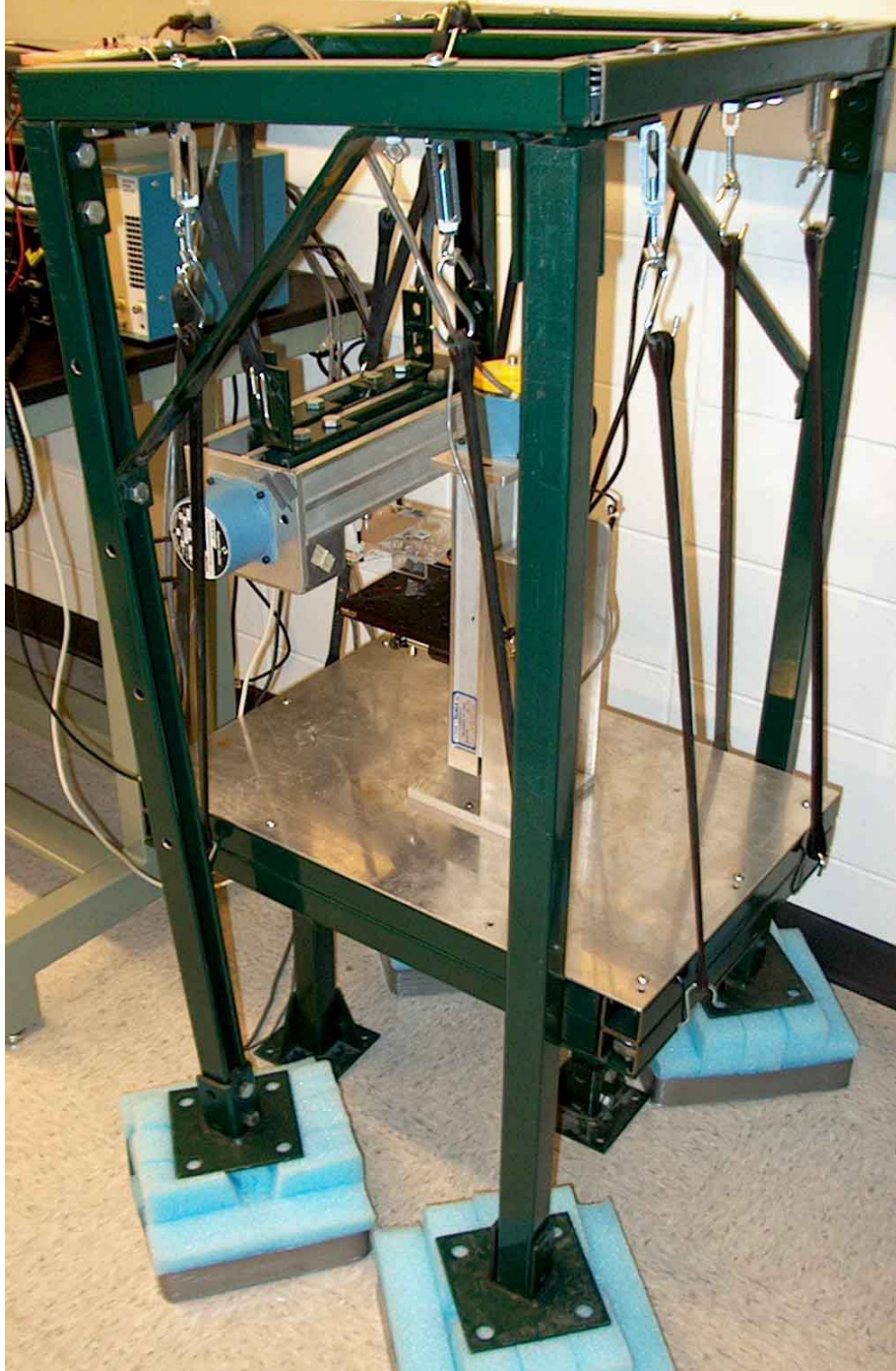


Figure 15. Vibration isolation platform used to mount the motor controlled translation stages.

While this vibration isolation platform is larger than desired, it can easily be scaled down by selecting smaller motorized stages. Smaller stages would permit a smaller size of the STM. This design has proven very effective at meeting the prescribed objectives.

3.3) Scanner

The scanner is mounted on the motor controlled translation stages, which in turn are mounted on the vibration isolation platform. The scanner is one of the primary features of the microscope. The function of the scanner is to laterally translate the STM probe tip through very small displacements. The scanner has a rather large range of motion, capable of accurate translation over length scales ranging from fractions of nanometers to microns. While attempting to draw a tunneling current, the vertical actuator must be able to displace over length scales comparable to the displacement corresponding to the coarse adjustment. During operation of the microscope and during data acquisition, the vertical actuator is capable of motion over length scales on the order of nanometers. In addition, the actuators can also independently move in three dimensions.

Actuation of the probe tip in three dimensions on a finer scale is accomplished by using piezoelectric elements (PhysikInstrumente, PICMA Chip Monolithic Multilayer Piezo Actuators, PL055). These actuators utilize single piezoelectric crystals. The crystals have a unique property. When a voltage is applied across them, stresses are developed which cause the crystal to deform. Similarly when a stress is induced on these crystals, an electric potential develops across them. AFM microscopes rely on measuring this stress that is developed in order to image surfaces. In the case of a STM, however, a voltage bias is applied to these crystals that cause them to deform resulting in the motion of their surfaces and whatever may be attached to their surfaces. Using these piezoelectric actuators, the probe tip is moved very accurately.

Piezoelectric actuators exhibit the behavior of first order systems with a transfer function modeled as follows [21]:

$$T(s) = \frac{x(s)}{V(s)} = \frac{K\tau s}{\tau s + 1} \quad (22)$$

where

K = static sensitivity, $\mu\text{m}/\text{V}$

τ = time constant, s

Figure 16 shows the amplitude of the displacement as a function of frequency. As can be seen,

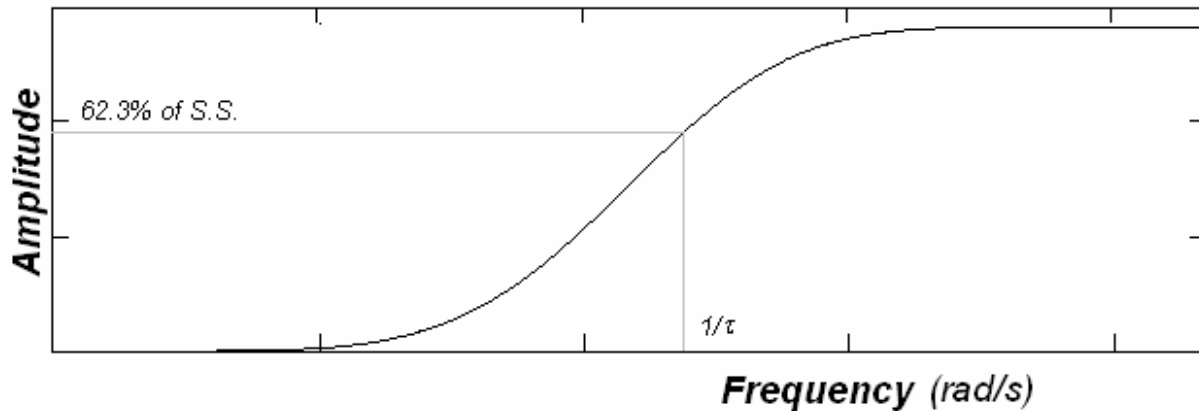


Figure 16. Typical first order frequency response of piezoelectric actuators

the response of these actuators is similar to that of a high pass filter. In other words, low frequency voltage signals do not cause actuation. The piezoelectric actuators are AC actuators and will not respond to DC signals but rather to the change in a DC signal. The equivalent electrical representation of a piezoelectric crystal is shown in Fig. 17.

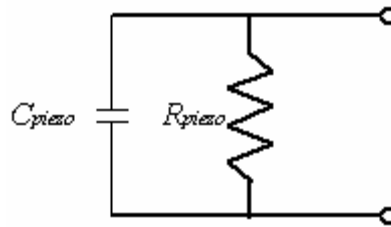


Figure 17. Equivalent electrical element representation of piezoelectric crystal

While a voltage is applied across the actuator the presence of piezoelectric resistance causes leakage. This leakage allows charge to propagate through the crystal causing electrical creep. This creep in turn disturbs the stresses in the crystal and causes spurious deflection. Over time, the actuators will exhibit creep as a constant voltage is applied across the crystal. This creep causes hysteresis in the actuator. The RC time constant influences the hysteresis. In other words, increasing the RC time constant causes the actuator to creep less thereby reducing the hysteresis. In addition, the RC time constant defines the cutoff frequency of the actuator itself. As long as the actuation frequencies are much larger than the cutoff frequency, then little attenuation of the actuation signal will occur. In this respect, increasing the time constant reduces the cutoff frequency for the high pass nature of the actuators making them more

susceptible to low frequency noise. While a larger RC time constant is good for reducing hysteresis, it permits low frequency signals corresponding to low frequency vibration noise to influence the actuator.

The static sensitivity of the piezoelectric actuators also depends on the RC time constant. The capacitance and the resistance of the piezoelectric actuators are difficult to measure and therefore one typically relies on the specifications supplied by the manufacturer. A static sensitivity of 2 microns at 100 volts is specified by the manufacturer of the piezoelectric actuators (PhysikInstrumente). Coincidentally, these are also the maximum recommended displacement and voltage of the actuators. The static sensitivity is typically defined as follows for piezoelectric actuators:

$$\frac{1}{K} = \frac{K_q}{C_{piezo}} = (20 \text{ nm/V})^{-1} \quad (23)$$

where

K_q = charge sensitivity of the crystal, coulombs/volt

C_{piezo} = piezoelectric crystal capacitance, F

From the system perspective, there are cables and instruments connected to the actuators. These cables and instruments add their own capacitance to the system. Therefore, the equivalent electrical representation is better depicted by the schematic shown in Fig.18.

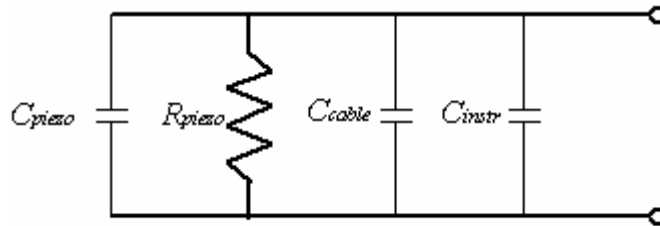


Figure 18. More realistic electrical representation of the piezoelectric actuators

Capacitances of the cable and instrument increase the overall capacitance of the system. This results in an increase in the sensitivity of the actuator, an increase in the time constant, a decrease in the hysteresis of the system, and a decrease in the cut off frequency. All the aforementioned effects are desirable except for the decrease in the cut off frequency. This allows

more low frequency vibrations from noise to pass through and influence the actuator. The realistic static sensitivity is better defined for using the overall capacitance of the system as [21]:

$$\frac{1}{K} = \frac{K_q}{C_{piezo} + C_{cable} + C_{instr}} \quad (24)$$

where

K_q = charge sensitivity of the crystal, coulombs/volt

C_{piezo} = piezoelectric crystal capacitance, F

C_{cable} = cable capacitance, F

C_{instr} = instrument capacitance, F

With these aforementioned considerations, a final design was selected for the actuators. First, three separate piezoelectric actuators are mounted on a T-support made from ABS plastic. The T-support was printed using a rapid prototyping fused deposition modeling (FDM) machine due to its unique shape and nature. The T-support holds the tungsten STM probe tip, which is mounted with a brass fitting in order to enable electrical contact with the tungsten tip. The piezoelectric crystals are also mounted on steel disks. These disks are magnetic so that the entire scanner assembly can be held in place by ceramic disk magnets (available at a local hardware store). A thin layer of motor oil is applied between the steel disks and the magnets to prevent the slip-stick friction conditions of the contact between the magnet and the steel disk. Thus, the actuators are allowed to independently move and slide the scanner over the magnets that hold the scanner in place. A model of the scanner is shown in Fig. 19 and additional details are given in Appendix A1.

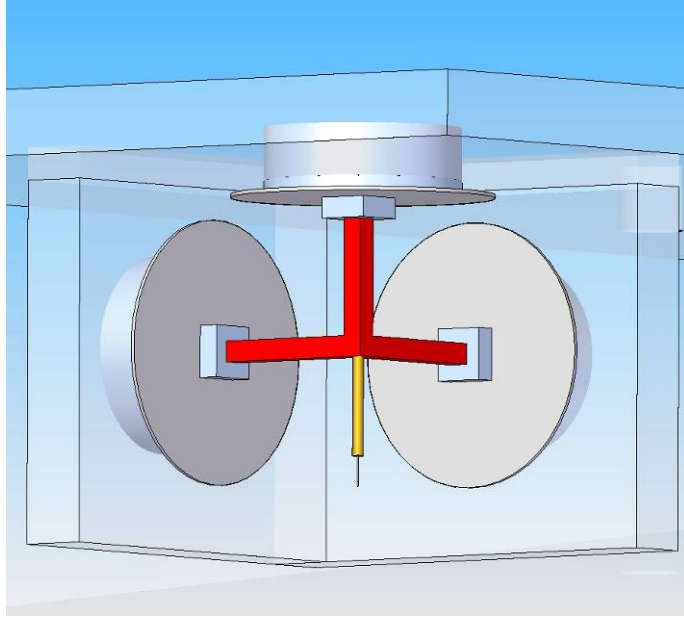


Figure 19. Schematic of the scanner assembly

3.4) Control Circuit

The primary purpose of the control circuit is to control the piezoelectric actuators. First, the circuit converts the tunneling current into a characteristic voltage signal. Next, the controller compares the voltage signal to a preset setpoint and determines the appropriate control signal. An integrator integrates that signal before sending it to the actuator. Since the actuator responds to changes in voltage, this integrator is necessary. Simultaneously, a signal from the DAQ system is sent to the control circuit in order to cause the scanner to sweep. The control circuit once again integrates this signal before sending it to the horizontal actuators. This is the basic concept behind the control circuit, and circuit diagrams are given in the Appendix A2.

A few remarks regarding operation of the STM must be made. First, a voltage bias must be induced between the sample and the probe tip. In order to accomplish this, a potentiometer and a voltage follower are used to apply a potential difference between the tip and sample. This potential difference is necessary in order to draw a tunneling current. It is difficult, however, to distinguish a tunneling current from currents produced by means other than tunneling currents. The voltage follower inhibits other currents that may be attributable to eddy currents, capacitance effects between the tip and sample, or other electromagnetic noise.

The integrator is essential. Not only does it add integral control aspects to the circuit but it also permits the actuators to operate correctly. The actuators respond to a change in voltage or in other words, the derivative of a voltage signal. So in order for the actuators to respond to a given voltage signal, that signal is first integrated and then the actuators respond to the derivative of the integrated signal which is then the original signal. See Fig. 20 for further explanation.

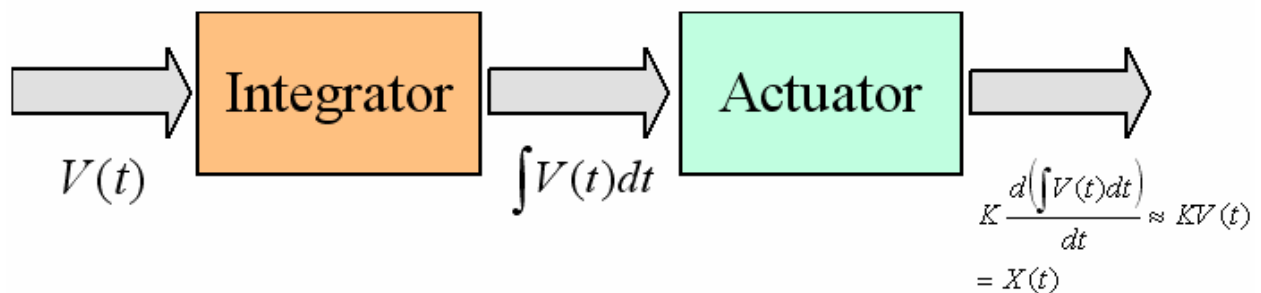


Figure 20. Integral-derivative control scheme used in the prototype STM

In addition to the differential nature of the actors, there is a gain associated with the actuating circuits. A 4x gain is associated with the horizontal actuators and a 2x gain is associated with the

vertical actuators, which is taken into consideration during scanning. These gains are easily incorporated into the desired scanning pattern and into the imaging software. For example, if the static sensitivity of the actuators is 37.5 nm/V, then with a 4x gain, the sensitivity of the horizontal actuators is 150 nm/V from the input signal.

Power for these actuators and the control circuit is provided by two 9V batteries. Batteries are used to eliminate noise. The noise present in the standard wall outlet at 110V can cause problems with the actuators such as false signals, if the frequency of electrical noise is greater than the cutoff frequency of the actuators. Therefore, a floating ground internal power source is selected. In addition, several capacitors are placed across the power supply in order to eliminate possible 60 Hz noise.

The control circuit is rather simple and utilizes three integrated chips (purchased from Digi-Key). The first chip is used in the tunneling current transducer. This chip is a LF411 low offset, low drift, junction field-effect transistor (JFET) input operational amplifier. This op-amp is inexpensive (see Table I) and has a fast response time in comparison to standard low-end op-amps. For scanning purposes, it is necessary that the op-amp be capable of operating quickly (with response frequencies on the order of kilohertz or millisecond response time). The other two chips are TL074 each of which actually has four integrated op-amps. These chips are designed to be low noise, JFET input operational amplifiers. One is used for the controller, vertical actuator, and sample bias. The other chip is used for the horizontal actuators.

The control circuit truly is the brains behind the microscope. In addition to the electronic circuit, the characteristics of the potentiometers and connecting wires must also be taken into consideration. The potentiometers are variable resistances used to tune and adjust the microscope. The wire connectors are used to send signals to the actuators and to the DAQ system. These interfaces consist of BNC connectors and a 15 pin D-sub connector. The 15 pin D-sub connector is used to carry the appropriate signals to and from the scanner and the BNC connectors are used to carry signals to the oscilloscope and DAQ system.

3.5) DAQ and Imaging Software

The last of the significant components are the DAQ system and the imaging software. These components record data and produce images that can be easily interpreted. The DAQ board is a National Instruments NI-USB 6211 card. This DAQ system is compatible with LabVIEW. A LabVIEW virtual instrument (VI) file is created in order to acquire and save data on a computer. This VI file is given in Appendix A3.1. The data is then visualized and interpreted using MATLAB. Within the MATLAB environment, a user-friendly graphic user interface (GUI) is developed in order to manipulate and interpret the images. The script and the explanation behind using this software are also given in Appendix A4

The data recorded by the DAQ system consists of voltage signals sent to the actuators. These voltages correspond to a specific position in space. In other words, there is a voltage signal that corresponds to a given position on the X axis, another voltage signal that corresponds to a position on the Y axis and yet another voltage signal that corresponds to a position on the Z axis. The three voltages can be thought of as representing the three Cartesian coordinates, which describe the tip's location. The imaging software simply takes these voltage traces and produces an image from them using the known static sensitivity of the actuators. This sensitivity can be taken from the manufacturer supplied data, but should be adjusted by the user upon calibration.

The imaging software is designed to produce three images and permit digital filtering. The software is linked to MATLAB's digital signal processing toolbox. In this environment the data can be filtered in order to potentially refine the images. The first plot produced by the program is a three dimensional representation of the data that can be rotated and interrogated further. The second plot is a contour plot that can be used to view surface characteristics. The final plot is a black and white 2D representation. This last image is typical of what is expected from a STM. In this image, high surface features, such as peaks, appear in white and low surface features, such as troughs, appear in black. In addition, quantitative information regarding the voltages, and hence coordinates (x,y,z) of various features on a surface can be stored in a data file for further use.

3.6) Cost

A major goal of this work is to design an inexpensive microscope, one that could potentially be used as a common laboratory instrument. Consequently, it is assumed that certain other laboratory apparatus such as a computer, oscilloscope, or data acquisition board are readily available and therefore not included in the cost. With these considerations, the various component costs are listed in Table I. As can be seen, the total cost for the various components is on the order of \$300.

Table I. Cost Estimate for the STM components¹

Part	Quantity	Price/Part	Price	Supplier	
Vibration Isolator					
Unistrut Frame	1	N/A	\$0.00	(Spare Parts)	
Bungee	12	\$1.24	\$14.88	Hardware Store	
Adjustable Hooks	8	\$2.70	\$21.60	Hardware Store	
Dashpot ²	1	\$67.94	\$67.94	McMaster-Carr	
Motor Controlled Stages	2	N/A	\$0.00	Velmex	
Motor Controller	1	N/A	\$0.00	Velmex	
Foam Block	4	N/A	\$0.00	(Spare Parts)	
Scanner					
Piezoelctric Actuators	3	\$50.00	\$150.00	Physik Instrumente	
Steel Disks	3	N/A	\$0.00	(Spare Parts)	
Ceramic Disk Magnets	3	\$0.25	\$0.75	Hardware Store	
T-Support	1	\$0.06	\$0.06	(Rapid Prototyping Machine)	
STM Tip	1	N/A	\$0.00	Veeco	
Brass Fitting	1	N/A	\$0.00	(Spare Parts)	
Acrylic Plastic	1	N/A	\$0.00	(Spare Parts)	
Circuit					
100 pF Capacitor	6	\$0.14	\$0.84	Digi-key	P4925-ND
0.1 μF Capacitor	4	\$0.15	\$0.60	Digi-key	P4924-ND
2.2 pF Capacitor	1	\$0.10	\$0.10	Digi-key	311-1146-6-ND
15 pin D-sub Male	1	N/A	\$0.00	Digi-key	T815M-ND
15 pin D-sub Female	1	N/A	\$0.00	Digi-key	T815F-ND
15 pin D-sub Cable	1	N/A	\$0.00	(Spare Parts)	
BNC	4	\$3.94	\$15.76	Digi-key	ARFX1064-ND
Battery Connector	2	\$0.99	\$1.98	Radio Shack	
100 K Resistor	6	\$0.33	\$1.99	Radio Shack	
10 M Resistor	1	\$0.33	\$0.33	Digi-key	10.0KXTR-ND
20 K Resistor (two 10K)	1	\$0.67	\$0.67	Radio Shack	
2.2 K Resistor	1	\$0.33	\$0.33	Radio Shack	
220 Ω Resistor	7	\$0.33	\$2.31	Radio Shack	
10 K Resistor	10	\$0.33	\$3.30	Radio Shack	
4.99 K Resistor	1	\$0.09	\$0.09	Digi-key	4.99KXTR-ND
LF411 Chip	1	\$1.63	\$1.63	Digi-key	LF411CN-ND
TL074 Chip	2	\$0.76	\$1.52	Digi-key	TL074CN
10 K Potentiometer	3	\$2.71	\$8.13	Digi-key	CT2205-ND
100 K Potentiometer	2	\$2.71	\$5.42	Digi-key	CT2208-ND
Prototyping Board	2	N/A	\$0.00	(Spare Parts)	
Wires	N/A	N/A	\$0.00	(Spare Parts)	
Solder	N/A	N/A	\$0.00	(Spare Parts)	
			TOTAL	\$300.23	

¹Computer, DAQ, and oscilloscope not included

²Optional dashpots

Chapter 4

Procedure for Imaging

4.1) Procedure for Coarse Adjustment

The procedures for operating the STM are rather simple but do require some attention to detail. Tunneling currents are small (on the order of a few nA to ten nA) so it is essential that the impedance of the measuring instruments be sufficiently large. The basic procedure involves bringing the STM tip close to the sample without establishing contact. When a tunneling current is drawn, the DAQ system begins to scan and acquire data. After the data is acquired it is processed using the imaging software. The details behind this procedure are, however, slightly more involved and are described in detail next.

The first step in imaging a surface is preparing the sample. The sample must be electrically conducting in order to conduct a tunneling current. A voltage bias must be applied between the sample and the STM tip. In order to accomplish this, the sample must first be electrically connected to the STM. A wire lead can easily be attached to the sample using conductive glue or a conductive pen such as those produced by Chemtronics (CW2200MTP). This specific wire lead can be seen on the electrical circuit shown in Fig. 59 of Appendix A2. A good electrical connection is essential and a resistance of less than 2Ω is necessary at this connection.

After the sample is prepared, coarse adjustment of the microscope can be enacted to position the sample at the desired location beneath the STM tip. The horizontal coarse adjustment is simply used to position the sample in the desired location whereas the vertical coarse adjustment is used to approach the sample. The vertical coarse adjustment is adjusted in steps of $2.5 \mu\text{m}$, a limitation imposed by the motorized translation stages. Since this is much too coarse of a distance to detect a tunneling current, fine adjustment is necessary. Even though the $2.5 \mu\text{m}$ adjustment is much too large to detect a tunneling current, it is also much too small to be noticed with the naked eye. Therefore, a clever approach is necessary in order to know when the STM tip is within one stage step of the surface in order to avoid running into the surface.

One useful technique in determining this limit is to rely on arcing since the tip and sample are exposed to air. Electrical breakdown of air or arcing occurs when an electric field of order $3 \text{ V}/\mu\text{m}$ is imposed across the gap. This breakdown field is of course dependent on the

presence of other impurity species such as CO_2 , H_2O , etc., but the value of $3 \text{ V}/\mu\text{m}$ is a reasonably approximate rule-of-thumb. This value of the breakdown field can also vary with ambient pressure and humidity, presence of adsorbate molecules on the surface of the sample, and sample surface roughness. Specifically, the electrical breakdown of most gases is described by Paschen's limit[22], which infers a correlation between the product of the pressure and gap distance (Pd) and the breakdown voltage. If the applied tip-to-sample bias is greater than this breakdown voltage defined by the Paschen minimum, then the air ionizes and arcing is likely. Below this limit, however, electrical breakdown is unlikely because the mean free path of an electron is greater than the electrode separation. So any current detected is small and steady and likely a tunneling current. The general trend of this dependence of Pd on the breakdown voltage indicates that at large values of Pd , the breakdown voltage decreases as Pd decreases. There comes a point, however, known as the Paschen minimum, where as Pd decreases the breakdown voltage will increase exponentially. Below this minimum, arcing is unlikely for even large voltages. The Paschen's curve is shown in Fig. 21.

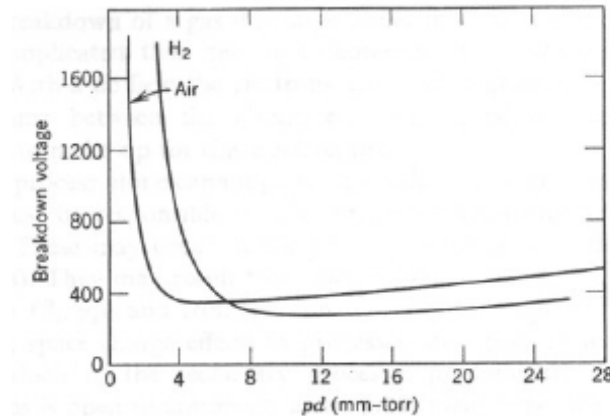


Figure 21. Paschen's limit curve

Using the rule-of-thumb regarding the electrical breakdown of air, at a sample bias 7.5 V the air is likely to break down when the STM tip and the sample are within 2.5 microns apart. This relationship is actually very useful in coarse positioning the STM tip. During the vertical coarse adjustment procedure, the sample bias is held at a constant 7 V relative to the tip as the STM tip approaches the sample using the vertical motor controlled stage. This is done until the first sign of arcing is detected. Arcing can be easily detected as the sample bias will fluctuate on orders greater than one hundred mV during arcing. In addition, the output of the microscope to

the DAQ and oscilloscope will indicate large spikes. The magnitude of these spikes depends on the gain of the microscope set by the user; however, they are sufficiently large that they can easily be distinguished. As soon as such arcing is detected, this is an indication that the gap distance between the tip and the sample is less than 2.5 microns. At this point, the microscope is shut off and the resistance between the gap and the tip is measured, typically yielding a large resistance, on the order of several $M\Omega$, since the tip and sample are not in contact. Being within 2.5 microns of the surface is the limit of the coarse adjustment, and the procedure shifts to one involving fine adjustment, which is discussed next.

4.2) Procedure for Fine Adjustment

After the coarse adjustment procedure described in Section 4.1 has positioned the STM probe tip at its limiting distance without contacting the sample, fine adjustment is enacted. The feedback control of the microscope actually performs the fine adjustment automatically. First, however, the setpoint must be established before imaging is initiated. The setpoint is a datum at which the magnitude of an anticipated value of the tunneling current is set. A simple circuit test was established in order to determine the initial setpoint. This test consisted of imposing a sinusoidal voltage with amplitude of 100mV and a frequency of 100Hz on a 10 M Ω resistor connected in series with the microscope. The voltage to resistance ratio yielded a sinusoidal current with amplitude of 10 nA. According to published measurements of the magnitude of tunneling currents, this is a typical value and can therefore be used to initialize the setpoint. The configuration and results of this test are shown in Fig. 22.

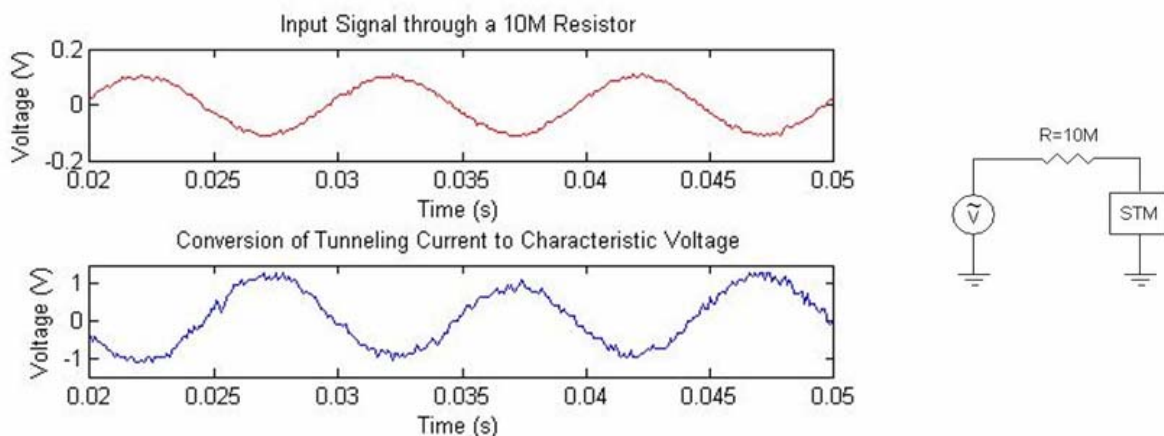


Figure 22. Establishing the setpoint

It can be seen from Fig. 22 that the output from the control circuit is shifted 90° out of phase with respect to the sinusoidal input. This is easily understood from the fact that the control circuit actually integrates the input current to produce an output voltage. The integral of a sinusoidal input therefore results in a cosine function as output, and the cosine function is 90° out of phase with the sine function. The setpoint and appropriate amplifying gains (discussed in detail later) are adjusted until a strong sinusoidal output is displayed. If the microscope gains are set too high, clipping of the output signal is likely since the op-amps will be at saturation. A strong

sinusoidal output is one where clipping is not present. This procedure is used to establish the setpoint, which is more finely adjusted if necessary, during operation of the microscope.

During the coarse adjustment, the tip is fully extended by the fine adjustment to its maximum position towards the sample because no current is detected and thus the current is below the setpoint. Once arcing is detected, however, the tip retracts by the fine adjustment to its minimum position furthest away from the sample because the arcing current is larger than the setpoint. Next, the sample bias is reduced to eliminate the arcing. Eventually the sample bias falls below the Paschen limit and breakdown stops. In this operating region, there is a reasonable certainty that any detected current is actually a tunneling current. Since tunneling currents are smaller in magnitude and more steady compared to currents detected during arcing, this serves to distinguish between the two.

During operation, the sample bias is reduced in order to eliminate arcing. While the sample bias is reduced, the control circuit actuates the piezoelectric elements responsible for vertical motion in order to meet the criterion dictated by the setpoint. This causes the actuator to extend as the arcing current is reduced and eventually eliminated. When the arcing stops, the actuators react to the tunneling current alone. Typical values for the sample bias range between 3 mV and 60 mV when a tunneling current is detected. Typical tunneling currents tend to be in the range of 0.2 nA and 10 nA for this range of voltages. These tunneling currents correspond to gap distances around 1 nm. The control circuit is then capable of maintaining the tunneling current and hence the tip-to-sample distance very accurately so that the tip can be rastered over the surface of the sample for imaging purposes.

In some instances, additional adjustments need to be made before scanning. Two gains and a voltage offset (refer to Fig. 59 in Appendix A2) may need to be adjusted in particular before the sample can be imaged. The two gains, referred to here as *integral gain* and simply *gain*, correspond to the amplifying gain of the integrator for the vertical actuator and the amplifying gain associated with the imaging signal sent to the DAQ board, respectively. The *integral gain* is used to allow greater displacement for smaller changes in the tunneling current. The *gain*, however, simply amplifies the output signal of the microscope sent to the DAQ so that it is within an acceptable voltage range for the DAQ board. Since the actuators respond to AC signals and not DC signals, the addition of a DC offset has no effect on the operation. However, this DC offset can be used to offset the signal sent to the DAQ so that it is within an acceptable

voltage range for the DAQ board. The range of the DAQ should be small such that the resolution of the 16 bit system can detect the small changes in the vertical actuator voltage signal.

Once a tunneling current is detected, the sample is imaged. Scanning the surface of the sample is rather simple and only requires the user to run the DAQ system via the computer. The controls circuit and the scanner make obtaining images effortless by the user. The actuators respond in such a manner that scans can be taken quickly and repeatably. A description on how to use the DAQ interface is given in Appendix A3. After the data is acquired by the DAQ, it is interpreted by the imaging software in the MATLAB environment. A description of the software as well as the MATLAB script is also given in Appendix A4. Using the MATLAB script, 2D, 3D, and black and white renderings of the surface can be displayed on a computer monitor. The procedures outlined in this section are summarized in the following section in order to provide a concise description of the operation of the microscope.

4.3) Summary of Imaging Procedures

The procedures discussed in this chapter are summarized below, for easy reference. In addition, Fig. 23 illustrates what occurs during the imaging procedures regarding the tip and sample separation, the sample bias, and the current.

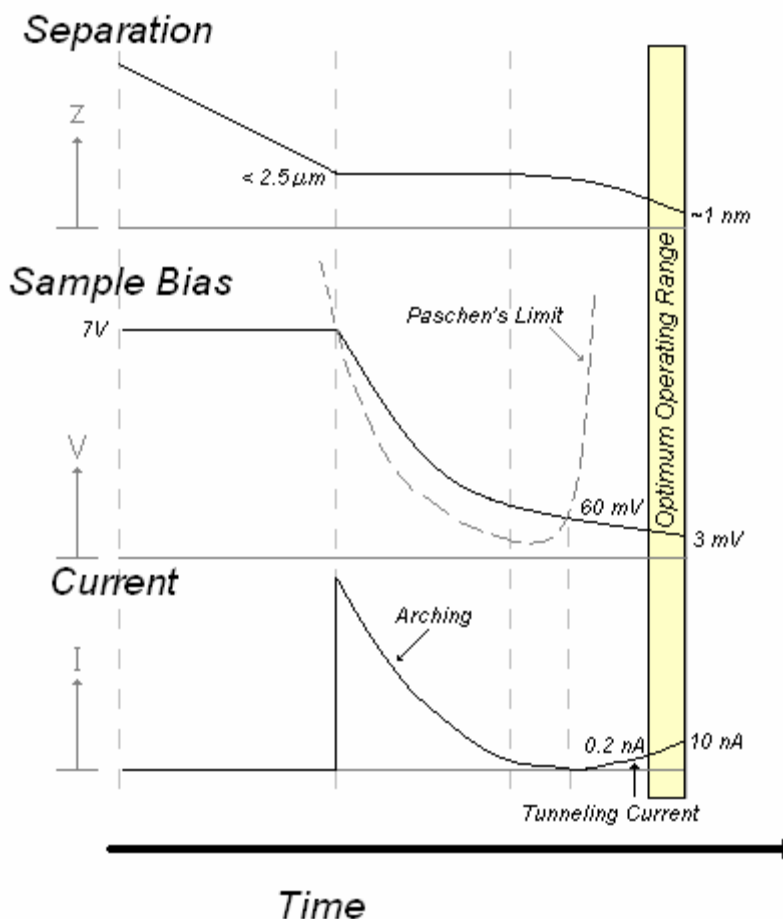


Figure 23. Separation, sample bias, and current depiction during imaging

1. Adjust the sample bias to 7 V by turning the potentiometer denoted as the sample bias found on the circuit diagram in Appendix A2.
2. Approach using coarse adjustment ($2.5 \mu\text{m}/\text{step}$).
3. When breakdown across the tip to sample gap is detected, the sample bias will fluctuate and current spikes will appear on the output of the microscope.
4. Turn off the microscope and verify that the resistance between sample and tip is on the order of $3 \text{ M}\Omega$ (i.e., that the tip is within $2.5 \mu\text{m}$ of the surface but not touching).

5. Turn on the microscope and reduce the sample bias until arcing stops. The offset may need to be adjusted so the output from the microscope is within the acceptable voltage range for the DAQ board.
6. The microscope control circuit will take over and attempt to acquire a tunneling current as the sample bias is reduced and arcing subsides.
7. If the tip is within 50 nm of the surface during the coarse adjustment, then the control circuit should get within Paschen's minimum and a larger voltage bias could be used. This will produce the strongest detectable tunneling current and potentially the best image. However, the microscope does not have to operate below Paschen's minimum rather it simply needs to operate below the Paschen curve.
8. Typical operating tunneling currents correspond to a sample bias between 3 mV and 60 mV.
9. Once these requirements are met, the DAQ system can be activated in order to scan and produce an image.

Chapter 5

Results

5.1) Overview

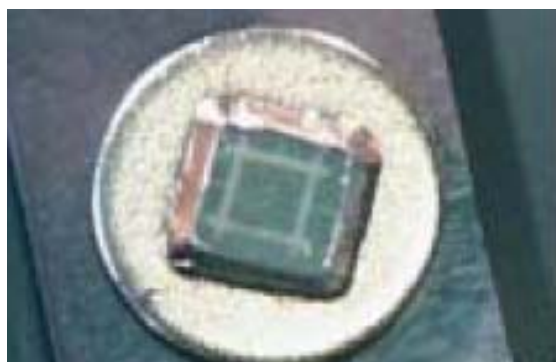
Images have been acquired from different samples in order to verify the operation of the prototype microscope. These samples include a gold STM calibration grid (Nanosurf, NanoGrid 160:T), a sputtered gold film of unknown thickness on an alumina substrate, another tungsten STM probe tip (Veeco Probes, Model TT), and a continuous fiber comprising bundles of single walled carbon nanotubes (SWCNT). Attempts at imaging these surfaces are described in this chapter.

Quantitative imaging of features observed on a sample's surface requires calibration of the tip-to-sample distance. A voltage signal represents the surface topology and a static sensitivity conversion factor relates the voltage to gap distance. Commercial STMs are calibrated using an optical deflection method[2]. Application of this method requires that the STM tip be suspended on a tiny cantilever beam. Deflection of the cantilever beam due to the voltage applied to the piezoelectric actuators is then inferred by monitoring the deflection of a laser beam that is reflected off the cantilever. In order to accomplish this measurement, the dimension of the cantilever must be known very accurately. This type of calibration could not be easily implemented in the prototype STM, at least while keeping the cost and system complexity down. Consequently, alternative means were sought for calibration of the prototype STM.

Calibration requires a sample with a known surface topology so that images acquired from the prototype microscope can be compared with known characteristics. A commercially available gold calibration grid is used for this purpose, and serves to relate the magnitude of the voltage recorded by the detection circuit to the scanner displacement. Once this information is obtained, voltages acquired from other samples can be used to infer the tip-to-sample distance, thereby yielding quantitative results for the surface topology of the sample.

5.2) Gold Calibration Grid

The prototype microscope is calibrated using a commercially available sputtered gold STM calibration grid (from Nanosurf). These grids are commonly used to calibrate commercial STMs. The grid consists of a plastic injection molded mount onto which a thin film of gold is sputtered. The sample is prepared in such a way that the surface topology is known over the 2 mm by 2 mm scanning area (See Figure 24). The grid has a pitch of 160 nm which is repeated over the entire scanning area. Along with the grid, Nanosurf provides an image of the surface taken with a commercial STM. This image is shown in Fig. 25.



Chip size: 5 x 5 mm²
Active area: 2 x 2 mm²
Pitch: 160 nm
Accuracy of pitch position: 5 nm
Accuracy of pitch (10 μm x 10 μm scan): ±1%

Figure 24. Photograph showing Nanosurf's sputtered gold grid used for calibration.

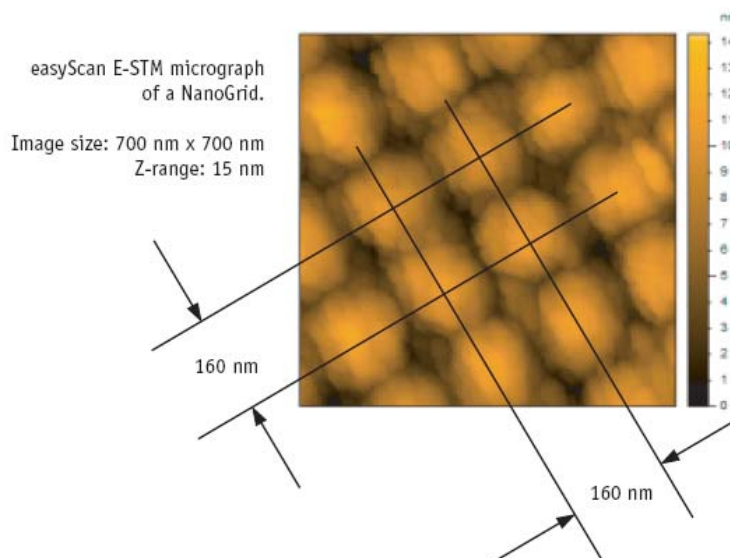


Figure 25. Image of Nanosurf's sputtered gold grid taken with a commercial STM.

Images of the sputtered gold grid obtained using the prototype microscope for comparison and calibration, are shown in Figs. 26-29. These images are used to calibrate both of the horizontal actuators. Visual alignment of repeated features on the grid is used to determine the length scale for the grid image obtained from the prototype microscope. The vertical actuator, however, cannot be calibrated with the same accuracy as the horizontal actuators since only a color map exists rather than a vertical grid or cross section. The vertical actuator is therefore assumed to have the same static sensitivity as the horizontal actuators.

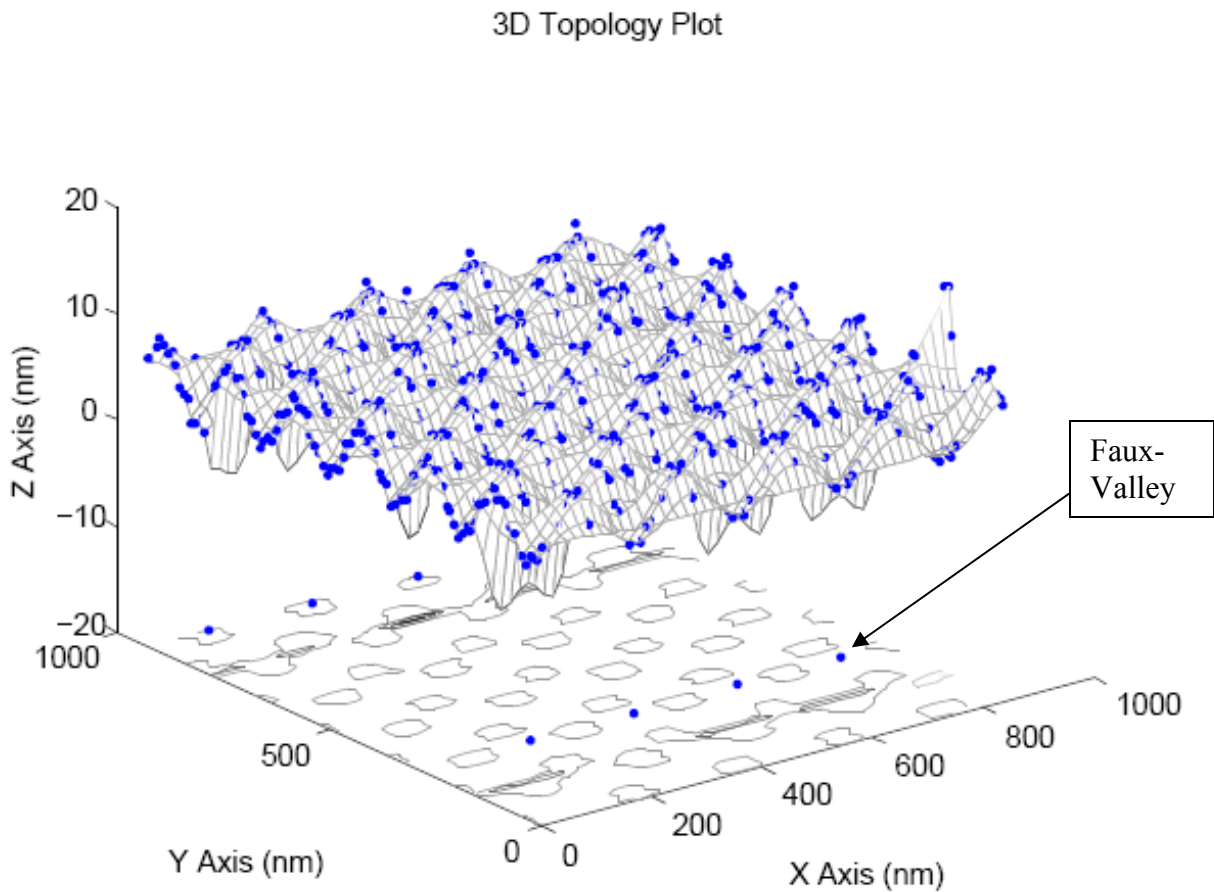


Figure 26. 3D gold sputtered calibration sample

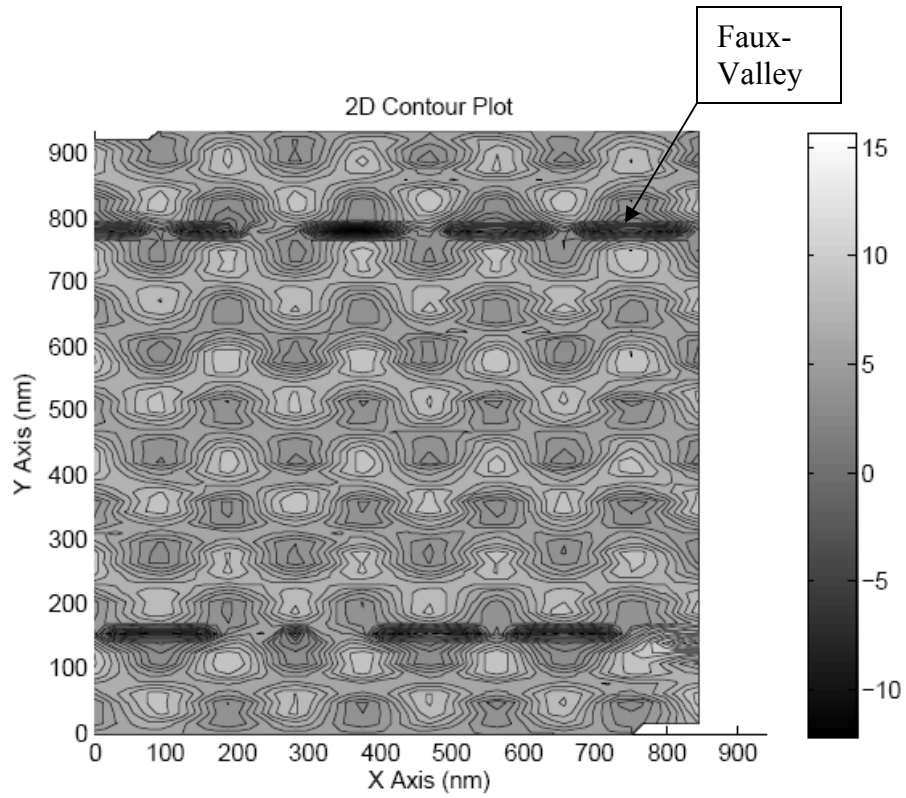


Figure 27. 2D gold sputtered calibration sample

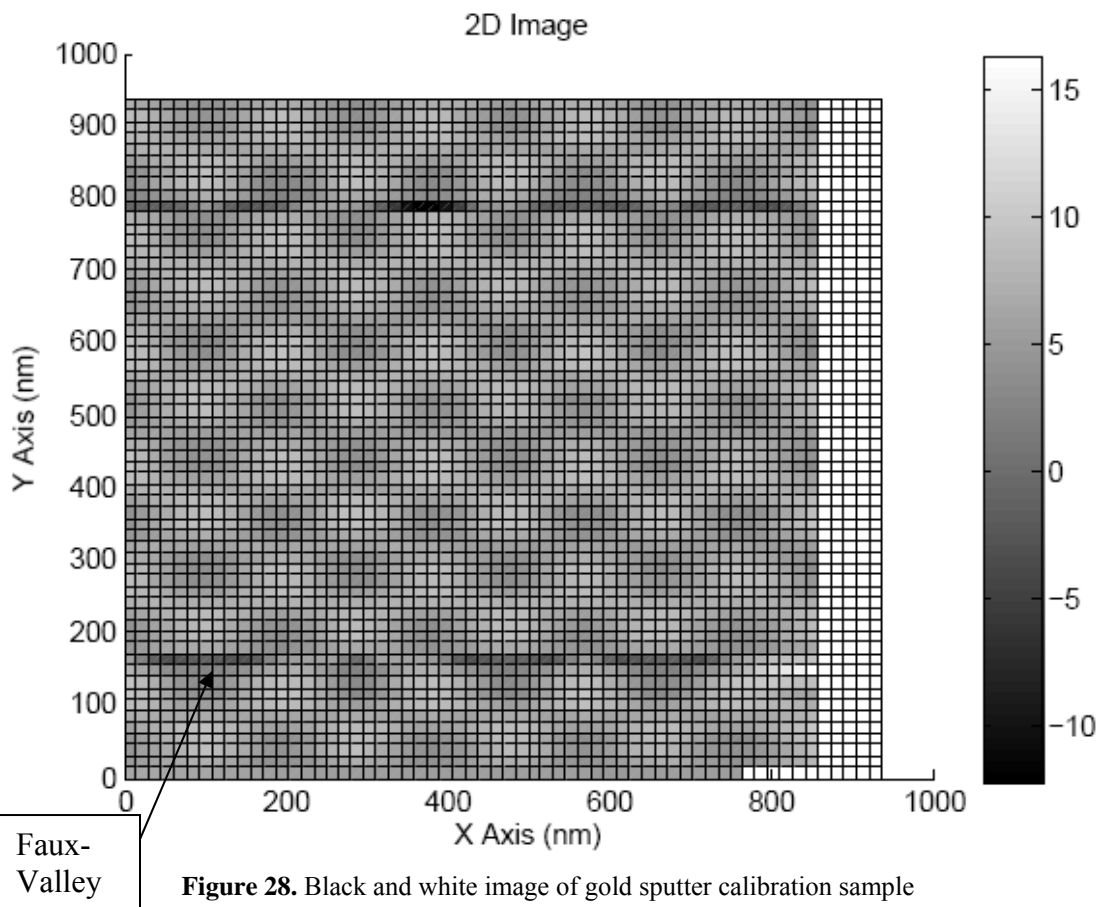


Figure 28. Black and white image of gold sputter calibration sample

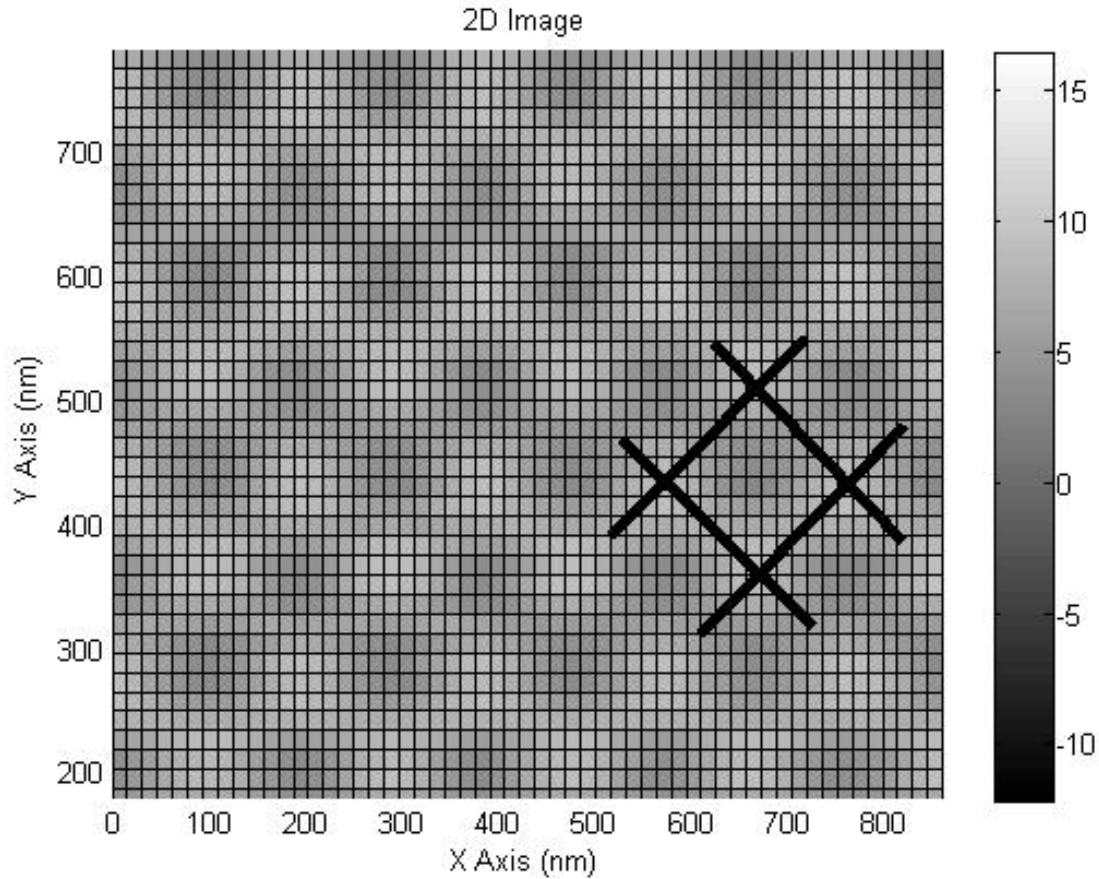


Figure 29. Center of gold sputtered calibration sample

The manufacturer (PhysikInstrumente) reports a value of 20 nm/V for the static sensitivity of the actuators themselves (see Equation (23)). However, as can be seen from Equation (24), the capacitance of the entire system affects this static sensitivity in such a way that the actual static sensitivity is *greater* than that reported by the manufacturer. Since the cables and instrument have a small capacitance, the actual sensitivity of the actuator systems is determined to be 37.5 nm/V. Inherent in the microscope's design, each actuator signal has its own inherent gain due to the configuration of the op-amp components. These inherent gains are known quantities. The horizontal actuators have an inherent gain of 4x and the vertical actuator has a gain of 2x. Therefore, the settings in the microscope's graphic user interface (GUI) are set to the default values of 150 nm/V for the horizontal actuators and 75 nm/V for the vertical actuator as can be seen in Fig. 68 in Appendix A3.2. These are the sensitivity values that result from the aforementioned calibration procedure.

Another issue arises during scanning. The horizontal actuators operate at an appreciable fraction of their design limits (maximum deflection of 1 μm under the reported static sensitivity) with regard to the size of the scanning area in order to image a large enough region of the sample. As a result, during rapid changes in direction, jerks produce faux-valleys (seen in Fig. 26-28) near the edges of the images. These effects are local and can easily be distinguished as deep valleys of singular events.

5.2) Sputtered Gold Film on an Alumina Substrate

A sputtered gold film of unknown thickness on an alumina substrate is also imaged. While this film does not have a known surface topology, it is selected because the surface is likely to be smoother than any machined surface. In addition, this sample is conducting and readily available.

A tunneling current is drawn and this sample reveals an interesting surface feature. A surface scratch only tens of nanometers wide is located, as can be seen in Figs. 30-32.

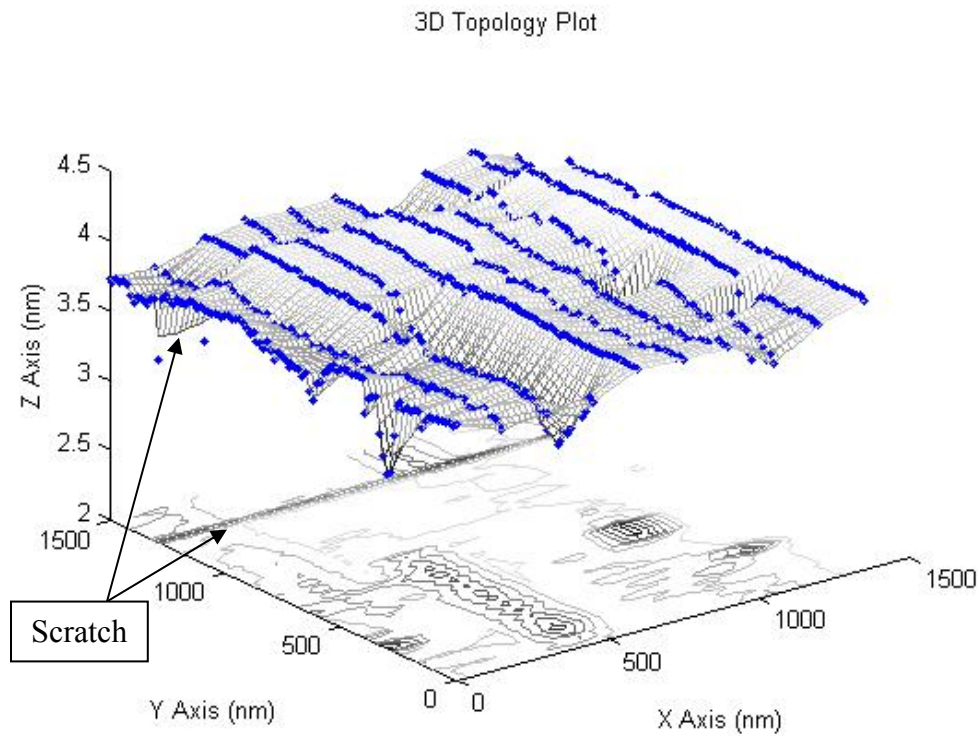


Figure 30. 3D surface scratch

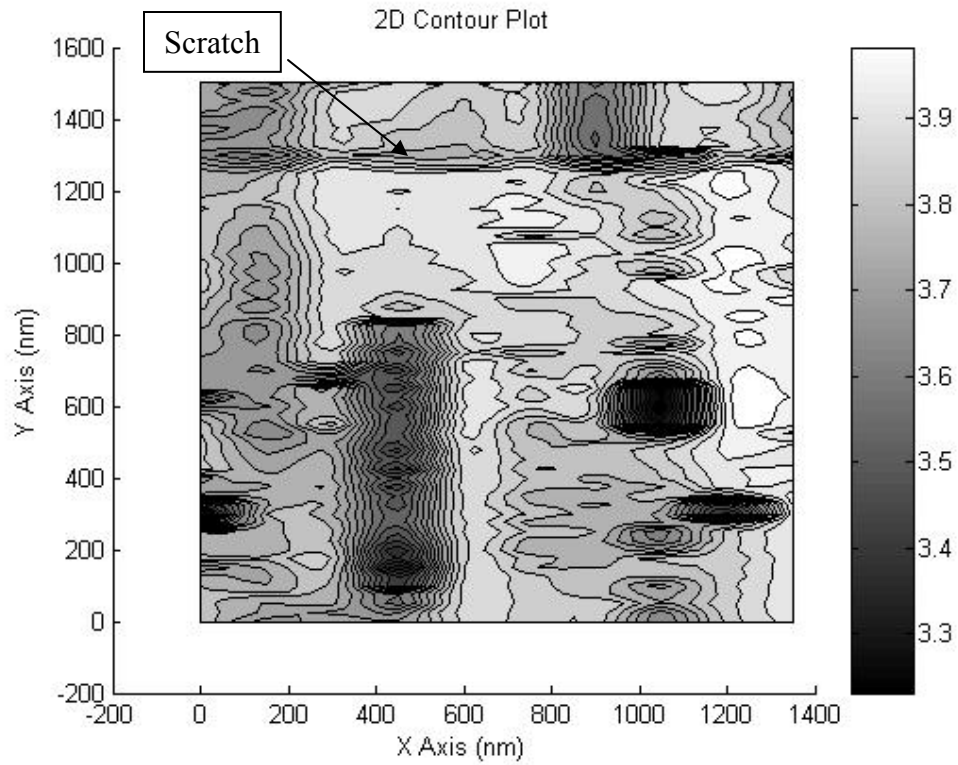


Figure 31. 2D surface scratch

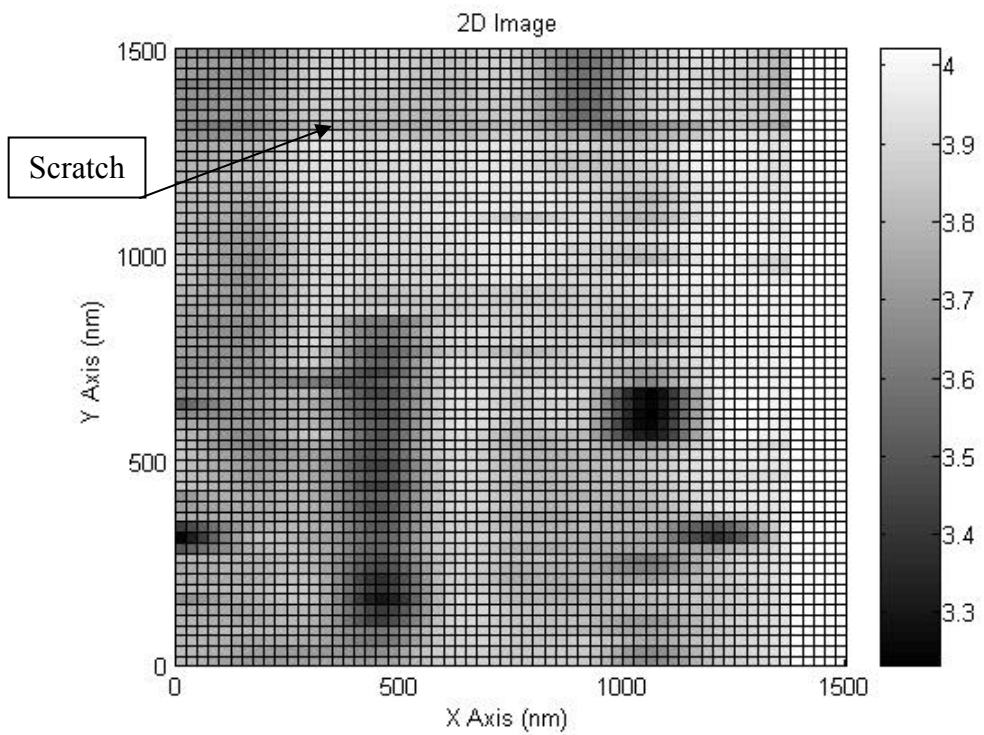


Figure 32. Black and white image of the surface scratch

Due to the rastering pattern of the scanner, the scratch was encountered periodically as illustrated in Fig. 33. The blue lines represent the scanning pattern traversed by the probe tip. As a result, two prominent frequencies are obtained in the frequency analysis of the data; one frequency for when the tip crosses the scratch coming down and one frequency when the tip crosses the scratch going up. This periodic encounter is visible on the fast Fourier transform (FFT) of the data as can be seen in Fig. 34.

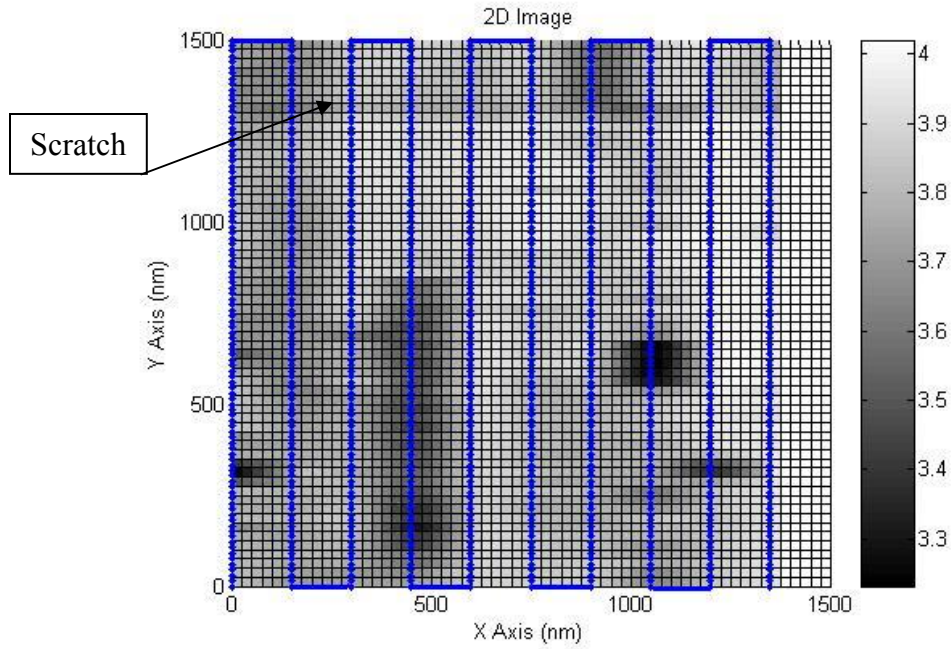


Figure 33. Rastering pattern encountering scratch

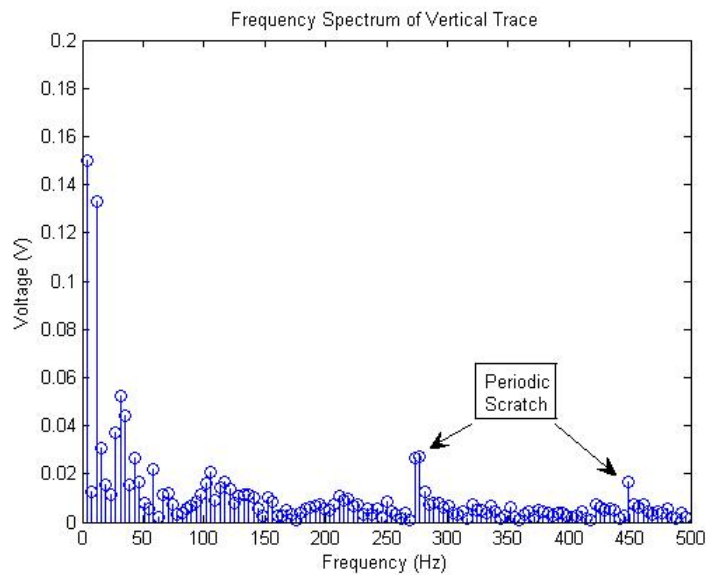


Figure 34. FFT of the data containing the scratch

Several images (Scan A and Scan B) of the scratch were acquired at different times, yielding repeatable results. In particular, other features located near the scratch, such as additional peaks and troughs were also noticed and were used to judge the repeatability of the scan. Those results are shown in Figs. 35-38.

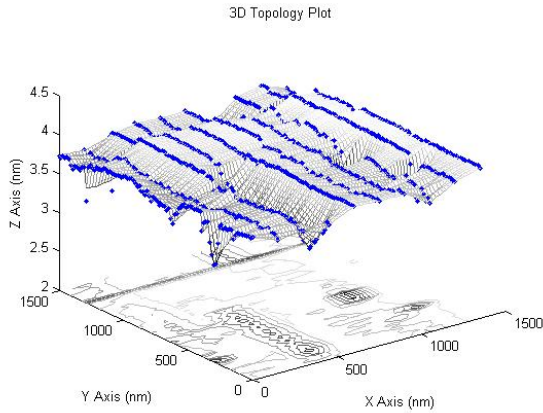


Figure 35. Scan A, 3D surface scratch

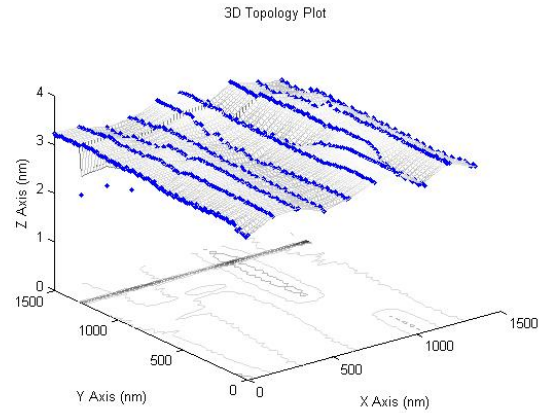


Figure 36. Scan B, 3D surface scratch

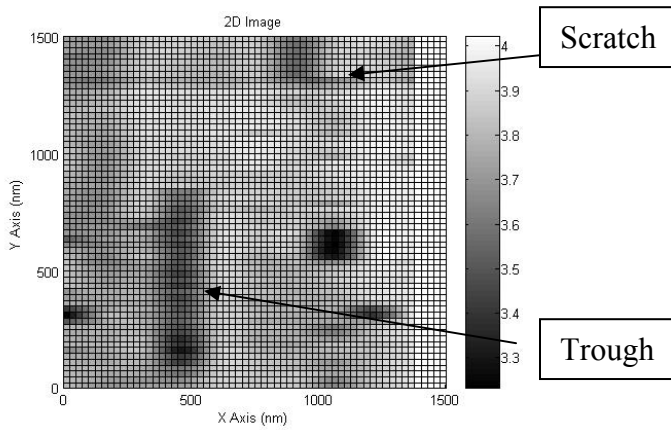


Figure 37. Scan A, Black and white surface scratch

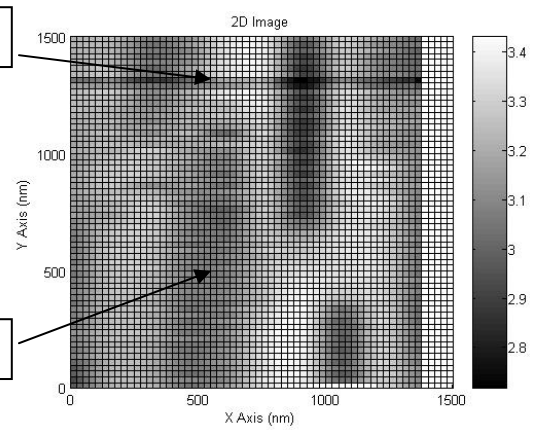


Figure 38. Scan B, Black and white surface scratch

5.3) STM Tungsten Probe Tip

In addition to the gold film on alumina, attempts were made to image a separate tungsten STM probe tip (see Fig. 10 for a photograph of a STM probe tip). The goal behind imaging a separate probe tip was to attempt to verify the radius of curvature of the probe tips. This attempt failed, however, because aligning the two tips proved too difficult to achieve given the coarse approach controls of the prototype microscope. Even though the hemispherical tip was not imaged, these results provided further evidence for the repeatability of the microscope as similar slopes of the surfaces were achieved in multiple scans. As can be seen from Figs. 39-42 a comparison of Scan C and Scan D reveals several similarities, especially in the slope, showing repeatability of results.

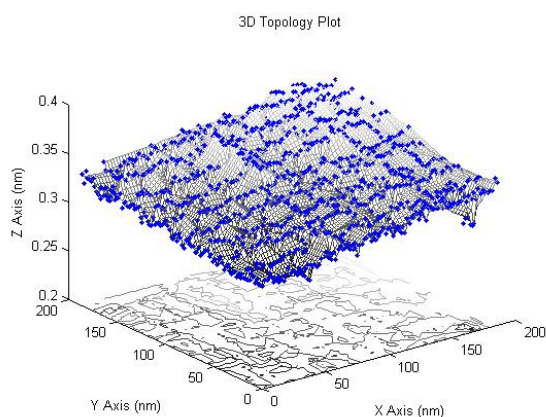


Figure 39. Scan C, 3D STM tip

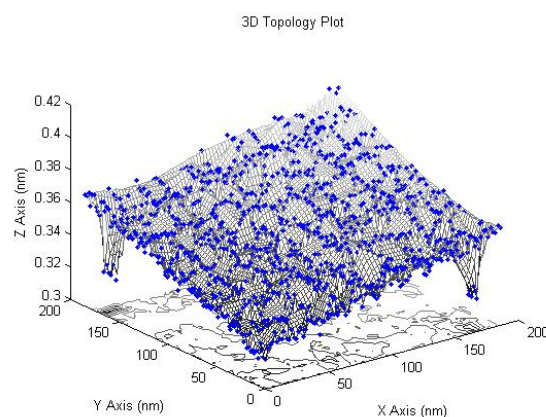


Figure 40. Scan D, 3D STM tip

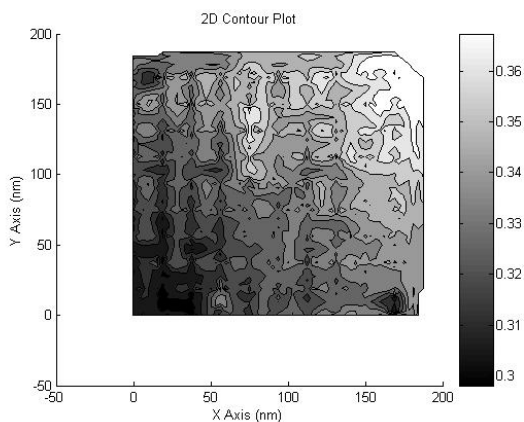


Figure 41. Scan C, 2D STM tip

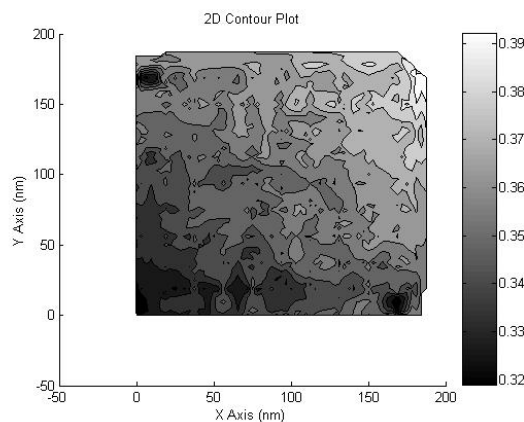


Figure 42. Scan D, 2D STM tip

5.4) SWCNT Bundle

A fiber consisting of bundles of SWCNT produced by electrophoretic drawing[23] was imaged. These bundles are known to have a diameter of approximately 20-40 nm as can be seen by the girth of the peaks in Figs. 43-46. Within these bundles, several SWCNTs are present and have a diameter of ~ 1 nm. The microscope was unable to image a individual SWCNTs but the bundles can be detected as the coarse surface roughness associated with a fiber.

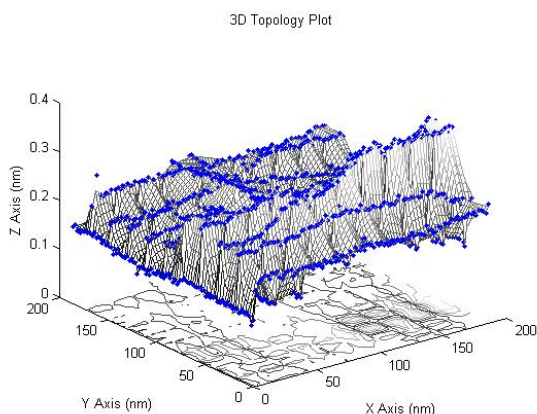


Figure 43. Fiber 1, 3D SWCNT bundle

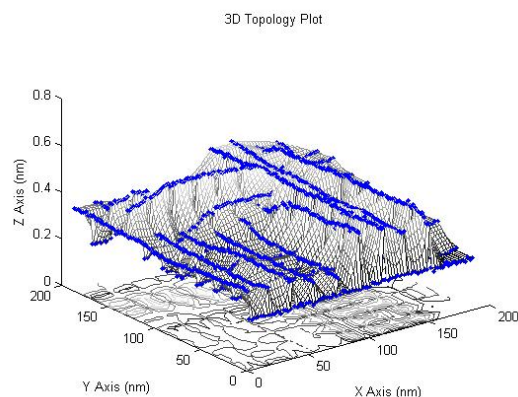


Figure 44. Fiber 2, 3D SWCNT bundle

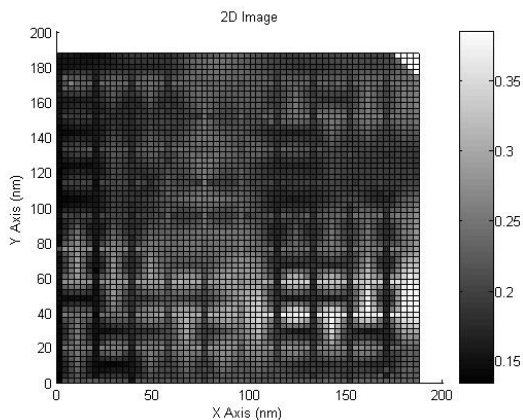


Figure 45. Fiber 2, SWCNT bundle

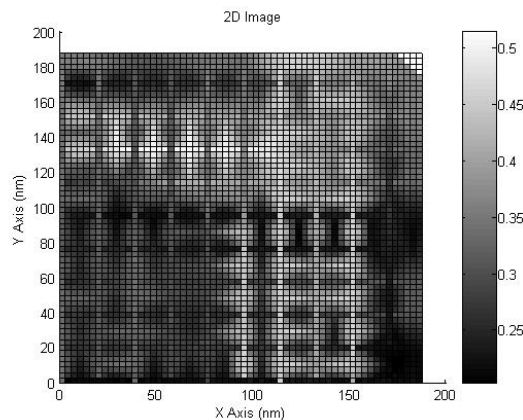


Figure 46. Fiber 3, SWCNT bundle

These bundles, while electrically conducting, are sensitive to electrostatic forces and they are brittle. They were so sensitive that upon attempting to draw a tunneling current, the fibers would move and eventually break under the electrostatic forces associated with the charged probe tip. This would cause the fibers to break free eliminating the sample bias and terminating the scan.

Summary & Conclusions

A relatively inexpensive, quotidian scanning tunneling microscope has been designed to serve as a basic laboratory research apparatus for potential use in nanotechnology research. Applications in nanotechnology require the use of such tools that can help visualize and manipulate structures at the nanoscale. The present approach consists of using off-the-shelf components and instrumentation commonly found in a university laboratory (such as oscilloscopes and multimeters) to construct the STM. Automatic feedback controls serve to acquire data and control the piezoelectric actuators to sub-nanometer displacements in order to obtain and maintain a tunneling current. This data is then recorded and analyzed by imaging software developed in MATLAB in order to produce topographical images of samples.

The present design was guided by well-developed ideas surrounding the quantum mechanical phenomena of tunneling. The design focuses on four components: the vibration isolators and sample stage, the scanner, and the control circuit. The sample stage consists of motor controlled translation stages anchored to a vibration isolator. These components are selected with the goal of utilizing common inexpensive equipment and materials. The scanner uses a novel approach incorporating three piezoelectric actuators mounted on a magnetically attached T-support. This scanner design differs from other existing designs and is inexpensive and versatile. Commonly available materials and components that can be found in a university laboratory, a hardware store, or at the neighborhood Radio Shack, are used. The prototype microscope was assembled at a cost of approximately \$300, not including the cost of a computer, oscilloscope, and DAQ board. The control strategy and circuit is adopted from the previous work[11]. Nevertheless, implementing this control strategy proved to be a challenge while attempting to keep the cost at a minimum. A new strategy for coarse adjustment of the microscope has also been developed. This too differs from approaches reported in the literature.

The prototype STM has been used to image several samples, after calibration. The STM was calibrated against a commercially available standard sputtered gold nanogrid from which the static sensitivities of the piezoelectric actuators are obtained. Following calibration, additional samples were imaged. These include a sputtered gold film on an alumina substrate, a tungsten STM probe tip, and a fiber containing bundles of SWCNT. Each of these images produced interesting results that provided evidence for the proper operation and repeatability of the microscope. While atomic resolution has not yet been demonstrated with this microscope, the

results obtained in atmospheric air imply that improved resolution may be attainable under vacuum conditions.

Recommendations for Future Work

The prototype STM developed in this work may be improved in several aspects. First, the coarse approach can be refined. While the motor controlled translation stages are effective, smaller step sizes on the coarse adjustment would permit more accurate placement of the sample under the tip. This improvement, however, may add to the cost. An alternative approach may be to stack additional piezoelectric actuators so that finer control may be exerted over larger vertical heights. Second, the vibration isolation units could be made significantly less bulky. The large size of the vibration isolator in this work was a result of using existing, large, motor controlled translation stages. Replacing these stages with smaller ones would permit the vibration isolator to be scaled down. Third, while this instrument is designed to operate open to atmospheric air, it is likely that higher resolution can be attained if the STM is operated under vacuum. Incorporating a vacuum chamber around the sample and scanner would not be a difficult task, given the versatility of the present design. However, the procedures for operating this microscope under vacuum will need to be developed since the breakdown distances will be altered at lower pressure. Finally, every component can be optimized and refined. For example, the controls circuit can be optimized and possibly even be simplified. The scanner can be improved by using newer piezoelectric technology as it becomes more affordable. The present design represents a small advance in the state-of-the-art in the design of inexpensive, quotidian scanning tunneling microscopes.

Appendix

A1) Schematic of the Scanner Assembly

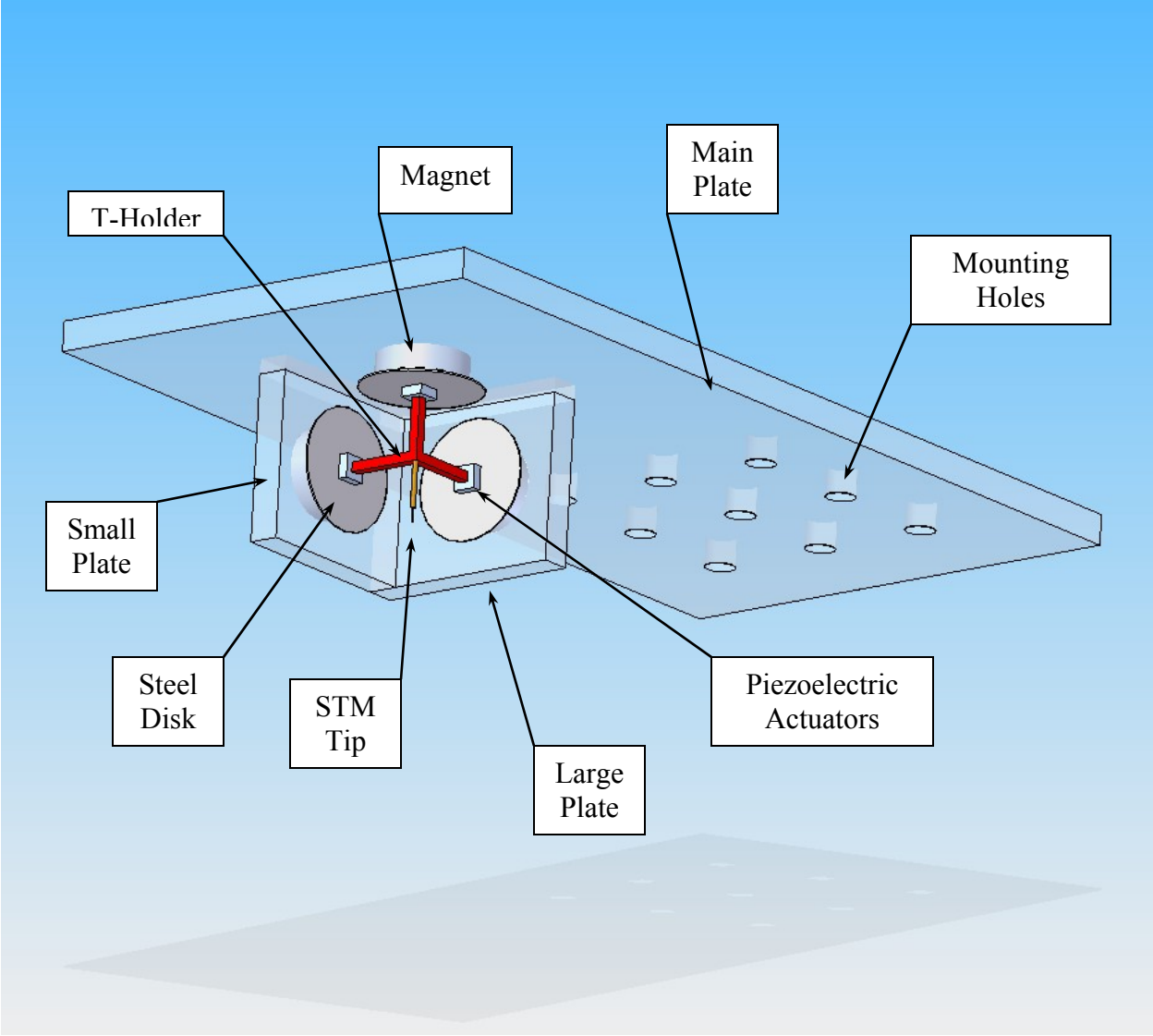


Figure 47. Schematic of the scanner assembly

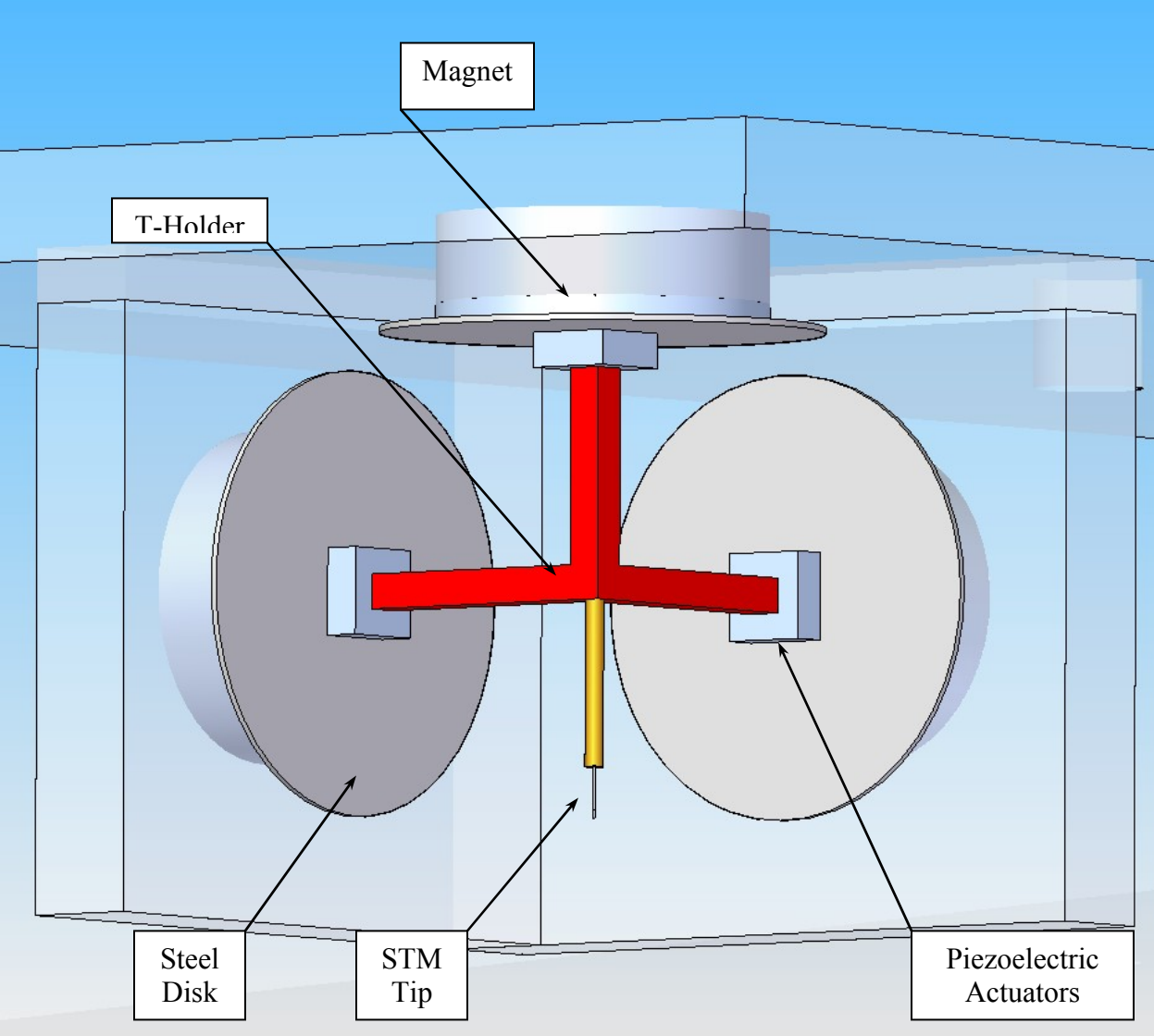


Figure 48. Close-up of scanner

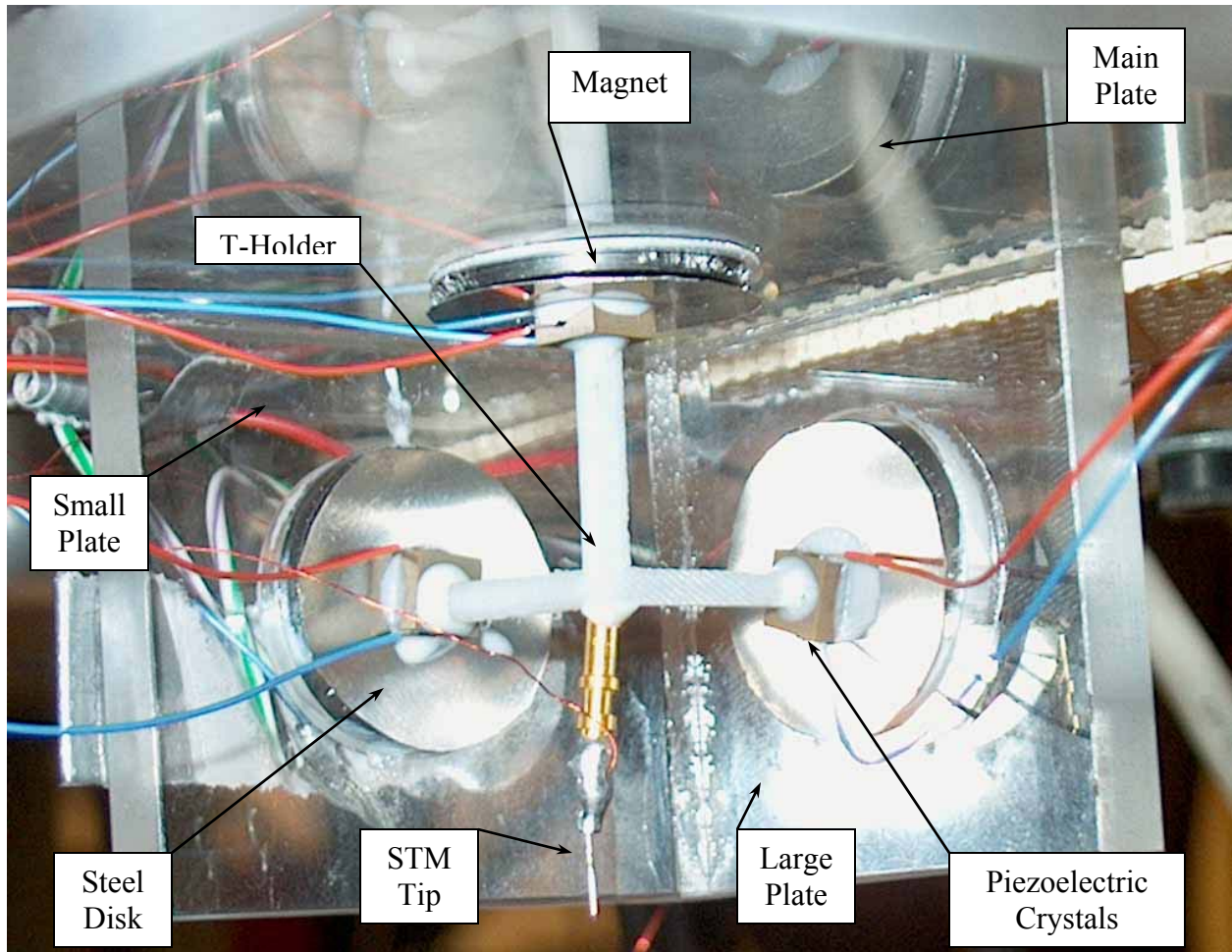


Figure 49. Photograph of the scanner assembly

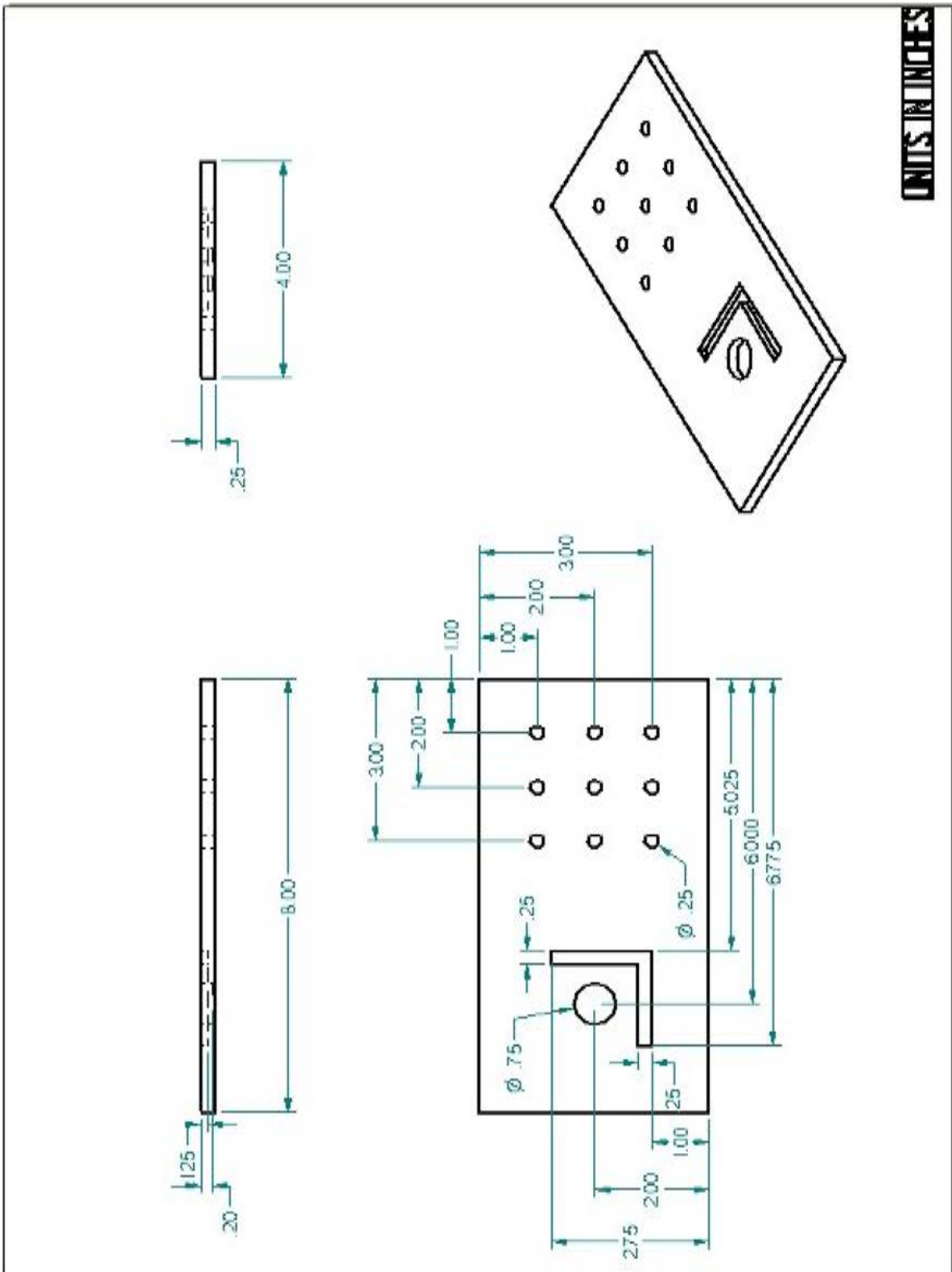


Figure 50. Mechanical drawing of the main support plate

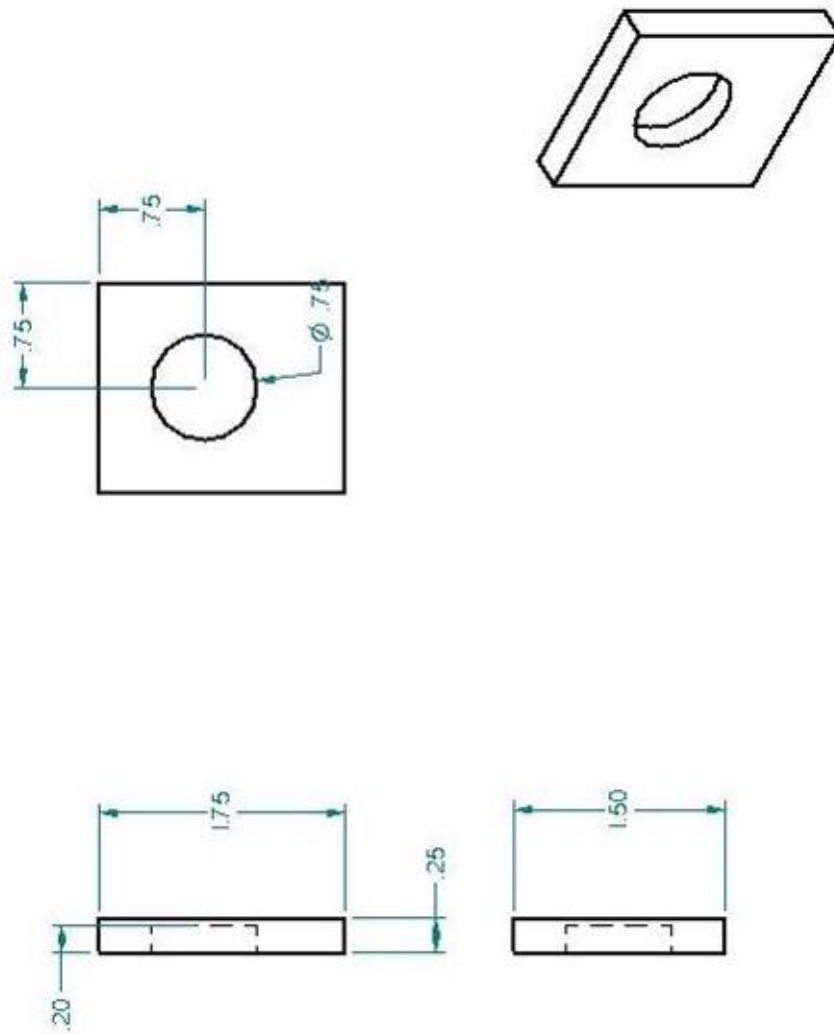


Figure 51. Mechanical drawing of the large support plate.

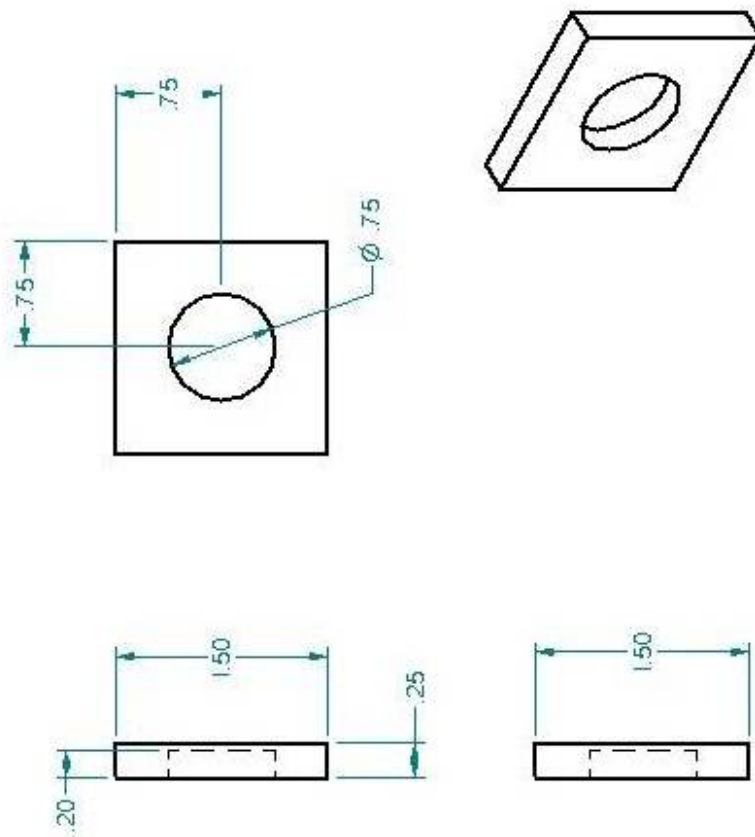


Figure 52. Mechanical drawing of the small plate

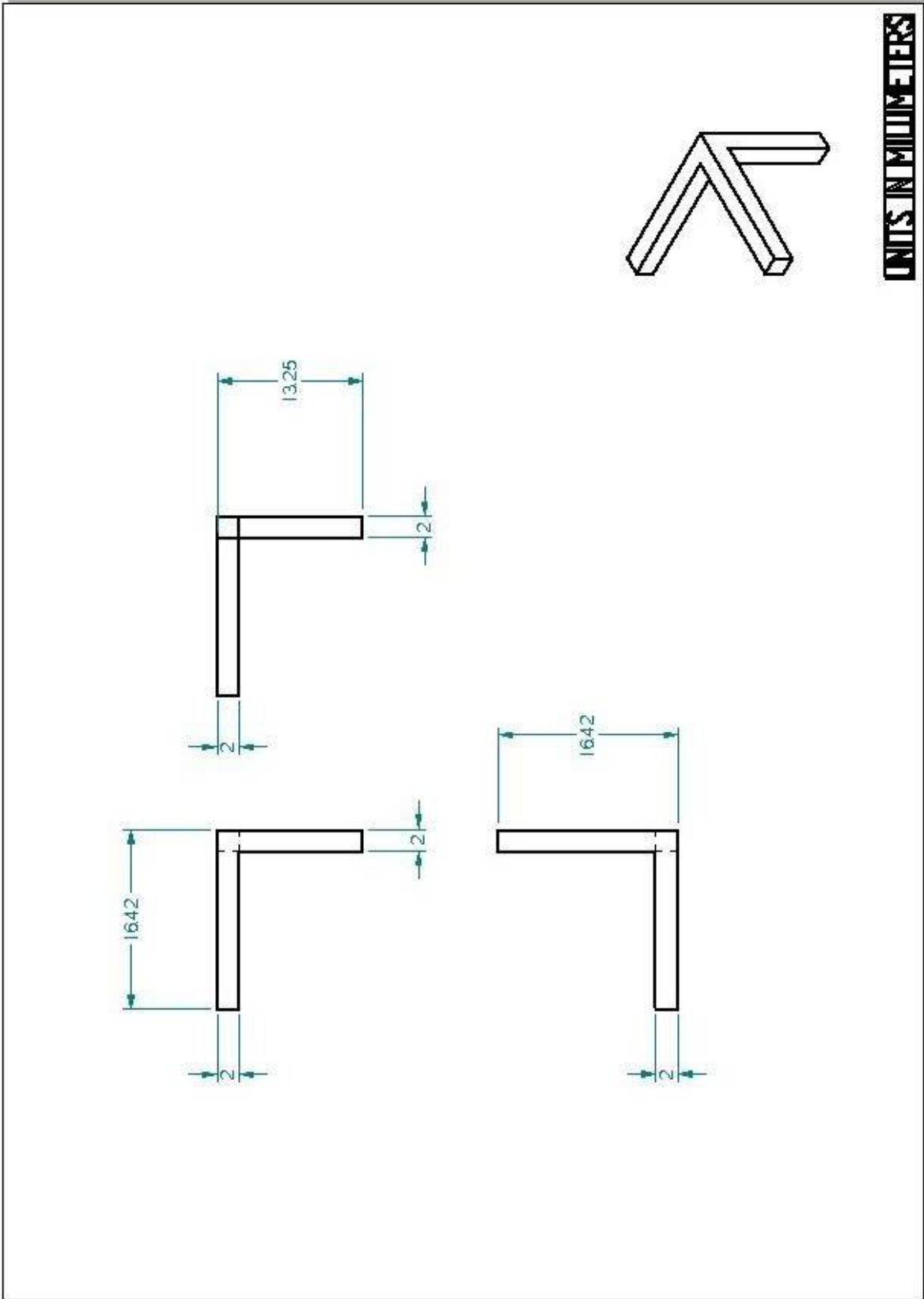


Figure 53. Mechanical drawing of the T-holder.

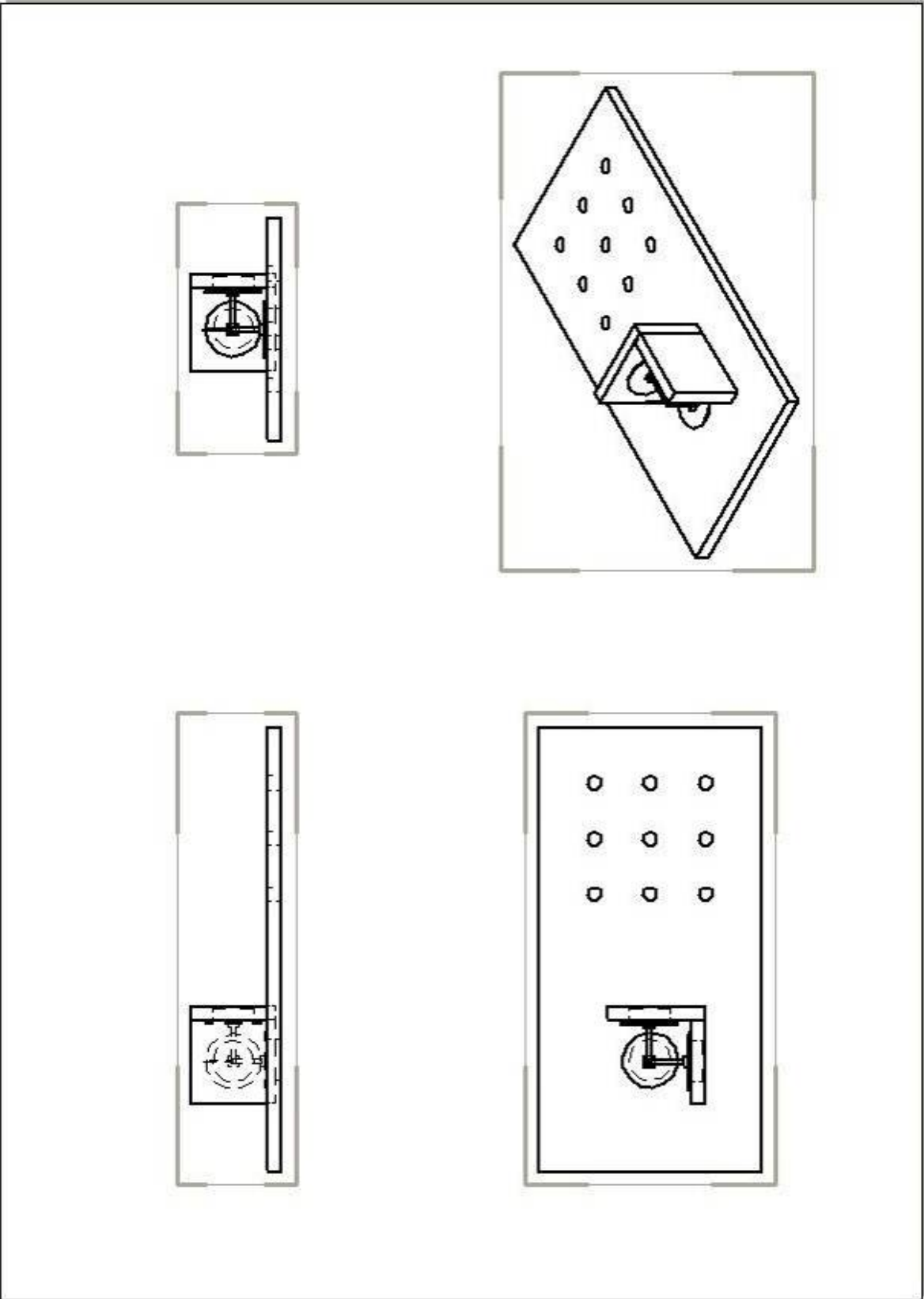


Figure 54. Mechanical Drawing of the scanner assembly

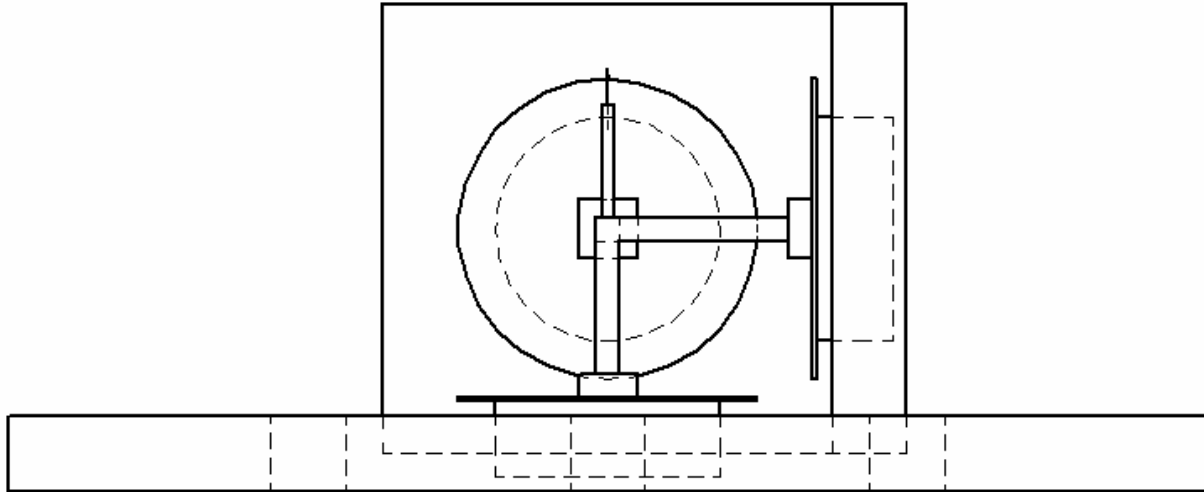


Figure 55. Close-up of scanner assembly (side view)

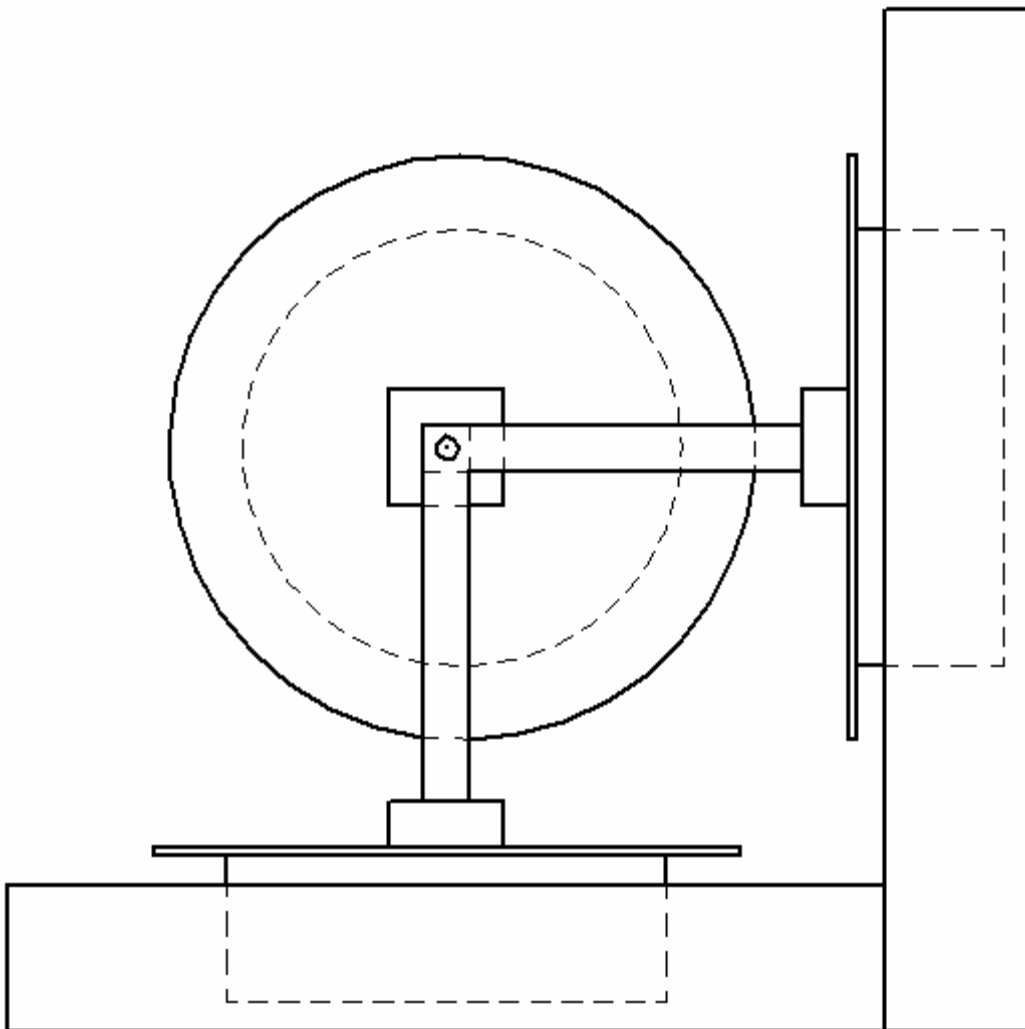


Figure 56. Close-up of scanner assembly (top view)

A2) Schematic of the Control Circuit

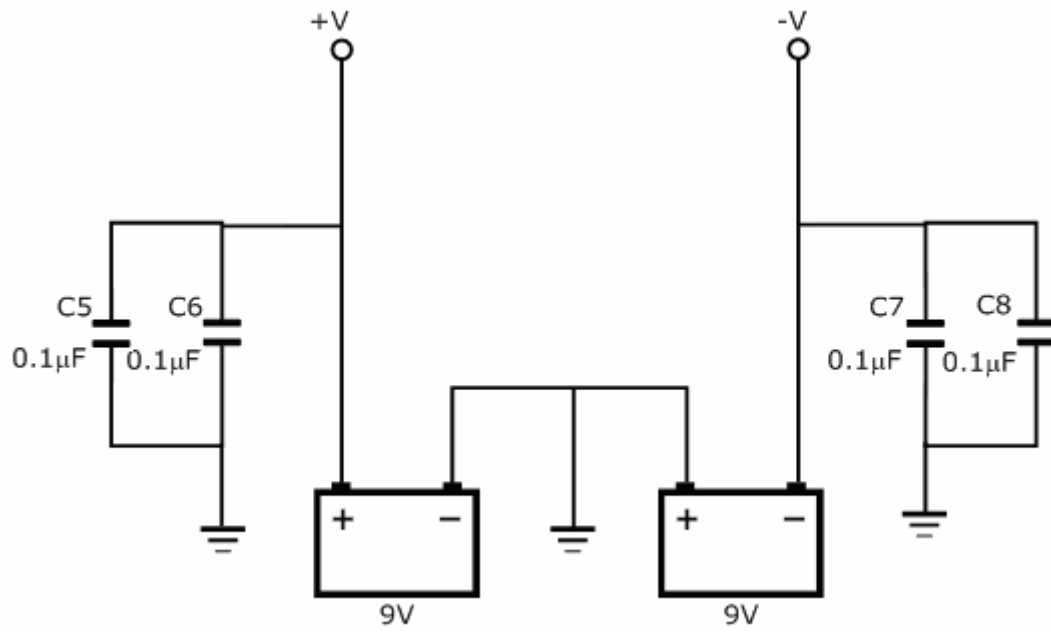


Figure 57. Schematic of the power supply for the control circuit.

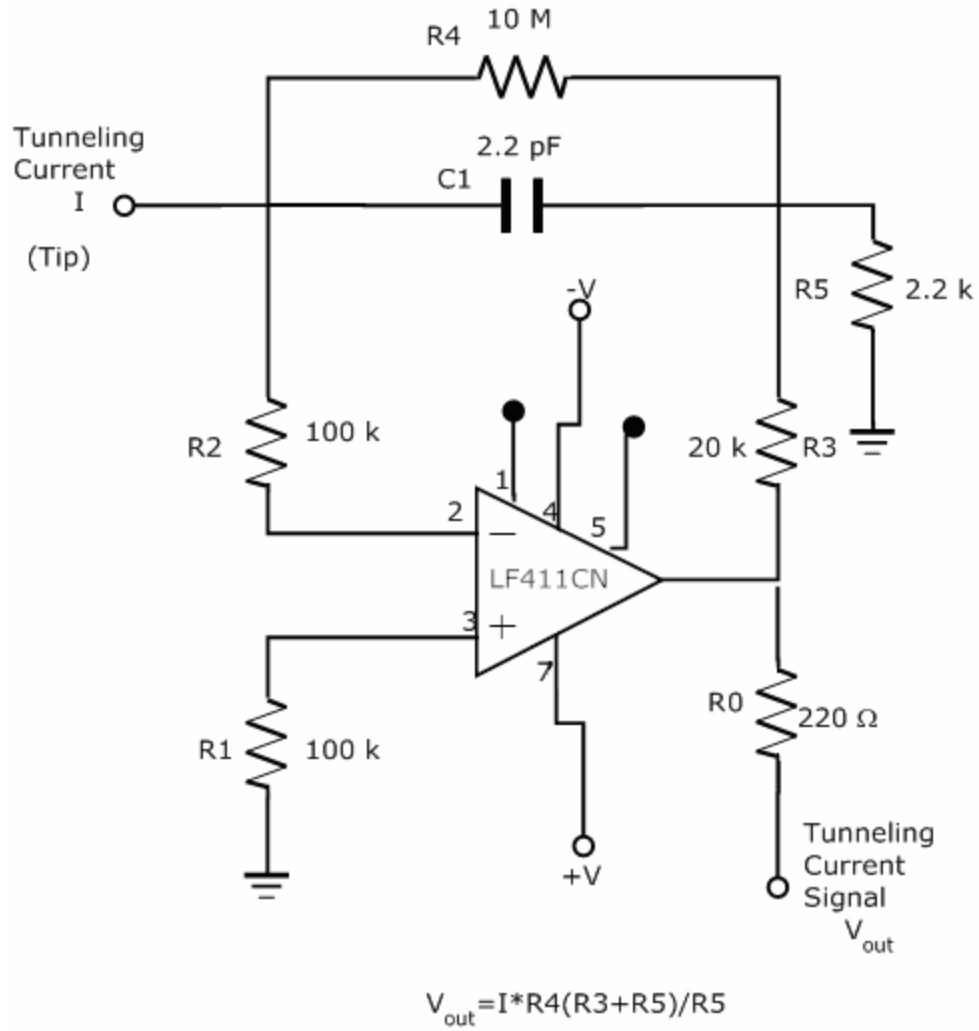


Figure 58. Circuit diagram of the tunneling current transducer

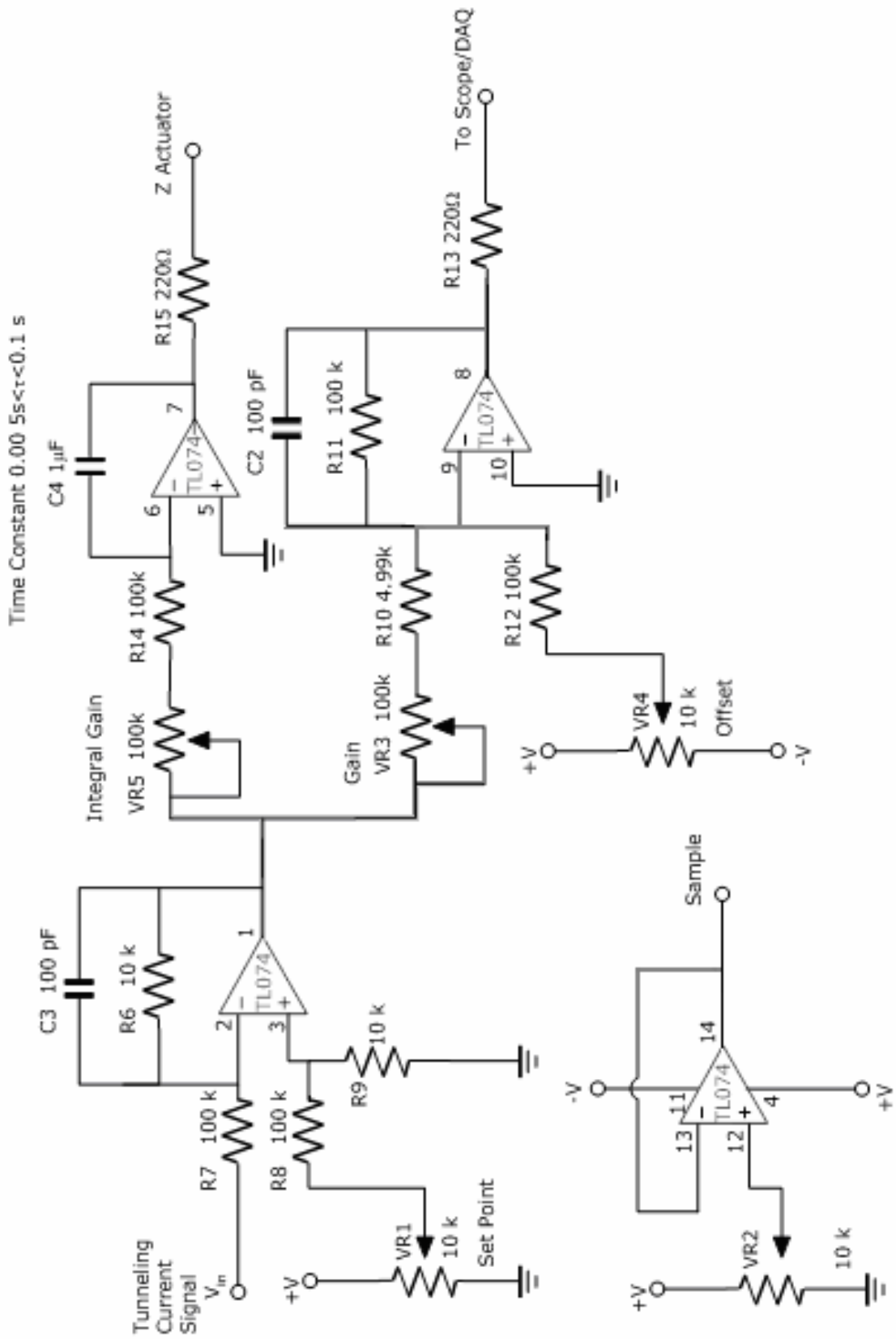


Figure 59. Controls circuit

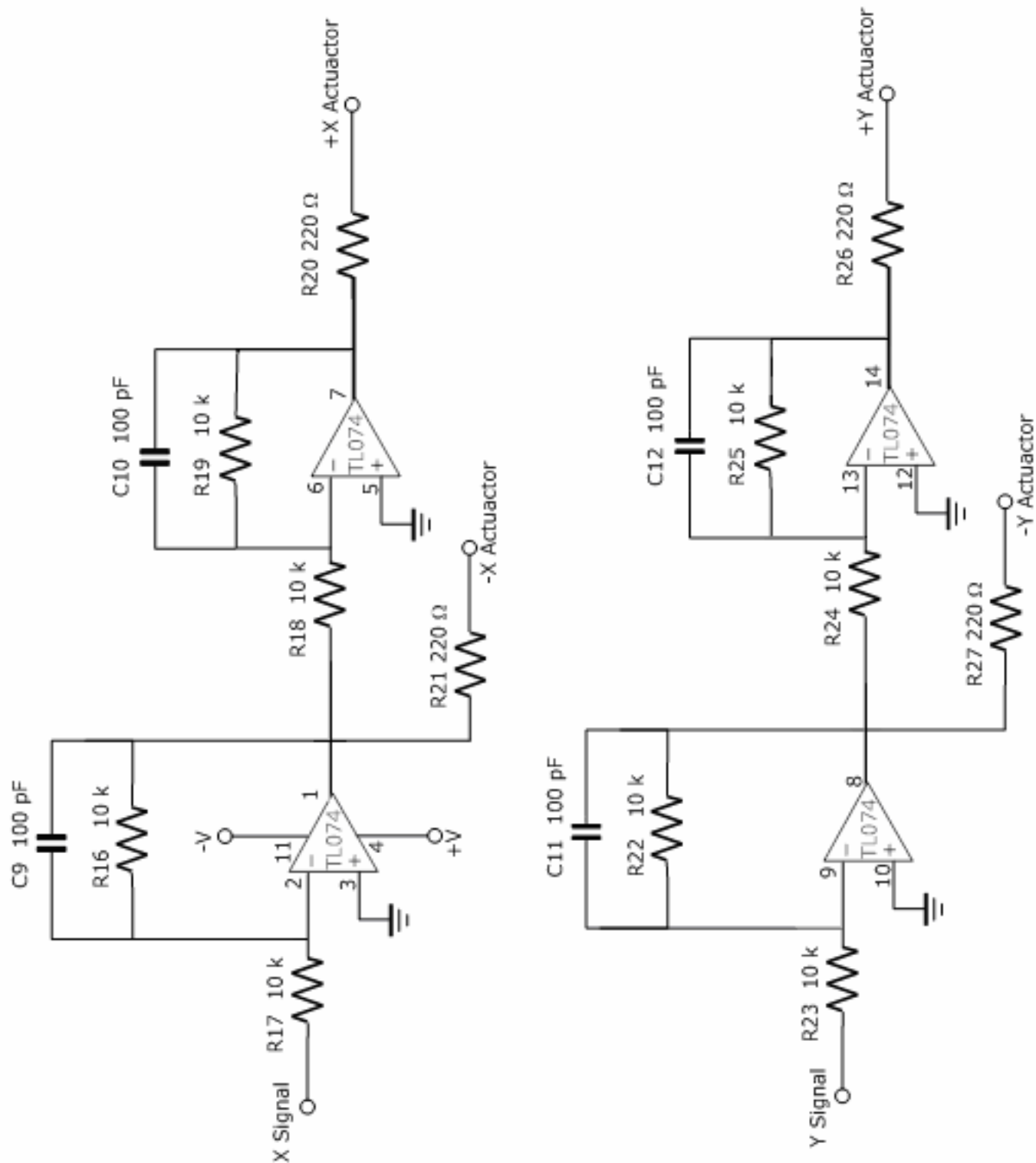


Figure 60. Control circuit for the lateral (XY) actuators.

A3) Explanation of the Software (ReadMe)

The STM software consists of two parts; the data acquisition (DAQ) and the data analysis. The DAQ is performed using a multifunction National Instruments (NI) DAQ board (NI-USB 6211). This DAQ system is selected because of the versatility of the analog inputs and outputs. The data analysis, however, is executed in MATLAB. MATLAB is selected because of its superior signal processing and imaging capabilities. A specific MATLAB script and a user interface have been written in order to interpret the voltage signals recorded by the DAQ system and in order to display images that can be easily interpreted by the user. The following discussion describes the process of recording and analyzing data. Note, however, that a different DAQ system could be used in place of the NI board with little or no changes made to the data analysis software.

A3.1 Data Acquisition

Two files are necessary to operate the data acquisition program. Those files are *2 Channel Analog Output.vi* and *STM DAQ&Analog Output.vi*. These two files must be located in the same directory. The primary program is *STM DAQ&Analog Output.vi*, which calls *2 Channel Analog Output.vi* during execution.

Opening *STM DAQ&Analog Output.vi* produces the following window (Fig. 61) which is the LabVIEW front panel:

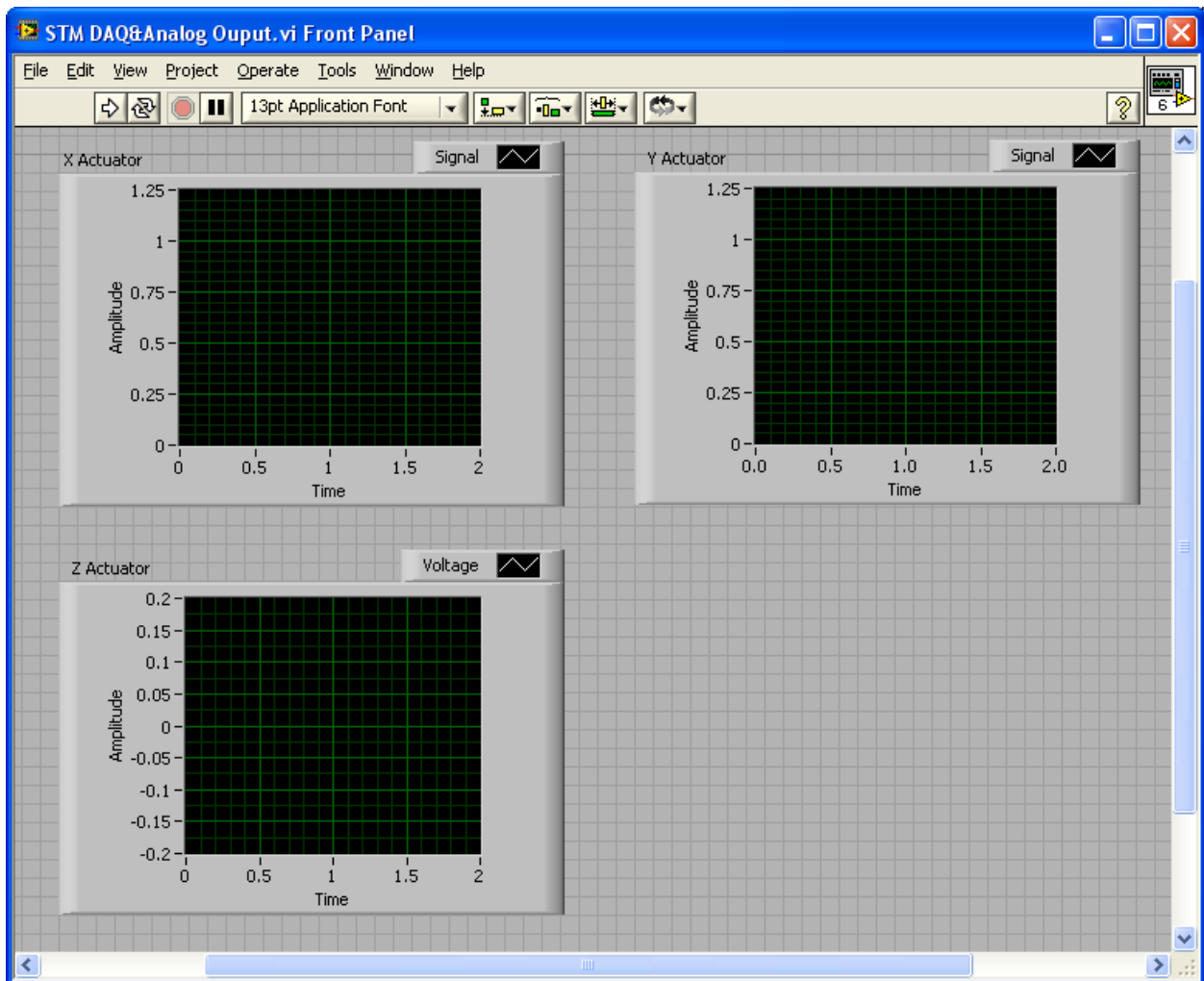


Figure 61. LabVIEW front panel for *STM DAQ&Analog Output.vi*

Selecting **Window>>Show Block Diagram** will call the block diagram. This is the logic behind the DAQ system. Calling the block diagram will produce the window in Fig. 62:

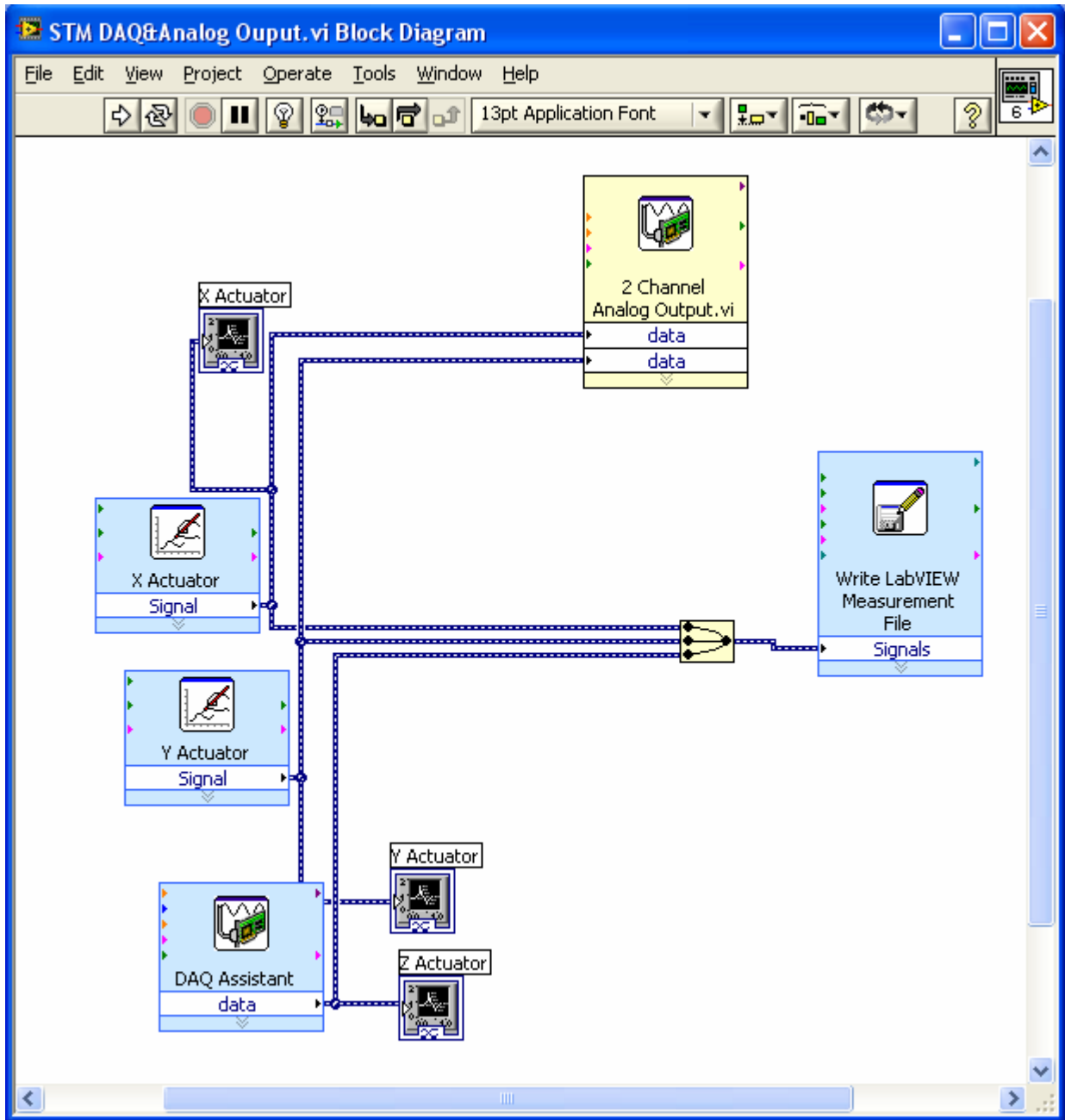


Figure 62. DAQ block diagram for *STM DAQ&Analog Output.vi*

There are eight blocks and one signal merging operator in this block diagram. There are three chart outputs (*X Actuator*, *Y Actuator*, *Z Actuator*), which correspond to the charts on the front panel. These are the voltage signals which are sent to the actuators via the DAQ board. A block labeled *DAQ Assistant* records the voltage signal of the Z (vertical) actuator from the DAQ board. Two signal generator blocks (*X Actuator (Signal)* and *Y Actuator (Signal)*) are also present for the lateral actuators. This is how various scanning patterns are generated. The generated signal is then sent to the actuators via the DAQ board through the block labeled *2 Channel Analog Output.vi*. This *.vi program is called during execution. The function of this program is to interact with the DAQ board in order to generate the necessary imaging signals. This block is specific to the DAQ board in use. In general, this block takes the generated signals and converts them to analog voltage signals via the DAQ board. The final block is a data recorder. This block, which may need to be altered during operation depending on the filename convention the user specifies, will write the acquired data to a specified file that is used during data analysis.

Double-clicking on the *DAQ Assistant* block will open the window shown in Fig. 63.

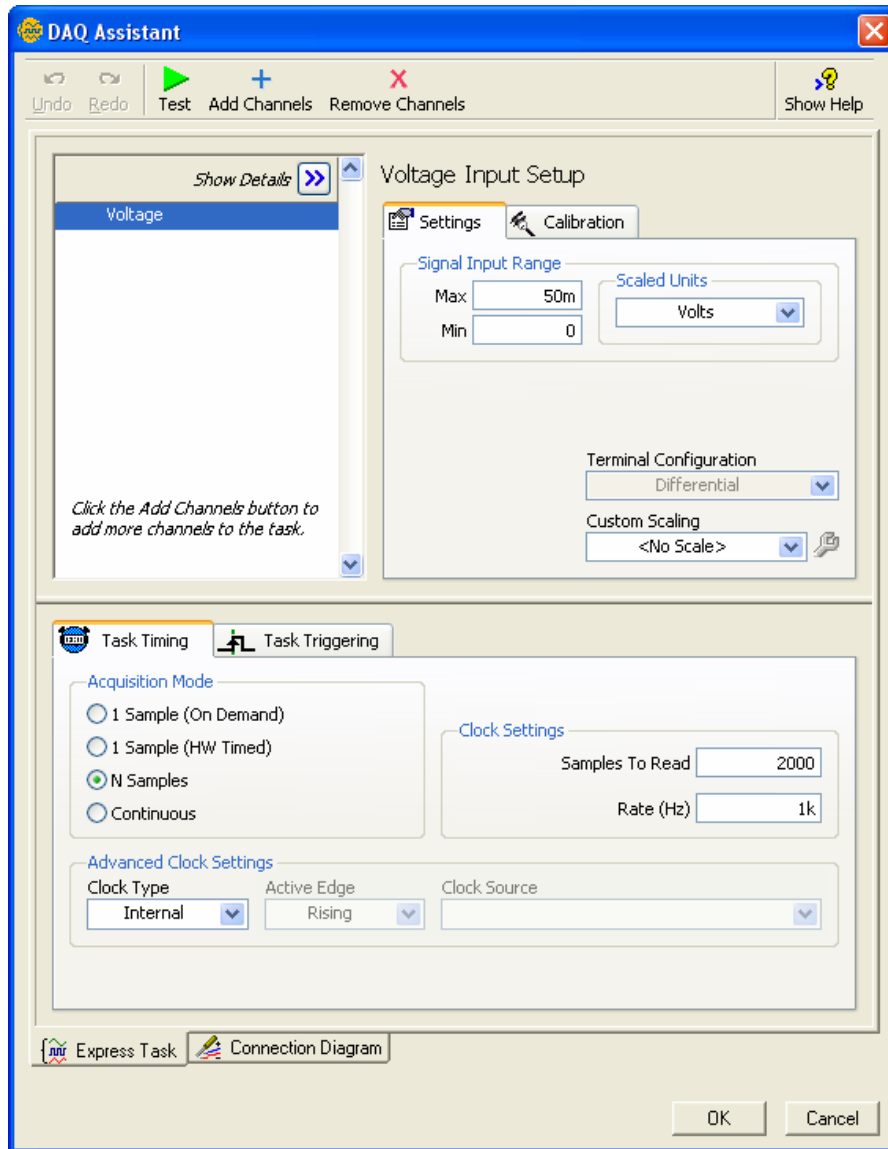


Figure 63. DAQ assistant window

In this block, the voltage range of the 16 bit DAQ board can be altered for maximum resolution. The *Acquisition Mode* must be specified as **N Samples**. The *Clock Setting* must also be set to **2000** and **1 kHz**. These two values can be altered but they must be the same for each channel.

Double-clicking on the *X Actuator (Signal)* block will open the window shown in Fig. 64.

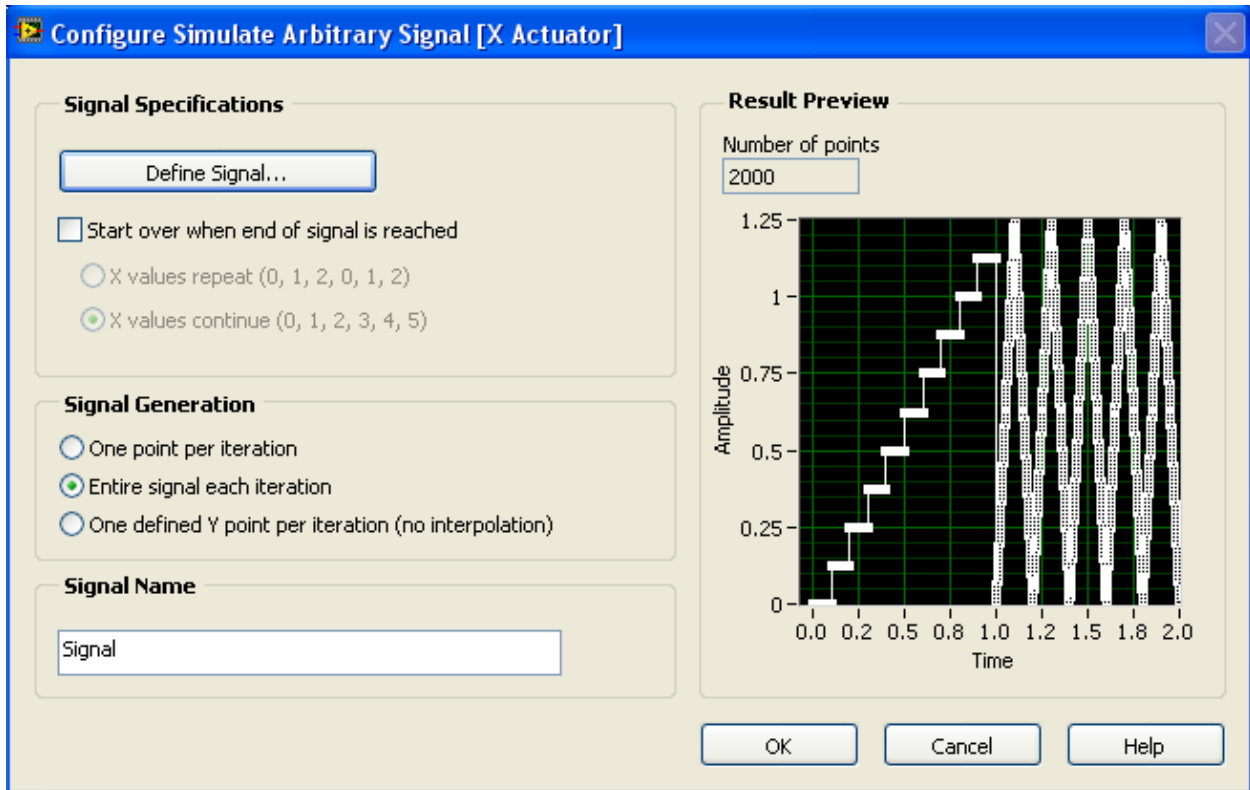


Figure 64. Signal generator window

This is how the X and Y actuator signals are defined. Note that the **Number of points** must agree with the number of samples (i.e. 2000).

By clicking on the *Define Signal...* button the window shown in Fig. 65 will open.

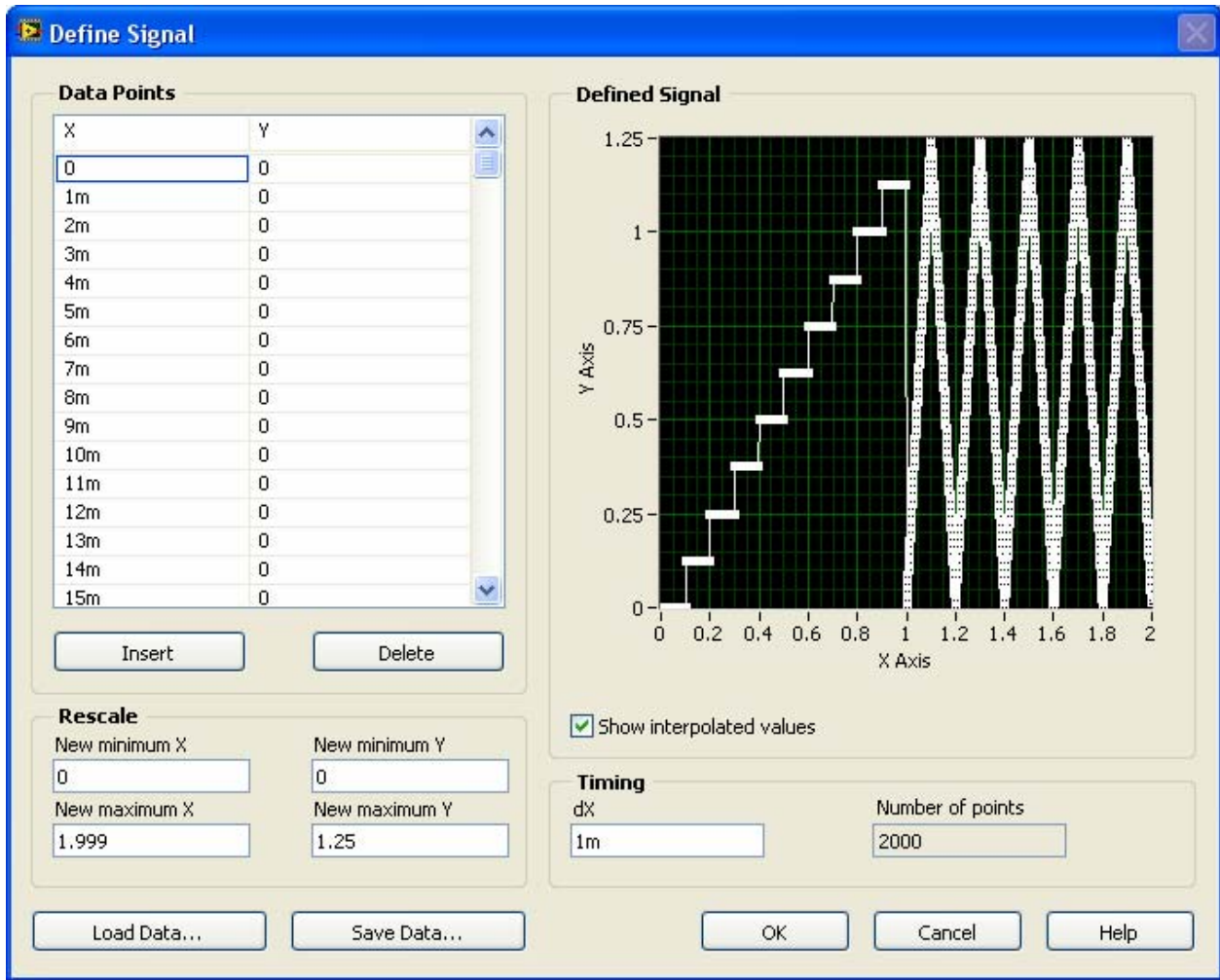


Figure 65. Define signal window

Here, data points and timing schemes can be set. Data can also be loaded by using the *Load Data...* button. The data to be loaded must be an *.lvm file and can be altered in Microsoft Excel. The Y Actuator can be set in an identical manner to the X Actuator. Again, it is important to make sure that the sampling frequency and time divisions agree.

Double-clicking on the *X Actuator (Signal)* block will open the window shown in Fig. 66.

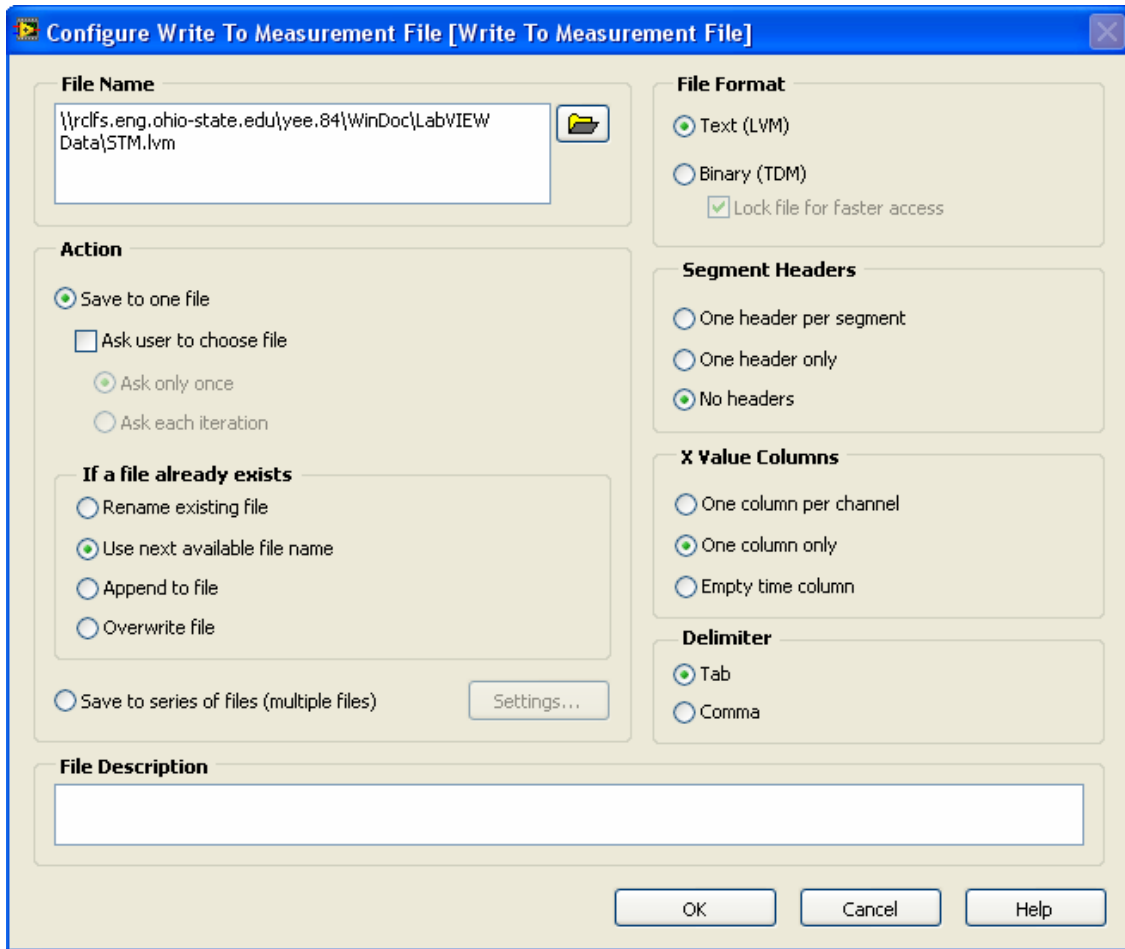



Figure 66. Write to file window

The filename and location can be altered here. The file should be written to the same directory as the MATLAB data analysis files. The *File Format* should also be **Text (LVM)**. In addition, it is important to make sure that the **Use next available file name** is selected to prevent overwriting data. Also select **No headers** under *Segment Headers* and **Tab** under *Delimiter*. This will properly format the file for the data analysis software.

To acquire data, go back to the front panel and click the *Run* button . This will initiate the DAQ system. The DAQ system will automatically stop after signals and have been sent, recorded, and written to a file. A preview of the continuous voltage signals can be viewed on the charts of the front panel.

A3.2 Data Analysis

The script behind the data analysis portion of the STM software is complicated and therefore only operation will be discussed. The imaging software has been incorporated into a MATLAB graphic user interface (GUI) in order to make the instrument more user-friendly. The files associated with the data analysis are: *STM.m*, *STMgui.m*, *STMgui.fig*, *Settings.m*, *Settings.fig*, *Explanation.fig*, and *removdup.m*. The function of these individual script files is not discussed but each file is crucial. The main script is the *STM.m* file. Once the *.lvm data and all the script files are in the same working directory, execute the *STM.m* script. This will initiate the GUI resembling the one shown in Fig. 67.

List of Script Files and Description

- *STM.m* – This is the main execution file that calls the STM GUI.
- *STMgui.m* – This is the GUI which interacts with the figure file.
- *STMgui.fig* – This is the figure for the STM GUI.
- *Settings.m* – This is the Settings GUI where the user can adjust parameters.
- *Settings.fig* – This is the figure for the Settings GUI.
- *Explanation.fig* – This is a window which provides further instruction for filtering.
- *removdup.m* – This sub-function deletes duplicate data points if they are present.

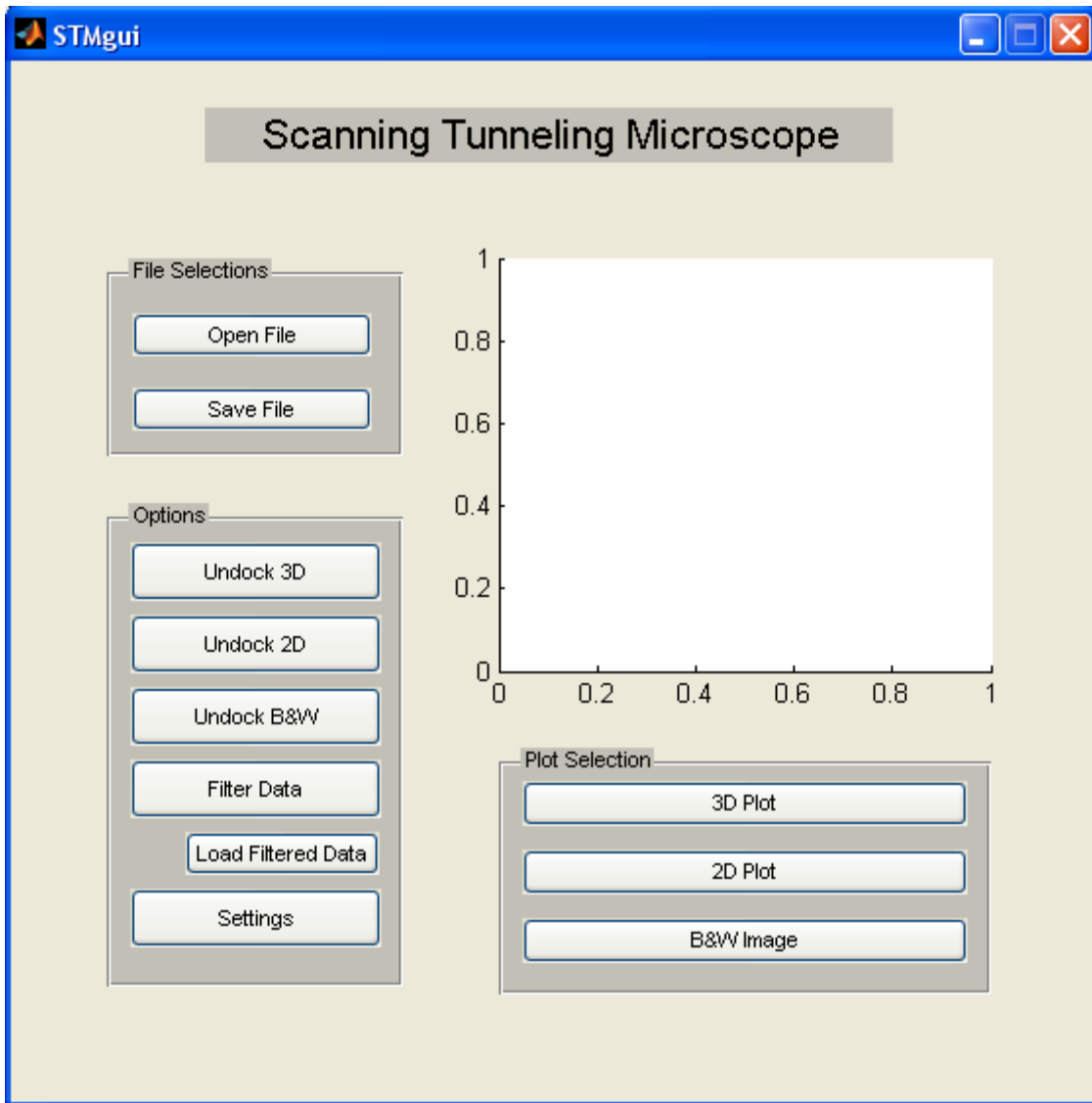


Figure 67. STM graphic user interface (GUI)

The features behind each button are summarized below:

File Selection:

- The *Open File* button allows the user to select the *.lvm file to analyze.
- The *Save File* button allows the user to save any data that has been manipulated during data analysis

Plot Selection:

- The *3D Plot* produces a preview image of the 3D plot in the inherent figure window.
- The *2D Plot* produces a preview image of the 2D contour plot in the inherent figure window.
- The *B&W Image* produces a preview image of the black and white rendering of the surface in the inherent figure window.

Options:

- The *Undock 3D* produces a 3D plot in a new figure window.
- The *Undock 2D* produces a 2D contour plot in a new figure window.
- The *Undock B&W* produces a black and white rendering of the surface in a new figure window.
- The *Filter Data* allows for data to be filtered using a signal processing toolbox.
- The *Load Filtered Data* loads the filtered data that was created using the *Filter Data* option.
- The *Settings* allows various microscope settings to be altered (e.g. static sensitivities, sampling frequencies, etc.)

The *File Selection* and *Plot Selection* features are self explanatory. The *Options*, however, need further explanation. Namely, using the filter commands and the setting commands.

Clicking the *Settings* button will produce the window shown in Fig. 68 and parameters can be altered by the user.

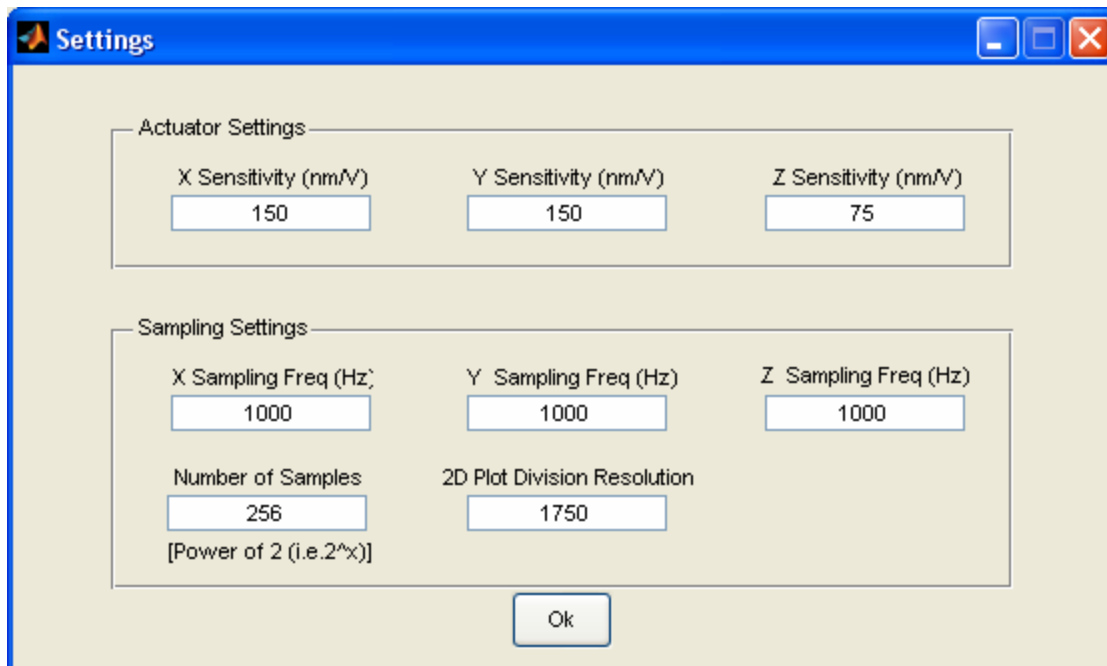


Figure 68. Settings window

Clicking the *Filter Data* button will produce the window shown in Fig. 69.

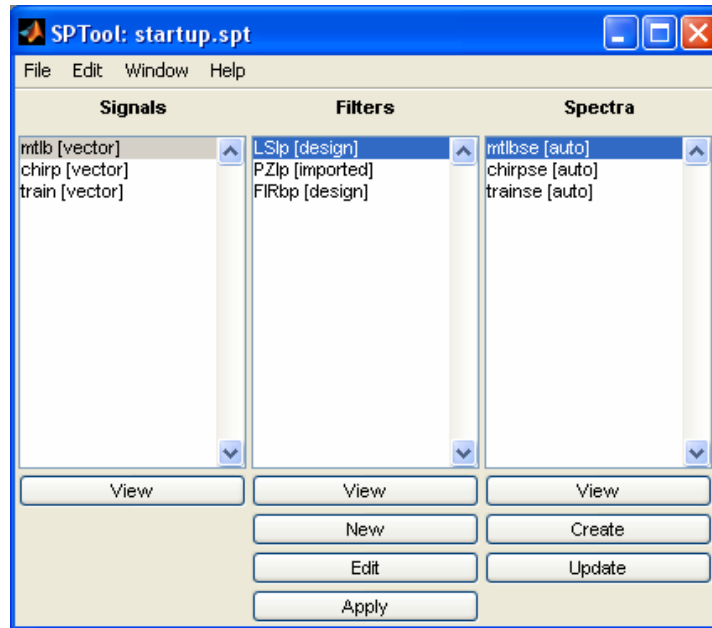


Figure 69. MATLAB SPTool toolbox

The MATLAB SPTool toolbox permits digital filtering. Use the built-in MATLAB help command to learn how to use the signal processing toolbox.

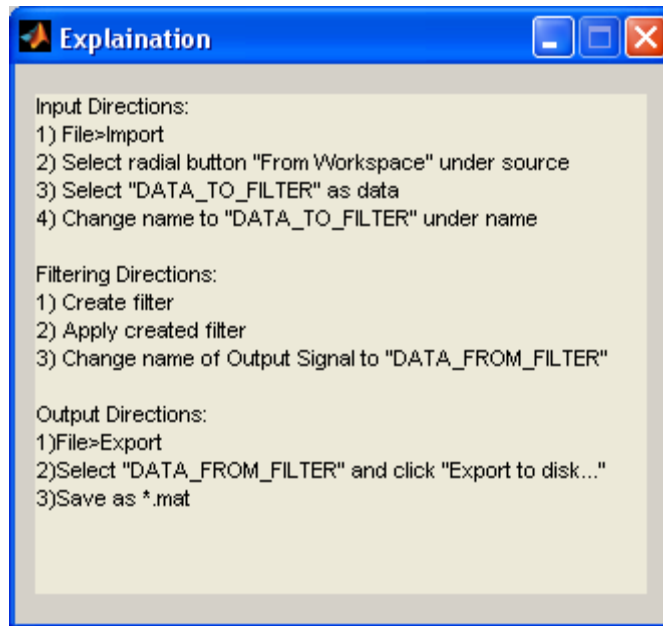


Figure 70. Explanation pop-up window

The explanation window provides the necessary instruction for filtering and saving filter data.

The FFT of the Z actuator data is also produced upon execution of the filtering command. Note that the FFT also appears in the inherent preview plot. The FFT can be used to investigate the presence of low frequency noise and also to check the periodicity of the surface. An example FFT is illustrated in Fig.71.

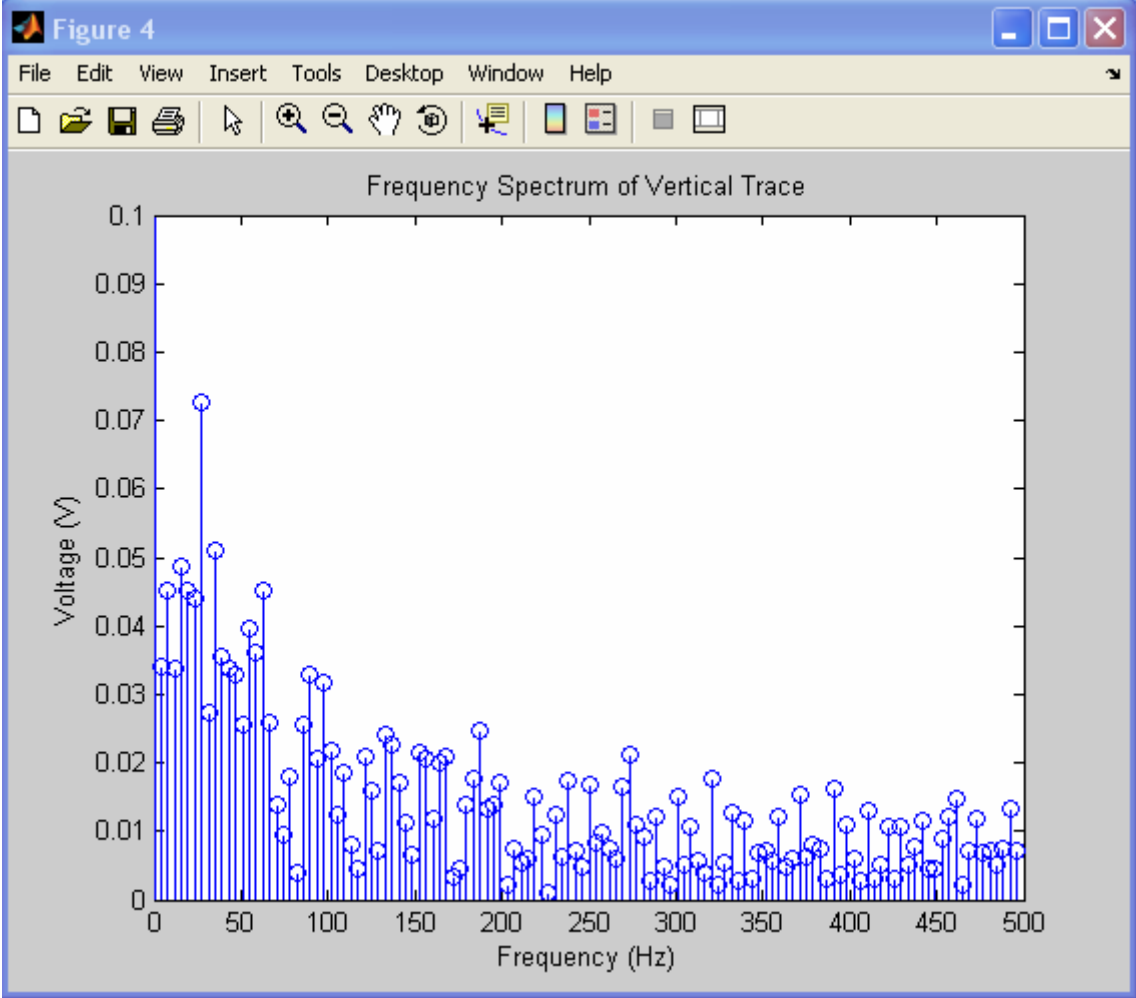


Figure 71. Sample FFT

Sample 3D, 2D, and black and white images are shown in Figs. 72, 73, and 74.

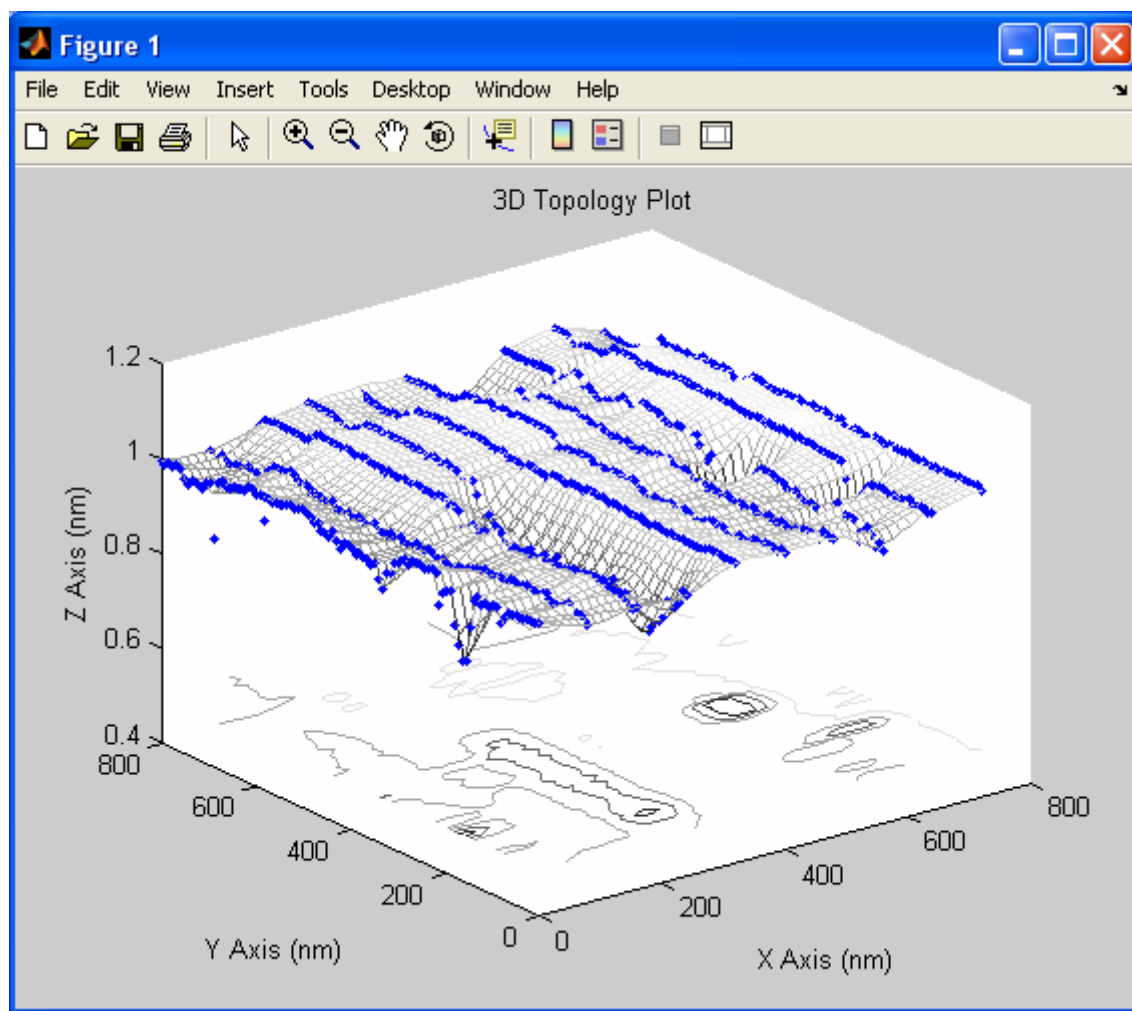


Figure 72. Example 3D image

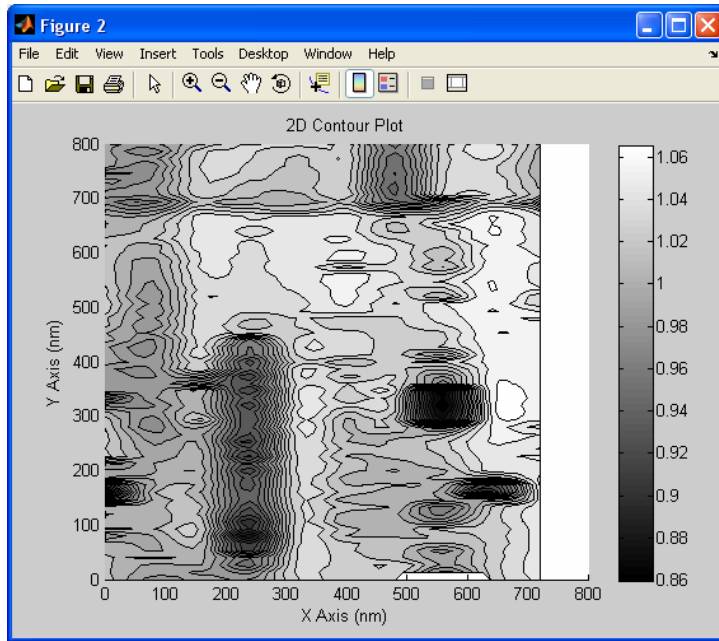


Figure 73. Example 2D image

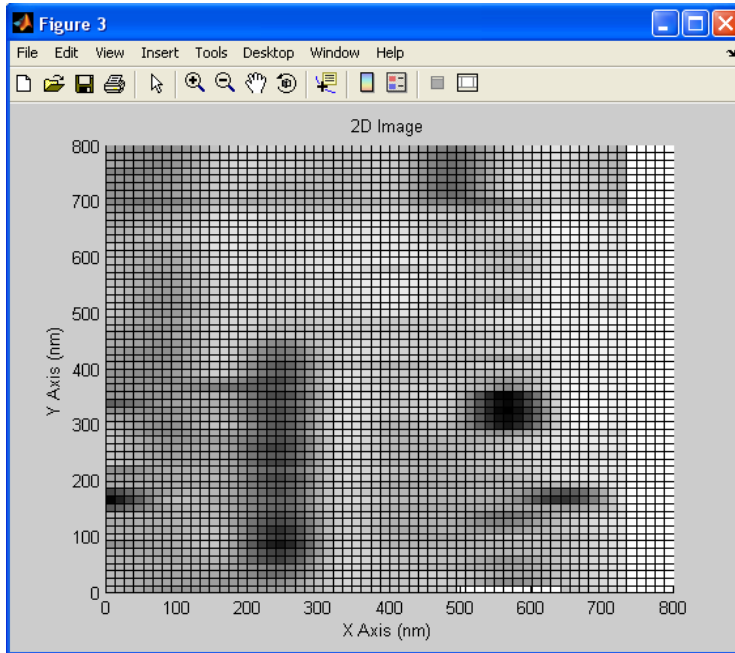


Figure 74. Example black and white image

A4) MATLAB Scripts

A4.1 STM.m

```
%This program will analyze, filter, and display the data collected
%from a Scanning Tunneling Microscope (STM) developed by Shannon Yee
%under the instruction of Dr. V. V. Subramaniam.
%
%Developed January 2006-June 2007
%The Ohio State University
%The Mechanical Engineering Department
%
%Contact:
%Shannon Yee
%email: yee.84@osu.edu
%
%Scott Laboratory
%201 W. 19th Ave
%Columbus, Ohio 43210

%*****Calls*****
clear all;
close all;
clc;

STMgui;
```

A4.2 STMgui.m

```
function varargout = STMgui(varargin)
%This command calls initialized the graphic user interface for the STM.
%
%
% STMGUI M-file for STMgui.fig
%     STMGUI, by itself, creates a new STMGUI or raises the existing
%     singleton*.
%
%     H = STMGUI returns the handle to a new STMGUI or the handle to
%     the existing singleton*.
%
%     STMGUI('CALLBACK',hObject,eventData,handles,...) calls the local
%     function named CALLBACK in STMGUI.M with the given input arguments.
%
%     STMGUI('Property','Value',...) creates a new STMGUI or raises the
%     existing singleton*. Starting from the left, property value pairs are
%     applied to the GUI before STMgui_OpeningFunction gets called. An
%     unrecognized property name or invalid value makes property application
%     stop. All inputs are passed to STMgui_OpeningFcn via varargin.
%
%     *See GUI Options on GUIDE's Tools menu. Choose "GUI allows only one
%     instance to run (singleton)".
%
% See also: STM, GUIDE, GUIDATA, GUIHANDLES

% Begin initialization code - DO NOT EDIT
gui_Singleton = 1;
gui_State = struct('gui_Name',       mfilename, ...
                  'gui_Singleton',  gui_Singleton, ...
                  'gui_OpeningFcn', @STMgui_OpeningFcn, ...
                  'gui_OutputFcn',  @STMgui_OutputFcn, ...
                  'gui_LayoutFcn',  [] , ...
                  'gui_Callback',   []);
if nargin && ischar(varargin{1})
    gui_State.gui_Callback = str2func(varargin{1});
end

if nargout
    [varargout{1:nargout}] = gui_mainfcn(gui_State, varargin{:});
else
    gui_mainfcn(gui_State, varargin{:});
end
% End initialization code - DO NOT EDIT

% --- Executes just before STMgui is made visible.
function STMgui_OpeningFcn(hObject, eventdata, handles, varargin)
% This function has no output args, see OutputFcn.
% hObject    handle to figure
% eventdata  reserved - to be defined in a future version of MATLAB
% handles    structure with handles and user data (see GUIDATA)
% varargin   command line arguments to STMgui (see VARARGIN)

%INITIALIZATIONS
    setappdata(0,'Xsens',150);    %nm/V                %The x sensitivity
```



```

setappdata(0, 'Ysens', 150);    %nm/V           %The y sensitivity
setappdata(0, 'Zsens', 75);    %nm/V           %The z sensitivity

setappdata(0, 'fs_x', 1e3);    %Hz The x voltage sampling frequency
setappdata(0, 'fs_y', 1e3);    %Hz The y voltage sampling frequency
setappdata(0, 'fs_z', 1e3);    %Hz The z voltage sampling frequency
setappdata(0, 'N', 256);       %Sample size (truncate of zero-pad)
setappdata(0, 'D2res', 1750);  %2D plot resolution division

% Choose default command line output for STMgui
handles.output = hObject;

% Update handles structure
guidata(hObject, handles);

% UIWAIT makes STMgui wait for user response (see UIRESUME)
% uiwait(handles.figure1);

% --- Outputs from this function are returned to the command line.
function varargout = STMgui_OutputFcn(hObject, eventdata, handles)
% varargout cell array for returning output args (see VARARGOUT);
% hObject handle to figure
% eventdata reserved - to be defined in a future version of MATLAB
% handles structure with handles and user data (see GUIDATA)

% Get default command line output from handles structure
varargout{1} = handles.output;

% --- Executes on button press in Open.
function Open_Callback(hObject, eventdata, handles)
% hObject handle to Open (see GCBO)
% eventdata reserved - to be defined in a future version of MATLAB
% handles structure with handles and user data (see GUIDATA)

%This function opens the designated STM data file
filein=uigetfile('*.lvm');

if filein~=0
    setappdata(0, 'fid', load(filein));
end

% --- Executes on button press in SaveAs.
function SaveAs_Callback(hObject, eventdata, handles)
% hObject handle to SaveAs (see GCBO)
% eventdata reserved - to be defined in a future version of MATLAB
% handles structure with handles and user data (see GUIDATA)

%This functions saves the current data set (Save filtered data).
fid=getappdata(0, 'fid');
[fileout, pathname, filterindex] = uiputfile('*.txt', 'Save As', 'STM
Filtered Output.txt');

%Write designated file
if fileout~=0

```

```

        fid_out=fopen(fileout,'w');
        for i=1:length(fid);

fprintf(fid_out,'%4.4f\t%4.4f\t%4.4f\t',fid(i,1),fid(i,2),fid(i,3));
        fprintf(fid_out,'\n');
        end
        fclose(fid_out);
    end

% --- Executes on button press in Plot3D.
function Plot3D_Callback(hObject, eventdata, handles)
% hObject    handle to Plot3D (see GCBO)
% eventdata  reserved - to be defined in a future version of MATLAB
% handles    structure with handles and user data (see GUIDATA)

%This function previews the 3D Image
Xsens=getappdata(0,'Xsens');    %nm/V           %The x sensitivity
Ysens=getappdata(0,'Ysens');    %nm/V           %The y sensitivity
Zsens=getappdata(0,'Zsens');    %nm/V           %The z sensitivity

fidl=getappdata(0,'fid');
fid=removdup(fidl);
[Xm,Ixm]=max(fid(:,1));
[Ym,Iym]=max(fid(:,2));
if Ym>=Xm
    ti = 0:Ym/60:Ym;
else
    ti = 0:Xm/60:Xm;
end
[X,Y] = meshgrid(ti,ti);
Z = griddata(fid(:,1), fid(:,2), fid(:,3),X,Y);

%Preview Plot
hold on;
title('3D Topology Plot');
xlabel('X Axis (nm)');
ylabel('Y Axis (nm)');
zlabel('Z Axis (nm)');
colormap(gray);
meshc(X*Xsens,Y*Ysens,Z*Zsens);
plot3(fid(:,1)*Xsens,fid(:,2)*Ysens,fid(:,3)*Zsens,'.');
view(-37.5,30);
hold off;

% --- Executes on button press in Plot2D.
function Plot2D_Callback(hObject, eventdata, handles)
% hObject    handle to Plot2D (see GCBO)
% eventdata  reserved - to be defined in a future version of MATLAB
% handles    structure with handles and user data (see GUIDATA)

%This function previews the 2D Image
Xsens=getappdata(0,'Xsens');    %nm/V           %The x sensitivity
Ysens=getappdata(0,'Ysens');    %nm/V           %The y sensitivity
Zsens=getappdata(0,'Zsens');    %nm/V           %The z sensitivity
fidl=getappdata(0,'fid');
fid=removdup(fidl);

```

```

[Xm,Ixm]=max(fid(:,1));
[Ym,Iym]=max(fid(:,2));
if Ym>=Xm
    ti = 0:Ym/60:Ym;
else
    ti = 0:Xm/60:Xm;
end
[X,Y] = meshgrid(ti,ti);
Z = griddata(fid(:,1), fid(:,2), fid(:,3),X,Y);

%Preview Plot
hold on;
title('2D Contour Plot');
xlabel('X Axis (nm)');
ylabel('Y Axis (nm)');
colormap(gray);
contourf(X*Xsens,Y*Ysens,Z*Zsens,20);
colorbar
hold off;

% --- Executes on button press in PlotBW.
function PlotBW_Callback(hObject, eventdata, handles)
% hObject    handle to PlotBW (see GCBO)
% eventdata  reserved - to be defined in a future version of MATLAB
% handles    structure with handles and user data (see GUIDATA)

%This function previews the B&W Image
Xsens=getappdata(0,'Xsens');    %nm/V    %The x sensitivity
Ysens=getappdata(0,'Ysens');    %nm/V    %The y sensitivity
Zsens=getappdata(0,'Zsens');    %nm/V    %The z sensitivity

fid1=getappdata(0,'fid');
fid=removdup(fid1);
[Xm,Ixm]=max(fid(:,1));
[Ym,Iym]=max(fid(:,2));
if Ym>=Xm
    ti = 0:Ym/60:Ym;
else
    ti = 0:Xm/60:Xm;
end
[X,Y] = meshgrid(ti,ti);
Z = griddata(fid(:,1), fid(:,2), fid(:,3),X,Y);

%Preview Plot
colormap(gray);
pcolor(X*Xsens,Y*Ysens,Z*Zsens);
title('2D Image');
xlabel('X Axis (nm)');
ylabel('Y Axis (nm)');

% --- Executes on button press in Undock3D.
function Undock3D_Callback(hObject, eventdata, handles)
% hObject    handle to Undock3D (see GCBO)
% eventdata  reserved - to be defined in a future version of MATLAB
% handles    structure with handles and user data (see GUIDATA)

%This function undocks the the 3D Image so it may be manipulated

```

```

Xsens=getappdata(0,'Xsens'); %nm/V %The x sensitivity
Ysens=getappdata(0,'Ysens'); %nm/V %The y sensitivity
Zsens=getappdata(0,'Zsens'); %nm/V %The z sensitivity

fid1=getappdata(0,'fid');
fid=removdup(fid1);
[Xm,Ixm]=max(fid(:,1));
[Ym,Iym]=max(fid(:,2));
if Ym>=Xm
    ti = 0:Ym/60:Ym;
else
    ti = 0:Xm/60:Xm;
end

[X,Y] = meshgrid(ti,ti);
[X,Y,Z] = griddata(fid(:,1), fid(:,2), fid(:,3),...
    X,Y,'cubic');

%Plot 3D Image
figure(1);
hold on;
plot3(fid(:,1)*Xsens,fid(:,2)*Ysens,fid(:,3)*Zsens, '.');
title('3D Topology Plot');
xlabel('X Axis (nm)');
ylabel('Y Axis (nm)');
zlabel('Z Axis (nm)');
colormap(gray);
meshc(X*Xsens,Y*Ysens,Z*Zsens);
view(-37.5,30);
hold off;

% --- Executes on button press in Undock2D.
function Undock2D_Callback(hObject, eventdata, handles)
% hObject handle to Undock2D (see GCBO)
% eventdata reserved - to be defined in a future version of MATLAB
% handles structure with handles and user data (see GUIDATA)

%This function undocks the the 2D Image so it may be manipulated
Xsens=getappdata(0,'Xsens'); %nm/V %The x sensitivity
Ysens=getappdata(0,'Ysens'); %nm/V %The y sensitivity
Zsens=getappdata(0,'Zsens'); %nm/V %The z sensitivity

fid1=getappdata(0,'fid');
fid=removdup(fid1);
[Xm,Ixm]=max(fid(:,1));
[Ym,Iym]=max(fid(:,2));
if Ym>=Xm
    ti = 0:Ym/60:Ym;
else
    ti = 0:Xm/60:Xm;
end

[X,Y] = meshgrid(ti,ti);
[X,Y,Z] = griddata(fid(:,1), fid(:,2), fid(:,3),...
    X,Y,'cubic');

```

```

%Plot 2D Image
figure(2)
    hold on
    title('2D Contour Plot');
    xlabel('X Axis (nm)');
    ylabel('Y Axis (nm)');
    colormap(gray);
    contourf(X*Xsens,Y*Ysens,Z*Zsens,20);
    colorbar
    hold off;

% --- Executes on button press in UndockBW.
function UndockBW_Callback(hObject, eventdata, handles)
% hObject      handle to UndockBW (see GCBO)
% eventdata    reserved - to be defined in a future version of MATLAB
% handles      structure with handles and user data (see GUIDATA)

%This function undocks the the B&W Image so it may be manipulated
Xsens=getappdata(0,'Xsens');    %nm/V          %The x sensitivity
Ysens=getappdata(0,'Ysens');    %nm/V          %The y sensitivity
Zsens=getappdata(0,'Zsens');    %nm/V          %The z sensitivity

fidl=getappdata(0,'fid');
fid=removdup(fidl);
[Xm,Ixm]=max(fid(:,1));
[Ym,Iym]=max(fid(:,2));
if Ym>=Xm
    ti = 0:Ym/60:Ym;
else
    ti = 0:Xm/60:Xm;
end
[X,Y] = meshgrid(ti,ti);
Z = griddata(fid(:,1), fid(:,2), fid(:,3),X,Y,'cubic');

%Plot B&W Image
figure(3)
    hold on;
    colormap(gray);
    pcolor(X*Xsens,Y*Ysens,Z*Zsens);
    title('2D Image');
    xlabel('X Axis (nm)');
    ylabel('Y Axis (nm)');
    hold off;

% --- Executes on button press in Filter.
function Filter_Callback(hObject, eventdata, handles)
% hObject      handle to Filter (see GCBO)
% eventdata    reserved - to be defined in a future version of MATLAB
% handles      structure with handles and user data (see GUIDATA)

%This functions previews the FFT and links to the SPTOOL box
fid=getappdata(0,'fid');
assignin('base', 'DATA_TO_FILTER', fid(:,3));

```

```

%Filter Initialization
ini_var.fs_x=getappdata(0,'fs_x'); %Hz The x voltage sampling frequency
ini_var.fs_y=getappdata(0,'fs_y'); %Hz The y voltage sampling frequency
ini_var.fs_z=getappdata(0,'fs_z'); %Hz The z voltage sampling frequency
ini_var.N=getappdata(0,'N'); %Sample size (truncate of zero-pad)

freq.Z_fft=fft(fid(:,3),ini_var.N); %Frequency transform
freq.f_fft=(0:(ini_var.N-1))/ini_var.N*ini_var.fs_z; %Frequencies

%FFT Plot
stem(freq.f_fft(1:ini_var.N/2),abs(freq.Z_fft(1:ini_var.N/2)));
title('Frequency Spectrum of Vertical Trace');
xlabel('Frequency (Hz)');
ylabel('Voltage (V)');
axis([0,ini_var.fs_z/2,0,.02])

figure(4)
stem(freq.f_fft(1:ini_var.N/2),abs(freq.Z_fft(1:ini_var.N/2)));
title('Frequency Spectrum of Vertical Trace');
xlabel('Frequency (Hz)');
ylabel('Voltage (V)');
axis([0,ini_var.fs_z/2,0,.02])
%Load SPTOOL box and explain linking procedures
sptool;
open Explanation.fig;

% --- Executes on button press in LoadFilter.
function LoadFilter_Callback(hObject, eventdata, handles)
% hObject handle to LoadFilter (see GCBO)
% eventdata reserved - to be defined in a future version of MATLAB
% handles structure with handles and user data (see GUIDATA)

%This functions loads filtered data
fid=getappdata(0, 'fid');
filein=uigetfile('*.mat');

%Replace current data with filtered data
if filein~=0
    DATA_STRUCT=load(filein);
    fid(:,3)=DATA_STRUCT.DATA_FROM_FILTER.data;
    setappdata(0,'fid',fid);
end

% --- Executes on button press in Settings.
function Settings_Callback(hObject, eventdata, handles)
% hObject handle to Settings (see GCBO)
% eventdata reserved - to be defined in a future version of MATLAB
% handles structure with handles and user data (see GUIDATA)

%This function loads the settings
Settings;

```

A4.3 Settings.m

```
function varargout = Settings(varargin)
%These are the setting used in the STM imaging software.
%
% See also: STM, STMgui, GUIDE, GUIDATA, GUIHANDLES

% Begin initialization code - DO NOT EDIT
gui_Singleton = 1;
gui_State = struct('gui_Name',       mfilename, ...
                  'gui_Singleton',  gui_Singleton, ...
                  'gui_OpeningFcn', @Settings_OpeningFcn, ...
                  'gui_OutputFcn',  @Settings_OutputFcn, ...
                  'gui_LayoutFcn',  [] , ...
                  'gui_Callback',   []);
if nargin && ischar(varargin{1})
    gui_State.gui_Callback = str2func(varargin{1});
end

if nargout
    [varargout{1:nargout}] = gui_mainfcn(gui_State, varargin{:});
else
    gui_mainfcn(gui_State, varargin{:});
end
% End initialization code - DO NOT EDIT

% --- Executes just before Settings is made visible.
function Settings_OpeningFcn(hObject, eventdata, handles, varargin)
% This function has no output args, see OutputFcn.
% hObject    handle to figure
% eventdata  reserved - to be defined in a future version of MATLAB
% handles    structure with handles and user data (see GUIDATA)
% varargin   command line arguments to Settings (see VARARGIN)

% Choose default command line output for Settings
handles.output = hObject;

% Update handles structure
guidata(hObject, handles);

% UIWAIT makes Settings wait for user response (see UIRESUME)
% uiwait(handles.figure1);

% --- Outputs from this function are returned to the command line.
function varargout = Settings_OutputFcn(hObject, eventdata, handles)
% varargout  cell array for returning output args (see VARARGOUT);
% hObject    handle to figure
% eventdata  reserved - to be defined in a future version of MATLAB
% handles    structure with handles and user data (see GUIDATA)

% Get default command line output from handles structure
varargout{1} = handles.output;
function XSens_Callback(hObject, eventdata, handles)
% hObject    handle to XSens (see GCBO)
```

```

% eventdata reserved - to be defined in a future version of MATLAB
% handles structure with handles and user data (see GUIDATA)

% Hints: get(hObject,'String') returns contents of XSens as text
% str2double(get(hObject,'String')) returns contents of XSens as a double

%This function returns and stores the X sensitivity
get(hObject,'String');
Xsens=str2double(get(hObject,'String'));
setappdata(0,'Xsens',Xsens); %nm/V %The x sensitivity

% --- Executes during object creation, after setting all properties.
function XSens_CreateFcn(hObject, eventdata, handles)
% hObject handle to XSens (see GCBO)
% eventdata reserved - to be defined in a future version of MATLAB
% handles empty - handles not created until after all CreateFcns called

% Hint: edit controls usually have a white background on Windows.
% See ISPC and COMPUTER.
if ispc && isequal(get(hObject,'BackgroundColor'),...
get(0,'defaultUicontrolBackgroundColor'))
set(hObject,'BackgroundColor','white');
end

function YSens_Callback(hObject, eventdata, handles)
% hObject handle to YSens (see GCBO)
% eventdata reserved - to be defined in a future version of MATLAB
% handles structure with handles and user data (see GUIDATA)

% Hints: get(hObject,'String') returns contents of YSens as text
% str2double(get(hObject,'String')) returns contents of YSens as a double

%This function returns and stores the Y sensitivity
get(hObject,'String');
Ysens=str2double(get(hObject,'String'));
setappdata(0,'Ysens',Ysens); %nm/V %The y sensitivity

% --- Executes during object creation, after setting all properties.
function YSens_CreateFcn(hObject, eventdata, handles)
% hObject handle to YSens (see GCBO)
% eventdata reserved - to be defined in a future version of MATLAB
% handles empty - handles not created until after all CreateFcns called

% Hint: edit controls usually have a white background on Windows.
% See ISPC and COMPUTER.
if ispc && isequal(get(hObject,'BackgroundColor'),...
get(0,'defaultUicontrolBackgroundColor'))
set(hObject,'BackgroundColor','white');
end

function ZSen_Callback(hObject, eventdata, handles)
% hObject handle to ZSen (see GCBO)
% eventdata reserved - to be defined in a future version of MATLAB
% handles structure with handles and user data (see GUIDATA)

```



```

% Hints: get(hObject,'String') returns contents of ZSen as text
%       str2double(get(hObject,'String')) returns contents of ZSen as a double

%This function returns and stores the Z sensitivity
get(hObject,'String');
Zsens=str2double(get(hObject,'String'));
setappdata(0,'Zsens',Zsens);      %nm/V           %The z sensitivity

% --- Executes during object creation, after setting all properties.
function ZSen_CreateFcn(hObject, eventdata, handles)
% hObject    handle to ZSen (see GCBO)
% eventdata  reserved - to be defined in a future version of MATLAB
% handles    empty - handles not created until after all CreateFcns called

% Hint: edit controls usually have a white background on Windows.
%         See ISPC and COMPUTER.
if ispc && isequal(get(hObject,'BackgroundColor'),...
get(0,'defaultUicontrolBackgroundColor'))
    set(hObject,'BackgroundColor','white');
end

function XFreq_Callback(hObject, eventdata, handles)
% hObject    handle to XFreq (see GCBO)
% eventdata  reserved - to be defined in a future version of MATLAB
% handles    structure with handles and user data (see GUIDATA)

% Hints: get(hObject,'String') returns contents of XFreq as text
%       str2double(get(hObject,'String')) returns contents of XFreq as a double

%This function returns and stores the X sampling frequency
get(hObject,'String');
fs_x=str2double(get(hObject,'String'));
setappdata(0,'fs_x',fs_x);      %Hz           %The x frequency

% --- Executes during object creation, after setting all properties.
function XFreq_CreateFcn(hObject, eventdata, handles)
% hObject    handle to XFreq (see GCBO)
% eventdata  reserved - to be defined in a future version of MATLAB
% handles    empty - handles not created until after all CreateFcns called

% Hint: edit controls usually have a white background on Windows.
%         See ISPC and COMPUTER.
if ispc && isequal(get(hObject,'BackgroundColor'),...
get(0,'defaultUicontrolBackgroundColor'))
    set(hObject,'BackgroundColor','white');
end

function YFreq_Callback(hObject, eventdata, handles)
% hObject    handle to YFreq (see GCBO)
% eventdata  reserved - to be defined in a future version of MATLAB
% handles    structure with handles and user data (see GUIDATA)

% Hints: get(hObject,'String') returns contents of YFreq as text
%       str2double(get(hObject,'String')) returns contents of YFreq as a double

```

```

%This function returns and stores the Y sampling frequency
    get(hObject,'String');
    fs_y=str2double(get(hObject,'String'));
    setappdata(0,'fs_y',fs_y);           %Hz           %The y frequency

% --- Executes during object creation, after setting all properties.
function YFreq_CreateFcn(hObject, eventdata, handles)
% hObject    handle to YFreq (see GCBO)
% eventdata  reserved - to be defined in a future version of MATLAB
% handles    empty - handles not created until after all CreateFcns called

% Hint: edit controls usually have a white background on Windows.
%         See ISPC and COMPUTER.
if ispc && isequal(get(hObject,'BackgroundColor'),...
get(0,'defaultUiControlBackgroundColor'))
    set(hObject,'BackgroundColor','white');
end

function ZFreq_Callback(hObject, eventdata, handles)
% hObject    handle to ZFreq (see GCBO)
% eventdata  reserved - to be defined in a future version of MATLAB
% handles    structure with handles and user data (see GUIDATA)

% Hints: get(hObject,'String') returns contents of ZFreq as text
%         str2double(get(hObject,'String')) returns contents of ZFreq as a double

%This function returns and stores the Z sampling frequency
    get(hObject,'String');
    fs_z=str2double(get(hObject,'String'));
    setappdata(0,'fs_z',fs_z);           %Hz           %The z frequency

% --- Executes during object creation, after setting all properties.
function ZFreq_CreateFcn(hObject, eventdata, handles)
% hObject    handle to ZFreq (see GCBO)
% eventdata  reserved - to be defined in a future version of MATLAB
% handles    empty - handles not created until after all CreateFcns called

% Hint: edit controls usually have a white background on Windows.
%         See ISPC and COMPUTER.
if ispc && isequal(get(hObject,'BackgroundColor'),...
get(0,'defaultUiControlBackgroundColor'))
    set(hObject,'BackgroundColor','white');
end

function NSamp_Callback(hObject, eventdata, handles)
% hObject    handle to NSamp (see GCBO)
% eventdata  reserved - to be defined in a future version of MATLAB
% handles    structure with handles and user data (see GUIDATA)

% Hints: get(hObject,'String') returns contents of NSamp as text
%         str2double(get(hObject,'String')) returns contents of NSamp as a double

%This function returns and stores the number of samples to use in the FFT
    get(hObject,'String');
    N=str2double(get(hObject,'String'));

```

```

        setappdata(0, 'N', N);           %#           %The number

% --- Executes during object creation, after setting all properties.
function NSamp_CreateFcn(hObject, eventdata, handles)
% hObject    handle to NSamp (see GCBO)
% eventdata  reserved - to be defined in a future version of MATLAB
% handles    empty - handles not created until after all CreateFcns called

% Hint: edit controls usually have a white background on Windows.
%         See ISPC and COMPUTER.
if ispc && isequal(get(hObject, 'BackgroundColor'), ...
get(0, 'defaultUiControlBackgroundColor'))
    set(hObject, 'BackgroundColor', 'white');
end

function D2res_Callback(hObject, eventdata, handles)
% hObject    handle to D2res (see GCBO)
% eventdata  reserved - to be defined in a future version of MATLAB
% handles    structure with handles and user data (see GUIDATA)

% Hints: get(hObject, 'String') returns contents of D2res as text
%        str2double(get(hObject, 'String')) returns contents of D2res as a double

%This function returns and stores the number of samples to use in the FFT
    get(hObject, 'String');
    D2res=str2double(get(hObject, 'String'));
    setappdata(0, 'D2res', D2res);           %#           %The number

% --- Executes during object creation, after setting all properties.
function D2res_CreateFcn(hObject, eventdata, handles)
% hObject    handle to D2res (see GCBO)
% eventdata  reserved - to be defined in a future version of MATLAB
% handles    empty - handles not created until after all CreateFcns called

% Hint: edit controls usually have a white background on Windows.
%         See ISPC and COMPUTER.
if ispc && isequal(get(hObject, 'BackgroundColor'), ...
get(0, 'defaultUiControlBackgroundColor'))
    set(hObject, 'BackgroundColor', 'white');
end

% --- Executes on button press in OK.
function OK_Callback(hObject, eventdata, handles)
% hObject    handle to OK (see GCBO)
% eventdata  reserved - to be defined in a future version of MATLAB
% handles    structure with handles and user data (see GUIDATA)
close Settings

```

A4.4 removdup.m

```
function fid=removdup(fid1)
%This function removes duplicate data points
%
% See also: STM, STMgui

i=1;
while i<length(fid1)
    I=find(fid1(i,1)==fid1(:,1) & fid1(i,2)==fid1(:,2));
    for j=length(I):-1:2
        fid1(I(j),:)=[];
    end
    i=i+1;
end
fid=sortrows(fid1);
```

References

- [1] Griffiths, David J. *Introducing Quantum Mechanics*. Prentice Hall. Upper Saddle River, New Jersey 1995.

- [2] Bhushan, Bharat (Ed). *Springer Handbook of Nanotechnology*. Springer-Verlag Berlin Heidelberg. Germany 2004.

- [3] Binnig, G., H. Rohrer, C. H. Gerber, and E. Weibel. "Surface Studies by Scanning Tunneling Microscopy." *Physical Review Letters* 49, 1 (1982a): 57-60.

- [4] Tersoff, J., and D. R. Hamann. *Theory of the Scanning Tunneling Microscope*. The American Physical Society. Physical Review B. Vol 31, Num 2. 15 Jan. 1985.

- [5] Binnig, G, and H. Rohrer, "Scanning Tunneling Microscopy-From Birth To Adolescence." Nobel Lecture, 8 Dec. 1986.

- [6] Güntherodt, H.-J., and R. Wiesendanger. *Scanning Tunneling Microscopy I*. Springer-Verlag, New York, 1992.

- [7] Wiesendanger, R., and H.-J. Güntherodt. *Scanning Tunneling Microscopy II*. Springer-Verlag, New York, 1992.

- [8] Park, Sang-il, and C.F. Quate, "Scanning tunneling microscope" *Rev. Sci. Instrum.* 58(11) 1987: 2010-2017.

- [9] Kleindiek, S., K. H. Herrman, "A miniaturized scanning tunneling microscope with large operation range" *Rev. Sci. Instrum.* 64(3) 1993: 692-693.

- [10] Jayadevaiah, M., and M. V. Lakshminarayanan, "Design of a compact scanning tunneling microscope with a feedback to coarse approach controller for low scan ranges" *Meas. Sci. Technol.* 15(5) 2004: N35-N38.
- [11] Alexander, John. *STM Project*. <<http://www.geocities.com/spm_stm/Project.html>>.
- [12] Müller, Jürgen *STM* 17 April 2006 << <http://www.e-basteln.de/index.htm>>>.
- [13] Pohl, D. W. "Dynamic piezoelectric translation devices" *Rev. Sci. Instrum.* 58 (1987) 54-57.
- [14] Koops, R., and G. A. Sawatzky "New scanning device for scanning tunneling microscope applications" *Rev. Sci. Instrum.* 63(8) 1992: 4008:4009
- [15] Rogers, B. L., J.G. Shapter, W. M. Skinner, K. Gascoigne, "A method for production of cheap, reliable Pt-Ir tips" *Rev. Sci. Instrum.* 71(4) 2000: 1702-1705.
- [16] Gupta, Anjan K., K. W. Ng, "Compact coarse approach mechanism for scanning tunneling microscope" *Rev. Sci. Instrum.* 72(9) 2001: 3552-3555.
- [17] Kuk, Y. and P. J. Silverman "Scanning tunneling microscope instrumentation" *Rev. Sci. Instrum.* 58 (1987) 165-180.
- [18] Maps, J., "Simple raster generator for use with scanning tunneling microscope" *Rev. Sci. Instrum.* 62(2) 1991: 357-359
- [19] Strom, V., R. D. Gomez, J. Nogues, B. Rodell, and K. V. Rao, "Inexpensive high-voltage low-current amplifier for driving long-range scanning tunneling microscope piezoactuators. *Meas. Sci. Technol.* 6 (1995):1072-1077.

- [20] Chen, Y..P., A. J. Cox, M. J. Hagmann, H. D. A. Smith, “Electrometer preamplifier for scanning tunneling microscopy” *Rev. Sci. Instrum.* 67(7) 1996: 2652-2653.
- [21] Doebelin, E. O. *Measurement Systems: Application and Design*. 5th ed. McGraw-Hill, 2004.
- [22] Brown, Sanborn C., *Introduction to Electrical Discharges in Gases*. John Wiley & Sons, New York, 1966.
- [23] Annamalai, R, J. D. West, A. Luscher, V. V. Subramaniam. “Electrophoretic drawing of continuous fibers of single-walled carbon nanotubes”, *Journal of Applied Physics* 98 (2005): 114307.